HIRDLS

SW-HIR-2046

HIGH RESOLUTION DYNAMICS LIMB SOUNDER

Originator: Charles Cavanaugh Date: 05/15/2013

Subject/Title:

Level 1 Algorithm Theoretical Basis Document – Post Launch Update

Description/Summary/Contents

In this document, we describe the scientific basis of the Level-1 processor algorithms used for the High Resolution Dynamics Limb Sounder (HIRDLS), flying on the Aura platform of the Earth Observing System (EOS) mission (EOS-Aura). The Level-1 processing stage ingests the Level-0 raw telemetry data and generated the Level-1 product consisting of calibrated and geo-located radiance data. HIRDLS is a joint US-UK project between the University of Colorado at Boulder and the University of Oxford.

Keywords:

L1PP, L1X, L1C, L1R, ATBD

Oxford University
Atmospheric, Oceanic &
Planetary Physics, Clarendon
Laboratory,
Parks Road,
OXFORD OXI 3PU,
United Kingdom

University of Colorado at Boulder
Center for Limb Atmospheric Sounding
3450 Mitchell Lane, Bldg. FL-0,
Boulder, Colorado,
80301
United States of America.

EOS

High Resolution Dynamics Limb Sounder

Level 1 Algorithm Theoretical Basis Document

Charles Cavanaugh[1], John Gille[1,2], Vince Dean[1], Gene Francis[1],
Chris Halvorson[1], Bruno Nardi[1], Maria Rivas[1], Bob Wells[3]

[1]National Center for Atmospheric Research, Boulder
[2]University of Colorado, Boulder
[3]University of Oxford, UK

Table of Contents

List of Figures

List of Tables

HIRDLS Acronym List (HAL)

AIRS	Atmospheric Infrared Sounder
APID	Application Process ID
ATBD	Algorithm Theoretical Basis Document
CC	Chopper Cycle
CEU	Cooler Electronics Unit
CLAES	Cryogenic Limb Array Etalon Spectrometer
CM	Calibration Mirror
CR	Chopper Revolution
DISC	Data and Information Services Center
ECI	Earth-Centered Inertial
ECIS	Earth-Centered Inertial Spacecraft
EDOS	EOS Data and Operations System
EOF	Empirical Orthogonal Function
EOS	Earth Observing System
EOSDIS	EOS Data and Information System
FFT	Fast Fourier Transform
FOV	Field-of-View
FPA	Focal Plane Array
GEU	Gyro Electronics Unit
GIRD	General Interface Requirements Document
GSFC	Goddard Space Flight Center
GSS	Gyroscope Subsystem
HAS	HIRDLS Acronym List
HDF	Hierarchical Data Format
HIRDLS	High Resolution Dynamics Limb Sounder
HPF	High-pass Filter
IFC	In-flight Calibrator
IFOV	Instrument Field-of-View
ISAMS	Improved Stratosphere and Mesosphere Sounder
LIMS	Limb Infrared Monitor of the Stratosphere
LOS	Line-of-Sight
LPF	Low-Pass Filter
LRIR	Limb Radiance Inversion Radiometer
LS	Least Significant
MaF	Major Frame
MiF	Minor Frame
MLS	Microwave Limb Sounder
MTF	Modulation Transfer Function
NASA	National Aeronautics and Space Administration
OAF	Open Area Fraction
PDS	Production Data System
PRHS	Primary Read Head Select
RDSR	Radiance Data Sample Rate

RMS	Root Mean Square
S/C	Spacecraft
SCRF	Spacecraft Reference Frame
SDP	Science Data Processing
SHFI	Science Housekeeping Format Identifier
SMA	Scan Mirror Assembly
SRHS	Secondary Read Head Select
SSH	Sunshield Door
SVD	Singular Value Decomposition
TOA	Top of the Atmosphere
TRCF	Telescope Reference Frame
TSS	Telescope Subsystem
UARS	Upper Atmosphere Research Satellite

Abstract

In this document, we describe the scientific basis of the Level-1 processor algorithms used for the High Resolution Dynamics Limb Sounder (HIRDLS), flying on the Aura platform of the Earth Observing System (EOS) mission (EOS-Aura). The Level-1 processing stage ingests the Level-0 raw telemetry data and generates the Level-1 product consisting of calibrated and geo-located radiance data. HIRDLS is a joint US-UK project between the University of Colorado at Boulder and the University of Oxford.

The HIRDLS instrument is a 21-channel infrared limb-scanning radiometer designed to sound an altitude range from the upper troposphere to the mesosphere to determine profiles of temperature, trace gas concentrations, aerosols, and the location of polar stratospheric clouds and cloud tops. The goals are to provide sounding observations with a horizontal and vertical resolution superior to those previously obtained, to observe the lower stratosphere with improved sensitivity and accuracy, and to improve understanding of atmospheric processes through data analysis, diagnostics, and the use of two- and three-dimensional models.

This release of the Level-1 Algorithm Theoretical Basis Document (ATBD) applies specifically to the algorithms developed for production, after the radiance anomaly was discovered.

1 Introduction

The purpose of this document is to present the physical and mathematical principles that underlie the algorithms developed by the HIRDLS team to generate calibrated, geo-located radiances and appropriate auxiliary data from the HIRDLS Level-0 telemetry and housekeeping data and from associated ephemeris and spacecraft attitude data. The generated Level-1 data is then further processed by HIRDLS Level-1 to Level-2 processing software to generate retrievals of atmospheric temperature, mixing ratios of 10 different trace gases, distributions of atmospheric aerosols, and cloud top heights, all with atmospheric pressure as the vertical profile. Further information on the HIRDLS experiment can be found in *Gille, J.C. and J.J. Barnett: Conceptual Design of the High Resolution Dynamics Limb Sounder (HIRDLS) for the EOS Aura Mission*. 1996, SPIE, 2830, 190-201

2 Overview and Background Information

This section details the scientific objectives, historical lineage, instrument subsystems, and applicable data processing stages of the HIRDLS experiment. Also detailed in this section is the anomalous effect of the unexpected partial blockage of the HIRDLS primary scan mirror, and the update to the mirror scan modes necessitated by the blockage.

2.1 Experiment Objectives

Concerns for the stability of the Earth's ozone layer have dominated research attention on the stratosphere and mesosphere since the middle 1970s, when attention originally focused on the impact of supersonic aircraft, but quickly shifted to the effects of chlorine released by photolysis of anthropogenic chlorofluorocarbons. The unexpected discovery of the rapid decline of the springtime ozone column over Antarctica resulted in many new measurements, theories and models, including chemistry taking place on particles, that provide a great deal of clarity on the processes involved. The development of our understanding of atmospheric dynamics has been less dramatic but no less important. Theoretical developments and observational studies have fundamentally changed the picture of the planetary scale circulation. These developments have had far-reaching implications for our understanding of the general circulation of the middle atmosphere, and the associated transport and mixing of trace constituents. Taken together, these advances have clarified our understanding of the ozone layer, and resulted in the Montreal Protocol and related agreements to phase out a wide range of species implicated in ozone depletion.

More recently attention is being paid to questions of global change and the possible effects of human activities on the climate system. As part of this study, the role of the stratosphere and stratospheric processes in climate has emerged as a critical area of study. The picture of the structure of the lower stratosphere and upper troposphere has been clarified, but there are still enduring questions about the ways in which exchange between these regions takes place. In addition, the distributions of particulates and radiatively important trace gases, such as ozone and especially water vapor, are not known well enough. For water there is not enough information to look for evidence of long term trends.

The general objectives of HIRDLS then are twofold; to provide information to assess the role of the stratosphere, especially the lower stratosphere and the upper troposphere (UT/LS) in climate processes; and to observe the processes that affect the stratospheric ozone layer at a time when the concentrations of active chlorine have reached a maximum and are beginning to decrease. These data

will improve our understanding of the dynamics of these chemical and dynamical processes, and improve our ability to model the future evolution of the atmosphere. These objectives are fully consistent with the objectives of the National Aeronautics and Space Administration (NASA) Earth Science Enterprise.

2.2 Scientific Objectives

Seven principal scientific objectives were chosen as the focus of the investigations for which the HIRDLS Science Team intends to use the data that is produced by the HIRDLS instrument. These objectives are:

1) To understand the fluxes of mass and chemical constituents (including greenhouse gases and aerosols) that affect the dynamics and composition of the troposphere, stratosphere, mesosphere, and thermosphere and link these regions together. These fluxes must be determined down to smaller scales than previously observed.

2) To understand the chemical processing, transport, and small-scale irreversible mixing of trace constituents in the middle atmosphere, including the chemical and dynamical processes responsible for creating the Antarctic (and perhaps Arctic) ozone holes.

3) To understand the momentum, energy, and potential vorticity balances of the middle atmosphere, by extending global observations to smaller horizontal and vertical scales than has previously been possible. These small-scale processes are believed to be fundamentally important to the determination of some large-scale characteristics and are thought to cause irreversible chemical mixing.

4) To obtain climatologies of upper tropospheric, stratospheric, and mesospheric quantities, in particular, profiles of temperature, ozone, several radiatively active gases, aerosol, gravity wave activity, and cloud top heights. Seasonal, interannual, and long-term trends will be obtainable because of the five-year measurement sequence that will be provided by each EOS instrument, combined with pre-EOS measurements and future EOS observations.

5) To provide data to validate and improve numerical models of the atmosphere, in order to gain confidence in their ability to predict climate change. These simulations are critically dependent on the treatment of horizontal and vertical scales that are much finer than those currently observed.

6) To improve the understanding of tropospheric chemistry through the use of temperature and constituent retrievals that extend into the upper troposphere, under favorable conditions. The combination of these observations with observations from other EOS instruments, and with chemical models, will yield information about the oxidation capacity of the atmosphere.

7) To improve the understanding of stratospheric and tropospheric aerosols and clouds by acquiring long-term high-resolution observations of their nature and distribution. Aerosols and polar stratospheric clouds are now known to play essential roles in the depletion of ozone in the lower stratosphere, and subvisible cirrus clouds in the upper troposphere significantly impact the radiative heating and cooling of the atmosphere.

2.3 Historical Perspective

The first successful proposal for the flight of an infrared limb viewing radiometer was that for the Limb Radiance Inversion Radiometer (LRIR), put forward for flight on Nimbus 6. Initial difficulties caused by the stringent requirements on pointing knowledge were solved by Gille and House (1971), who showed how the limb measurements themselves could be used to make this determination, or equivalently to solve for the vertical temperature profile as a function of pressure as a vertical coordinate. LRIR was launched in June, 1975; a brief discussion of its measurements of temperature and ozone is contained in Gille *et al.*(1980a,b).

A similar instrument, the Limb Infrared Monitor of the Stratosphere (LIMS) was flown on Nimbus 7 (Gille and Russell, 1984). It added the capabilities to measure water vapor, nitrogen dioxide, and nitric acid to the LRIR capabilities. Another limb sounder, the Stratosphere and Mesosphere Sounder (SAMS) also flew on Nimbus 7, measuring notably temperature, methane and nitrous oxide [*Drummond et al.*(1980)]. The results from these instruments added greatly to knowledge of stratospheric dynamics and chemistry.

Two infrared limb viewers flew on the Upper Atmosphere Research Satellite (UARS). The Improved Stratosphere and Mesosphere Sounder (ISAMS), a limb scanner [*Taylor et al.*(1993)] and the Cryogenic Limb Array Etalon Spectrometer (CLAES) [*Roche et al.*(1993)], a limb-staring instrument. These instruments together measured temperature and the distributions of ozone, water vapor, methane, nitrous oxide, nitric acid, nitrogen dioxide, chlorofluorocarbon 11 and 12, carbon monoxide and nitric oxide. In addition they determined the distributions and composition of aerosols. These measurements have greatly added to our knowledge of the distribution of trace species and aerosols in the stratosphere and mesosphere, and the processes that maintain them.

The HIRDLS instrument traces much of its instrument approach to LIMS, and the flight software to ISAMS.

2.4 Instrument Overview

HIRDLS is an infrared limb-scanning radiometer designed to measure atmospheric limb emission in 21 spectral channels operating over the wavelength range from 6 to 18 μm. Requirements for increased vertical and horizontal resolution, the ability to sound down into the lower stratosphere and upper troposphere, and the ability to measure simultaneously a large number of trace species with a range of chemical lifetimes, necessitate improvements over previous limb scanning instruments. Limb scanners, such as LIMS and ISAMS, provided vertical resolution of about 2 to 3 km, but their longitudinal sampling was limited to approximately 2600 km at the equator (and half that at 60° latitude). HIRDLS was designed to improve on the capabilities of previous limb scanners by incorporating azimuth scanning to obtain a horizontal spacing between vertical profiles of roughly 5° or 500 km at the equator. Furthermore, the vertical resolution was increased by continuously scanning a narrow 1-km vertical field-of-view and over-sampling the vertical radiance profile nominally every 0.2 km. Detailed simulations have shown that spatial features having wavelengths 1.5 km can be adequately resolved. A schematic diagram of the HIRDLS instrument is shown in Figure 1.

The instrument consists of nine subsystems; the key subsystems are described below. The structural-thermal subsystem (STH) provides an outer cover to create a stable mechanical and thermal environment for the instrument, a radiator panel for removing heat from the mechanical cryocooler, and a baseplate on which the telescope subsystem is mounted. The instrument views rearward from the spacecraft with the boresight inclined approximately 25 degrees from the local horizon. A sunshield subsystem (SSH) controls a moveable door to prevent sunlight from directly illuminating the instrument aperture when the satellite is in the high latitude portion of the orbit.

2.4.1 Telescope Subsystem

Limb radiation enters the instrument aperture and is collected by the optical telescope after reflection off the flat scan mirror. The telescope subsystem (TSS) consists of a two-axis scan mirror, an off-axis, 3-mirror Gregorian reflective telescope, and two Ge lenses to relay the image of the atmosphere produced by the telescope onto the focal plane consisting of 21 infrared detectors while maintaining good image quality. The optical system is designed to image a 1-km vertical dimension at the atmospheric limb a distance of 3000 km away onto detectors with a vertical dimension of 82 µm. The telescope forms an f/2.5 intermediate image at the focus of the off-axis parabolic primary mirror. The secondary, an off-axis ellipse, re-images this to a good quality but slow image which is transferred by Ge lenses to a nearly diffraction limited f/1.5 image at the detectors. A Lyot stop system is used to control diffracted stray radiation. The scan mirror (SMA) rotates about two axes to view the field at a given azimuth angle (variable over a 60° range) and scan in elevation angle to view the desired part of the atmospheric limb or to view the collimated beam of a small, high quality blackbody for in-flight radiometric calibration (IFC). The entrance pupil diameter is approximately 160 mm with an effective focal length of the optical system of 245 mm. Incoming atmospheric radiation, collected by the primary mirror, is mechanically chopped at a frequency of 500 Hz by a reflective rotary chopper located at the first focal plane. The chopper reflects a view of space via a relay mirror to the detectors when closed.

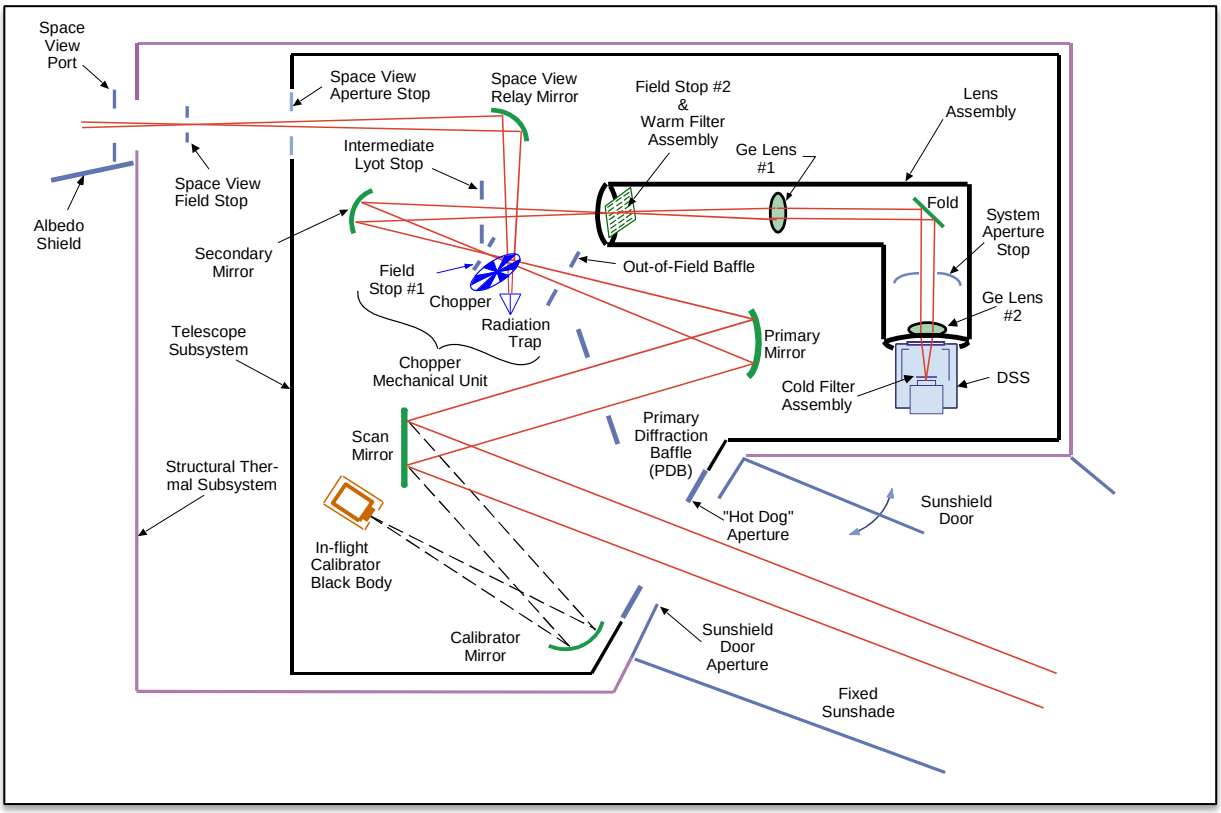

Figure 1. HIRDLS Optical Schematic

2.4.2 Detector Subsystem

The modulated atmospheric radiation and unmodulated background radiation emitted within the instrument is detected by 21 separate HgCdTe photoconductive detectors. The detector subsystem (DSS) contains the focal plane and vacuum dewar. The detectors and cold filters are cooled by a Stirling cycle cryocooler (CSS) operating at 60° K and controlled by a feedback loop between the focal plane and the cooler electronics unit (CEU). This maintained the detector temperature's stability to 0.001° K over the mission. The detector signals are ac-coupled to remove constant or slowly varying background signals before being amplified by low-noise preamplifiers. The amplified ac signal is passed through an analog bandpass filter with a bandwidth somewhat greater than two times the expected signal bandwidth and centered about the fundamental component of the chopping frequency to prevent aliasing of higher or lower frequency components into the signal band. The filtered signal is demodulated by sampling the waveform synchronously with the chopping frequency. The signal is digitized using a 16-bit analog-to-digital converter. A programmable lowpass digital filter for each channel allows the performance of the signal processing system to be optimized in orbit and minimizes sensitivity to drift or changes in electrical component values. After digital lowpass filtering, the signal samples are reduced by a factor of 6 to a final effective sampling rate of nominally 83.3 Hz before being output to the telemetry stream.

Spectral selection is achieved through the use of 21 individual interference filters operating at ambient temperature and located at an intermediate focal plane. A second set of filters is located on the cold focal plane in close proximity to the detectors, having roughly twice the spectral bandpass of the warm filters. The cold filters are necessary to achieve a high level of out-of-band spectral blockage and to significantly reduce unwanted optical cross talk due to scattering by or internal reflections from the Ge lens relay system. The thickness of the substrate of each of the cold filters is selected to compensate for the small residual longitudinal chromatic aberration in the relay system.

The detector focal plane dimensions and the relative positions of the spectral channels are shown in Figure 2. The center detector column has been offset from the middle to allow room for electrical connections to be made. The physical size of detector elements is 82 μm x 820 μm, with a corresponding angular field-of-view (FOV) of 0.332 mrad x 3.32 mrad. The vertical dimension of the instantaneous detector FOV is 1-km at the limb, with a horizontal dimension of 10 km. The composite field-of-view is 55 km x 55 km. The alignment quad-cell detector at the top of the array is to facilitate pre-flight testing of the line-of-sight and will not be operational in-flight.

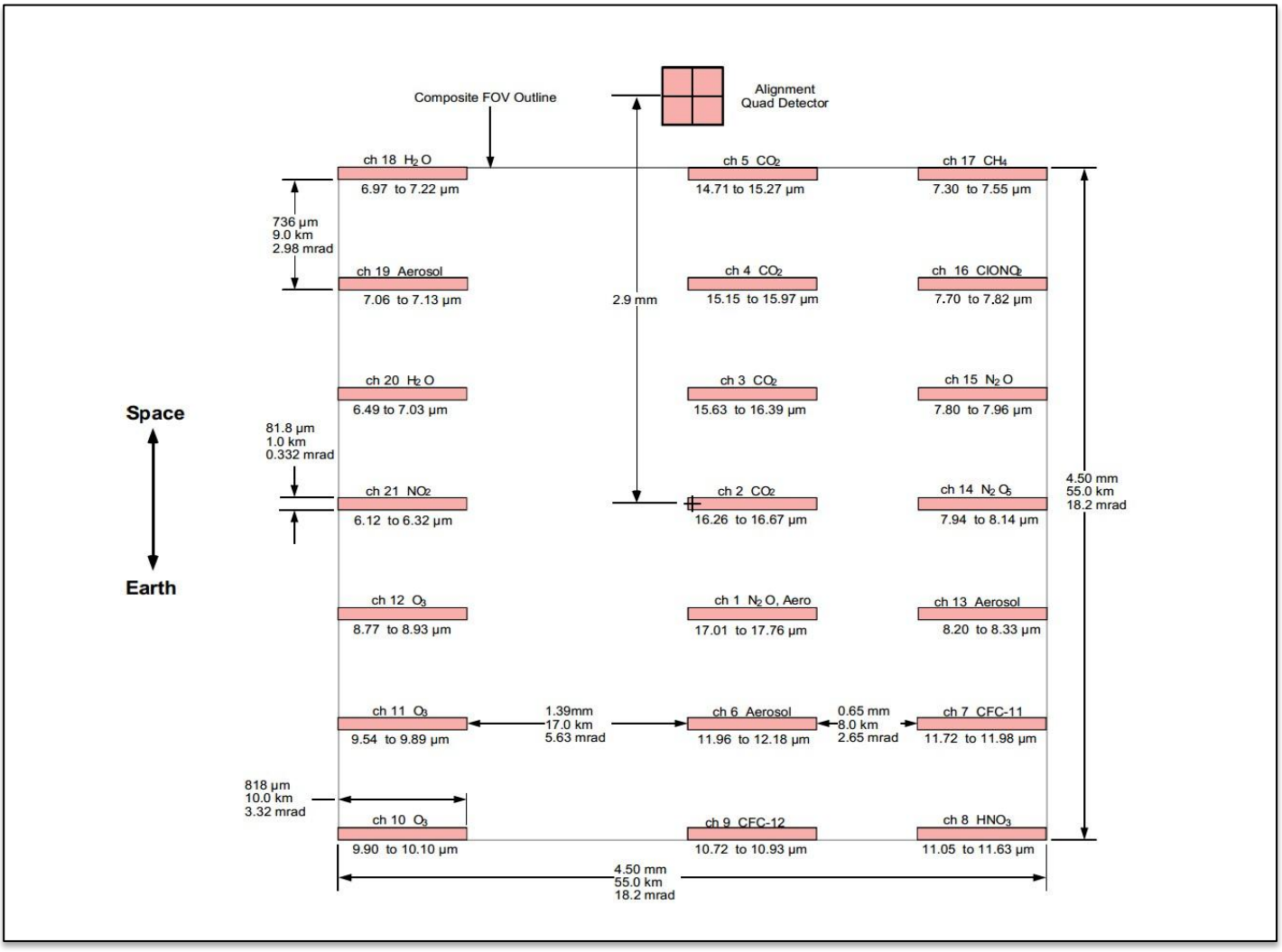

Figure 2. Detector Focal Plane Schematic

2.4.3 Gyroscope Subsystem

To facilitate the determination of accurate geopotential heights if there were significant spacecraft motions on a sub-orbital level, and to realize the full scientific potential of HIRDLS, more accurate pointing information is needed than that provided by the spacecraft location and spacecraft attitude data and rigid body geometry alone. The optical system was mounted on a separate optical bench. There will inevitably be small time-varying distortions between the optical bench and the instrument baseplate and between the instrument baseplate and the spacecraft altitude measurement system.

The detector fields-of-view are alternately scanned upward and downward across the limb at a nominal scan rate of 0.3 deg/sec in the global observation mode. The angular position of the scan mirror relative to the optical bench is measured by optical encoders every 12 msec, corresponding to approximately 14 arcsec. Any inertial motion of the optical bench produced by spacecraft and instrumental disturbances will introduce undesired motion of the line-of-sight (LOS), which will not be sensed by the encoders. It is expected that data from the spacecraft attitude control system will not be of sufficient precision nor will the relationship between the spacecraft gyro and HIRDLS line-of-sight be known precisely enough to meet this requirement. Therefore, a multi-axis gyroscope is

mounted to the optical bench to measure bench motion relative to inertial space, making corrections to pointing knowledge possible. The gyroscope subsystem (GSS) consist of a mechanical unit, which is mounted directly to the optical bench providing angular motion measurements of the bench. The gyroscope unit is a GEC-Marconi Avionics Type 125 gyro with an electronic unit (GEU) specifically designed for HIRDLS requirements.

2.5 Radiance Anomaly

HIRDLS was launched on the Aura spacecraft on 15 July 2004 from the Western Test Range into a 705 km Sun-synchronous orbit. After 24 days for outgassing from the instrument and satellite, the coolers were gradually turned on during the evening of 9 August, and reached the 62 K detector operating temperature early on 10 August. At this point the Sun shield door was opened, and the scan mirror was commanded to perform an exploratory scan across the entrance aperture, including the atmosphere, for ~10 minutes.

The first measurements were much different from what was expected. The radiance signal was much larger, and was much more vertically uniform than expected from the atmosphere and space. There was a region at the azimuth furthest from the Sun and orbit plane where the signal was a bit lower, and had more vertical variation. Clearly there had been a serious malfunction.

The HIRDLS team, working with a NASA review board, established that an obstruction in the optics was blocking the view from the scan mirror to the aperture, as well as the view to the IFC, preventing radiance from outside the aperture or the IFC, from reaching the detectors. Subsequent attempts to understand and simulate what happened suggest that there was air between the 2 layers of a plastic (Kapton®) film used to line the optical cavity to maintain cleanliness. During the depressurization at launch these layers could have separated, with the inner one contacting and being punctured by a sharp feature on the back of the scan mirror. Once cut, a tear in the plastic could propagate very rapidly, thus creating a flap from the inner layer. The force on it during the maximum acceleration of the launch rocket could have pulled it in front of the scan mirror. Efforts to move the blockage by various motions of the scan mirror were not successful.

Scans in azimuth confirmed that at the azimuths furthest from the orbital plane there was a partial view out past the blockage, establishing that the blockage covers most of the aperture, with the only clear area being at azimuths furthest from the Sun, or furthest left when looking backward along the orbit.

The most definitive effect of the blockage is the effect on horizontal coverage. Useful scans can only be made at the largest view angle away from the Sun, or a line of sight (LOS) of 47° on the anti-Sun side of the orbital plane, looking backward. This has three effects on coverage. Most obviously, it limits longitudinal resolution to the orbital spacing of 24.72°. Second, it prevents coverage south of 63°S, or north of 80°N, (resulting in global coverage similar to that of LIMS [Gille and Russell, 1984]). Finally, it precludes simultaneous measurements with other Aura or A-Train instruments at nearly the same time. Some locations can be seen on a preceding or following orbit, however. How the HIRDLS team was able to overcome this anomaly will be presented in further sections.

2.6 Scan Modes

As described in Section 2.6, an anomaly with the HIRDLS radiances forced a change to the pre-launch defined scan mirror movement modes. Figure 3 shows the pre-launch “Global Mode” scan pattern, which optimized global coverage by scanning in the vertical (elevation) axis at six different

horizontal (azimuth) angles. 2-point radiometric calibration was included in this mode by adding a short stare at the in-flight blackbody calibration point. Radiance data obtained from HIRDLS soon after launch exposed the anomaly, and invalidated the use of this global coverage scan pattern. The in-flight calibrator was no longer accessible to the scan mirror, and roughly 80% of the viewing aperture was no longer accessible to the scan mirror. The HIRDLS recovery focus was two-fold: moving the scan mirror in such a way as to define the extent of the blockage of the viewing aperture, and moving the scan mirror in such a way as to fulfill as many of the HIRDLS mission requirements as possible. To those ends, two different types of scan modes were utilized: raster scanning modes and science data scanning modes. The raster scanning modes formed the basis for the correction work detailed in Section 4 of this document. The remainder of this section describes these two scan mode types. In those descriptions, "chopper rotation" (CR) nomenclature is used. That nomenclature is fully detailed in Section 3.1, but for this section, it is only important to note that a CR is the basic unit of radiance data acquisition, and takes 12 milliseconds.

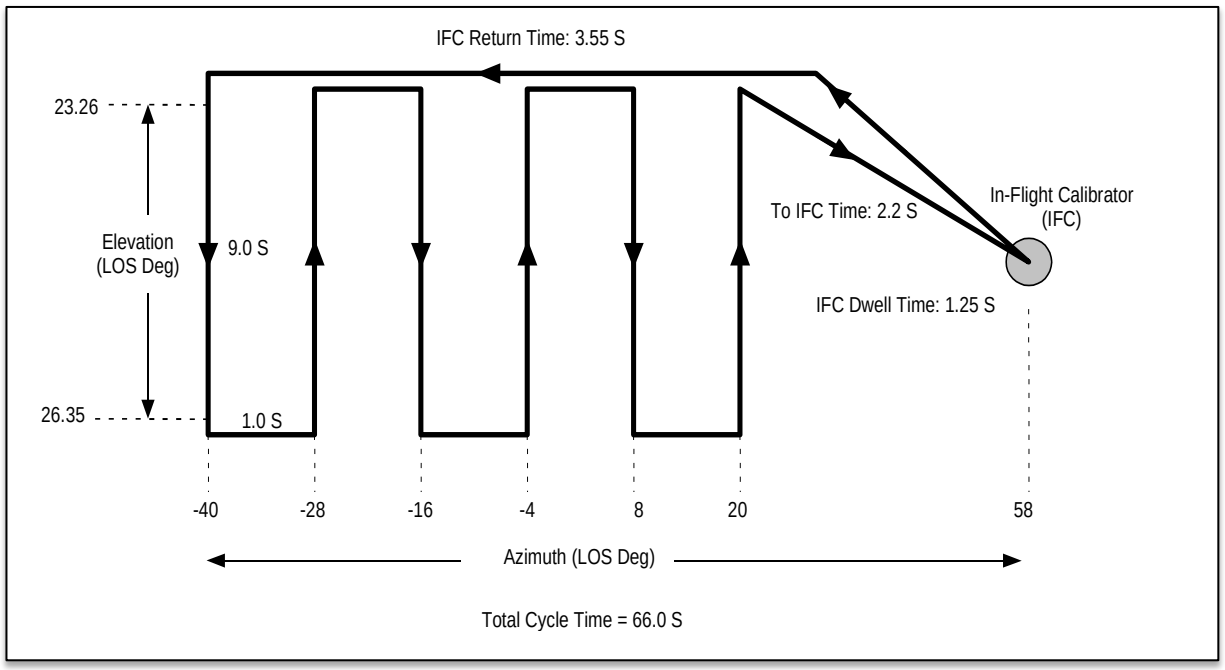

Figure 3 "Global Mode" Scan Pattern

2.6.1 Raster Scan Modes

The first task after discovery of the aperture blockage was to determine the blockage extent. Raster scanning of the mirror across the full azimuth angle range, while holding elevation angle constant, then repeating this azimuth scan for a different constant elevation angle, for the full elevation angle range, was used for this determination. Eight different raster scanning modes were employed, and were given the scan table numbers 7, 9, 14, 15, 17, 20, 27 and 29. Two of these scan tables, 7 and 20, which are representative of the eight scan tables, are detailed further in this section.

2.6.1.1 Scan Table 7

Figure 4 shows the scan pattern of scan table 7. Eight different elevation angles, representing the extent of the altitudinal atmospheric vertical range within the viewing aperture, are used for mirror slews across a limited azimuth angle range. The exact elevation angles used depend on the Earth's oblateness factor at the data point, with the intent to have this scan table's elevation range extent be constant in altitude, and to have each individual azimuth slew's altitude be constant for all cycles of this scan table. Movement of the mirror in the vertical at azimuth shaft angle -23.5° (or 47° off the Aura scan track) was chosen because preliminary scanning showed more radiance gradient at this azimuth angle than at any other. This scan table was run twice in March 2005; once for 16 full cycles of the scan table, and the other, five days later, for 32 full cycles. Table 1 details the timing of one full cycle of scan table 7.

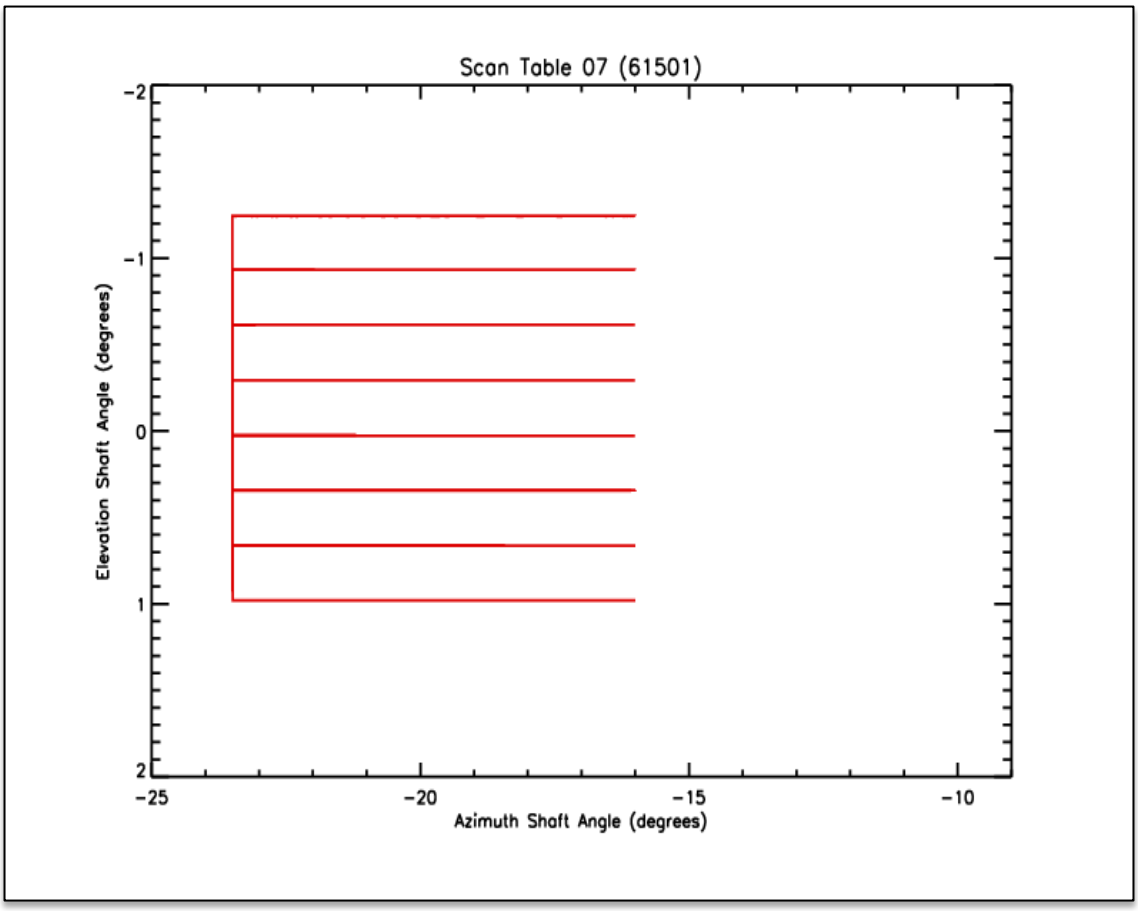

Figure 4. Scan Table 7 Scan Pattern

CRs	Time Extent (seconds)	Start Azimuth (degrees)	Start Elevation (Kilometers)	Stop Azimuth (degrees)	Stop Elevation (Kilometers)	Action / Segment
160	1.920	-23.5	-59	-23.5	150	Up Scan / A
166	1.992	-23.5	i	-16.0	i	Right Scan / B-1
252	3.024	-16.0	i	-16.0	i	Stare / B-2
166	1.992	-16.0	i	-23.5	i	Left Scan / B-3
3334	40.008	-23.5	i	-23.5	i	Stare / B-4
166	1.992	-23.5	i	-23.5	i + 1	Down Scan / B-5 Segment B loops 8 times (except B-5, which is not performed on loop 8), with "i" the loop index into [150, 122, 93, 64, 34, 4, -27, -59]
102	1.224	-23.5	-59	-23.5	-59	Stare / C

Table 1. Scan Table 7 Cycle Timing

2.6.1.2 Scan Table 20

Figure 5 shows the scan pattern of scan table 20. This scan table is more complex than the other type of raster scanning table (scan table 7 being representative of that type), in that all azimuth scans, including four addition ones, slew across the full azimuth angle range, and also in that five full elevation scans are included. One of the five elevation scans is at a known fully-blocked azimuth angle (-18.0°), the other four are at azimuth angles that show enough radiance gradient to be potentially useful for science data scanning. This scan table was run thrice in 2005; on February 1 for 77 full cycles of the scan table, on February 8 - 10 for 2371 full cycles, which included 177 full cycles during spacecraft pitch-down, and on May 12 for 1066 full cycles. Table 2 details the timing of one full cycle of scan table 20.

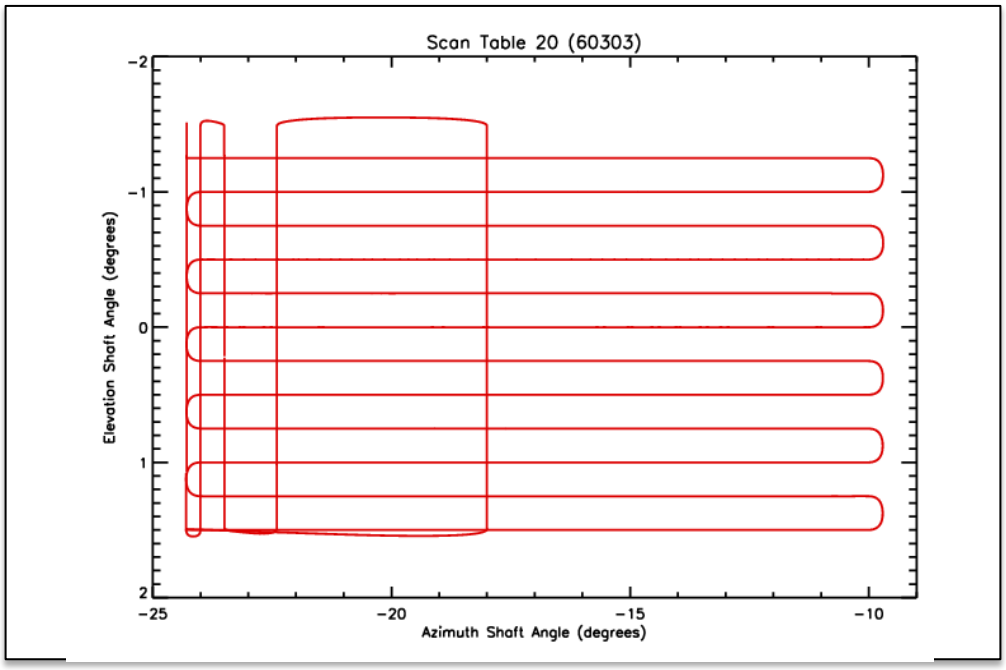

Figure 5. Scan Table 20 Scan Pattern

CRs	Time Extent (seconds)	Start Azimuth (degrees)	Start Elevation (degrees)	Stop Azimuth (degrees)	Stop Elevation (degrees)	Action / Segment
238	2.856	-24.3	1.50	-24.3	1.50	Stare / A-1
8	0.096	-24.3	1.50	-24.0	1.50	Right Scan / B
196	2.352	-24.0	i	-10.0	i	Right Scan / C-1
16	0.192	-10.0	i	-10.0	[i] - .250	Arc / C-2
194	2.328	-10.0	[i] - .250	-24.0	[i] - .250	Left Scan / C-3
16	0.192	-24.0	[i] - .250	-24.0	i + 1	Arc / C-4 Segment C loops 6 times (except C-4, which is not performed on loop 6), with "i" the loop index into [1.50, 1.00, 0.50, 0.00, -0.50, -1.00], and "[i]" the value at index i.
10	0.120	-24.0	-1.25	-24.3	-1.25	Left Scan / D
32	0.384	-24.3	-1.25	-24.3	-1.51	Up Scan / E
500	6.000	-24.3	-1.51	-24.3	1.50	Down Scan / F
34	0.408	-24.3	1.50	-24.0	1.50	Arc / G
500	6.000	-24.0	1.50	-24.0	-1.50	Up Scan / H
34	0.408	-24.0	-1.50	-23.5	-1.50	Arc / J
1500	18.000	-23.5	-1.50	-23.5	1.50	Down Scan / K
34	0.408	-23.5	1.50	-22.4	1.50	Arc / L
500	6.000	-22.4	1.50	-22.4	-1.50	Up Scan / M
42	0.504	-22.4	-1.50	-18.0	-1.50	Arc / N
500	6.000	-18.0	-1.50	-18.0	1.50	Down Scan / P
48	0.576	-18.0	1.50	-24.3	1.50	Arc / Q
224	2.688	-24.3	1.50	-24.3	1.50	Stare / A-2

Table 2. Scan Table 20 Cycle Timing

2.6.2 Science Data Scan Modes

By analyzing the radiance data from the raster scan modes, the HIRDLS team was able to devise four new science data acquisition scan modes. These scan modes all took advantage of the most open area of the aperture blockage, and moved the mirror in such a way as to minimize movement of the Kapton® that blocked the aperture. These scan modes were given the scan table numbers 13, 22, 23 and 30. All four of these scan table are detailed further in this section, in order of their deployment.

2.6.2.1 Scan Table 30

Scan Table 30 was the primary science data acquisition scan mode from January 21, 2005 to April 28, 2005. It was also run in November 2006, during spacecraft pitch-down, for 156 full cycles. Figure 6 shows the scan pattern of scan table 30, and Table 3 details the timing of one full cycle of the scan table. This pattern was devised to not only acquire science data, but also to learn more about the behavior of the Kapton® during science data acquisition. To facilitate that behavior analysis, an elevation scan at -18.0° was included in the pattern. Analysis of the science data during this scan table also showed that elevation scans at -22.4° azimuth angle were not sufficiently unaffected by the Kapton®, and therefore, later science scan modes did not include elevation scans at this azimuth angle. Elevation scan analysis of the science data acquired at -23.5° azimuth angle, with an angular velocity of 0.22005 degrees/sec, showed more Kapton® oscillation than expected, and that information fed forward into later science scan mode pattern development.

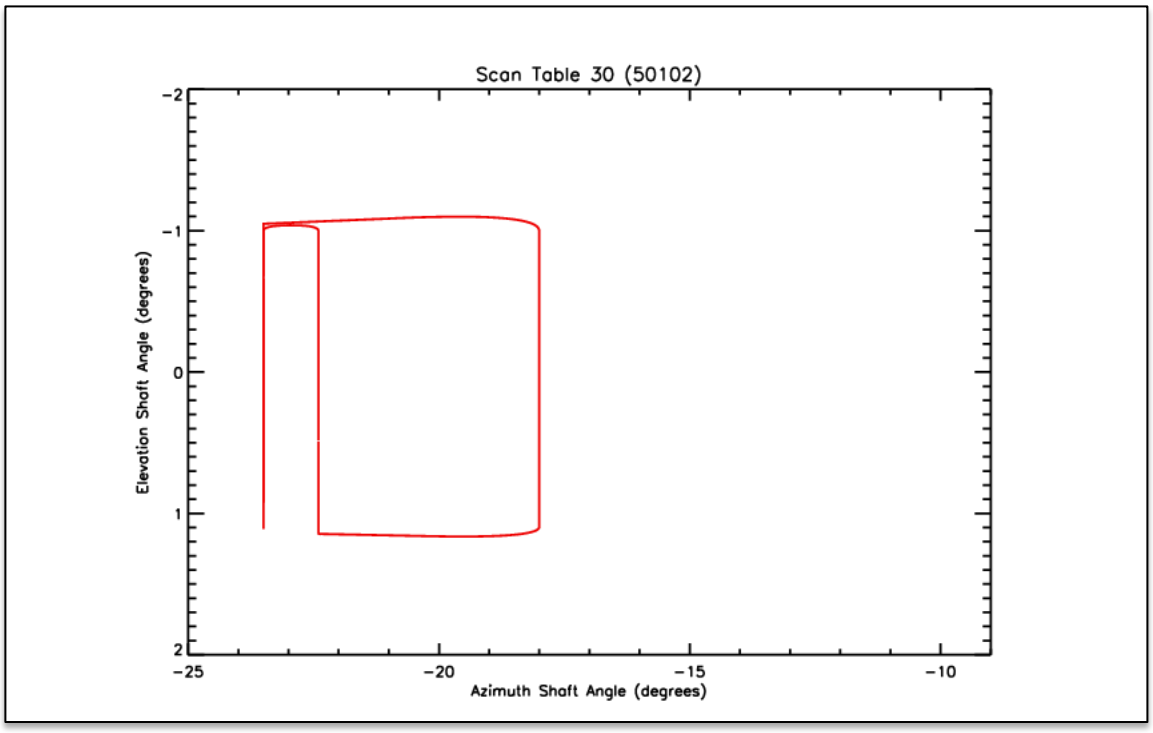

Figure 6. Scan Table 30 Scan Pattern

CRs	Time Extent (seconds)	Start Azimuth (degrees)	Start Elevation (degrees)	Stop Azimuth (degrees)	Stop Elevation (degrees)	Action / Segment
158	1.896	-23.5	-1.05	-23.5	-1.05	Stare / A-1
812	9.744	-23.5	-1.05	-23.5	1.11	Down Scan / B
804	9.648	-23.5	1.11	-23.5	-1.00	Up Scan / C
60	0.720	-23.5	-1.00	-22.4	-1.00	Arc / D
806	9.672	-22.4	-1.00	-22.4	1.15	Down Scan / E
2	0.024	-22.4	1.15	-22.4	1.15	Stare / F
38	0.456	-22.4	1.15	-18.0	1.11	Arc / G
266	3.192	-18.0	1.11	-18.0	-1.00	Up Scan / H
66	0.792	-18.0	-1.00	-23.5	-1.05	Arc / J
188	2.256	-23.5	-1.05	-23.5	-1.05	Stare / A-2

Table 3. Scan Table 30 Cycle Timing

2.6.2.2 Scan Table 13

Scan Table 13 was the primary science data acquisition scan mode from April 28, 2005 to April 24, 2006. It was also run in July 2006, during spacecraft pitch-down, for 11 full cycles, and it was also run in November 2006, during spacecraft pitch-down, for 24 full cycles. Figure 7 shows the scan pattern of scan table 13, and Table 4 details the timing of one full cycle of the scan table. Like scan table 30 before it, this pattern was devised to not only acquire science data, but also to learn more about the behavior of the Kapton® during science data acquisition. To facilitate that behavior analysis, an elevation scan at a different fully blocked azimuth angle, -14.0°, was included in the pattern. The main focus of the pattern was science data acquisition at -23.5° azimuth angle, and to that end, this pattern included 19 pairs of up/down elevation scans at that angle, for a total of 39 elevation scans (including the Kapton® scan at -14.0°). Elevation scan analysis of the science data acquired at -23.5° azimuth angle, with an angular velocity of 0.16944 degrees/sec, showed less, and more predictable, Kapton® oscillation than was exhibited in scan table 30 (due to the slower elevation scan rate), and that information fed forward into later science scan mode pattern development. Another important distinction of scan table 13 was that the elevation angle scanning extent for each scan was allowed to float, to provide for a constant top altitude of 153.5 kilometers for each scan (150 kilometers for the nominal science portion). Table 4 shows how this scan table allowed science data scanning in constant altitude space and allowed Kapton® data acquisition scanning in constant elevation angle space.

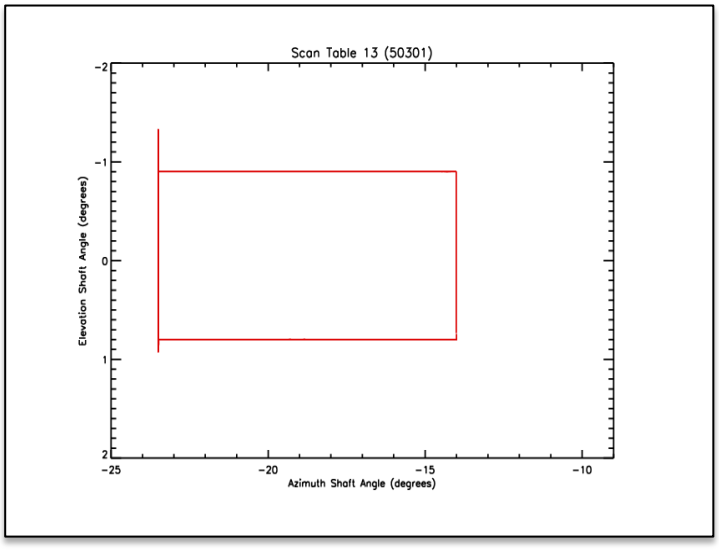

Figure 7. Scan Table 13 Scan Pattern

CRs	Time Extent (seconds)	Start Azimuth (degrees)	Start Elevation	Stop Azimuth (degrees)	Stop Elevation	Action / Segment
156	1.872	-23.5	-54.5 km	-23.5	-54.5 km	Stare / A
1120	13.440	-23.5	-54.5 km	-23.5	153.5 km	Up Scan / B-1
1120	13.440	-23.5	153.5 km	-23.5	-54.5 km	Down Scan / B-2 Segment B executed 19 times
1120	13.440	-23.5	-54.5 km	-23.5	153.5 km	Up Scan / C
128	1.536	-23.5	153.5 km	-23.5	-0.9 degrees	Down Scan & Stare / D
168	2.016	-23.5	-0.9 degrees	-14.0	-0.9 degrees	Right Scan / E
514	6.168	-14.0	-0.9 degrees	-14.0	0.8 degrees	Down Scan / F
250	3.000	-14.0	0.8 degrees	-23.5	0.8 degrees	Left Scan / G
224	2.688	-23.5	0.8 degrees	-23.5	-54.5 km	Down Scan or Up Scan & Stare / H

Table 4. Scan Table 13 Cycle Timing

2.6.2.3 Scan Table 22

Scan Table 22 was the primary science data acquisition scan mode from April 24, 2006 to May 4, 2006. Figure 8 shows the scan pattern of scan table 22. Unlike the two previous science data scan modes, scan table 22 included no Kapton® elevation scans. This scan table pattern remains at azimuth angle -23.5° for the duration of its cycle, performing 27 pairs of down/up elevation scans and then briefly "staring" out the aperture at an elevation angle pointing towards space. Table 5 details this scan table's timing pattern. Analysis of elevation scans of previous scan tables allowed the HIRDLS team to program the elevation scanning of this table at a rate, 0.15539 degrees/sec, that most minimized the oscillation of the Kapton®.

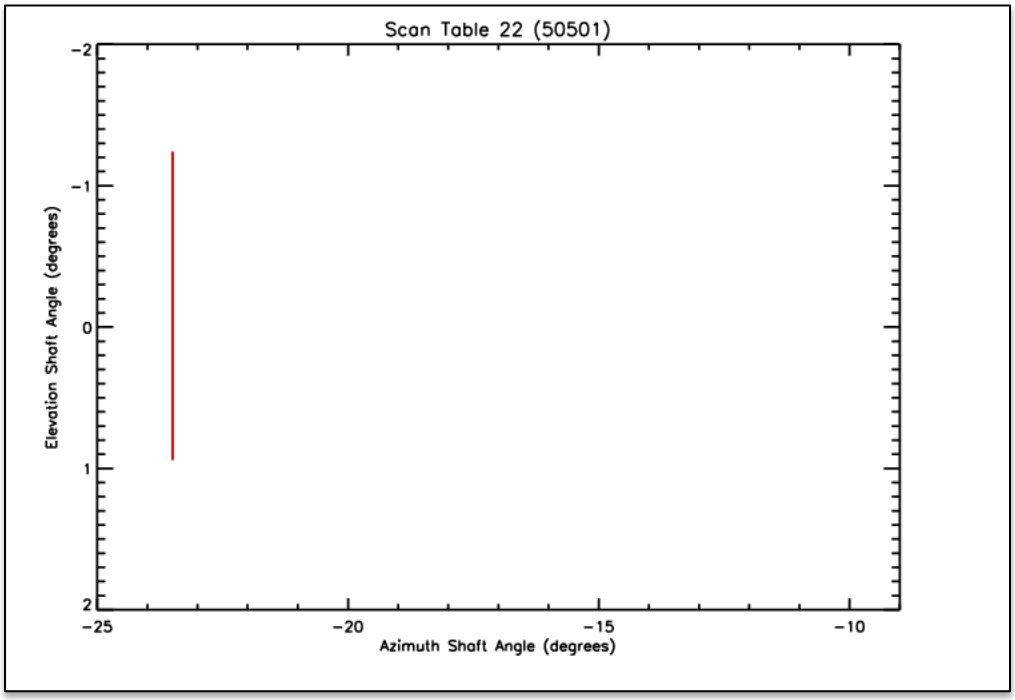

Figure 8. Scan Table 22 Scan Pattern

CRs	Time Extent (seconds)	Start Azimuth (degrees)	Start Elevation (degrees)	Stop Azimuth (degrees)	Stop Elevation (degrees)	Action / Segment
158	1.896	-23.5	-1.239	-23.5	-1.239	Stare / A-1
1209	14.508	-23.5	-1.239	-23.5	0.939	Down Scan / B-1
1210	14.520	-23.5	0.939	-23.5	-1.239	Up Scan / B-2 Segment B executed 27 times
193	2.316	-23.5	-1.239	-23.5	-1.239	Stare / A-2

Table 5. Scan Table 22 Cycle Timing

2.6.2.4 Scan Table 23

Scan Table 23 was the primary science data acquisition scan mode from May 4, 2006 to March 17, 2008, when the optical chopper stopped rotating. Figure 9 shows the scan pattern of scan table 23. The scan pattern for scan table 23 differs from scan table 22 only in the extent of its elevation scanning range. The top (spaceward) elevation angle for scan table 23 is 0.15° higher than scan table 22's. The elevation scan rate did not change, so therefore this scan table has approximately 80 more data acquisition points than scan table 22, as detailed in Table 6.

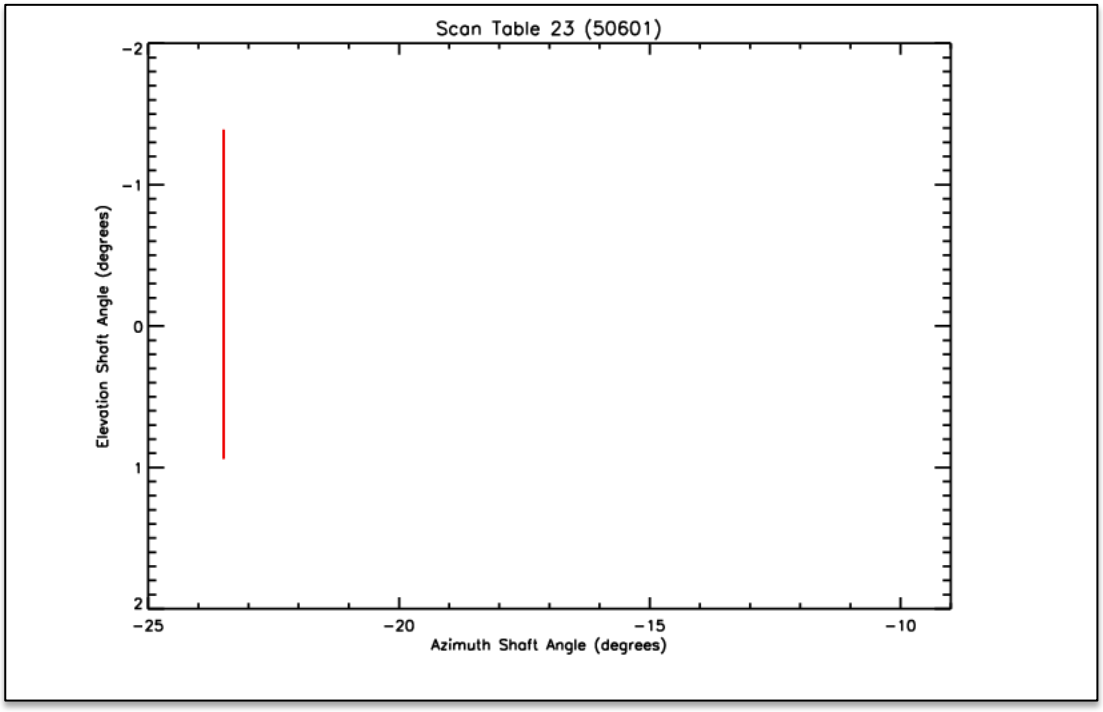

Figure 9. Scan Table 23 Scan Pattern

CRs	Time Extent (seconds)	Start Azimuth (degrees)	Start Elevation (degrees)	Stop Azimuth (degrees)	Stop Elevation (degrees)	Action / Segment
158	1.896	-23.5	-1.390	-23.5	-1.390	Stare / A-1
1290	15.480	-23.5	-1.390	-23.5	0.939	Down Scan / B-1
1290	15.480	-23.5	0.939	-23.5	-1.390	Up Scan / B-2 Segment B executed 27 times
198	2.376	-23.5	-1.390	-23.5	-1.390	Stare / A-2

Table 6. Scan Table 23 Cycle Timing

2.7 Processing Stages

HIRDLS Level 1 processing was designed to take place in two stages. The first stage, nicknamed L1X, would produce the required, by the Earth Science Data and Information System (ESDIS) project, standard NASA L1B time-series data product that would be made publicly available via NASA data servers. L1B is a NASA-created moniker that denotes the file contents are converted instrument data and/or calibrated radiances, rather than raw telemetry. The second stage, nicknamed L1R, would ingest the L1B data product and create a HIRDLS-designed profile-based data product for HIRDLS internal use only, containing only atmospheric scans and their respective ancillary data. This second data product isolated L1B file changes from the Level 2 processor. After launch, and therefore after the HIRDLS radiance anomaly, it became clear to the HIRDLS team that a third stage, inserted between the first and second stage, was necessary. This stage, nicknamed L1C, would ingest the L1B file, correct for the radiance anomaly effects, and create an output L1B file with the corrected radiances being the only difference between the input and output L1B files. While this decision did necessitate additional data storage, it was deemed the wisest choice in regards to isolating anomaly corrections and allowing development on all three processing stages to proceed independent of each other. A fourth processor, nicknamed L2PP, was added to run before L1X, to fix an anomaly in the raw L0 Files. It was also decided, post-launch, to release the previously-internal HIRDLS1R file. The remainder of this section, including Figure 10, further details these four processing stages.

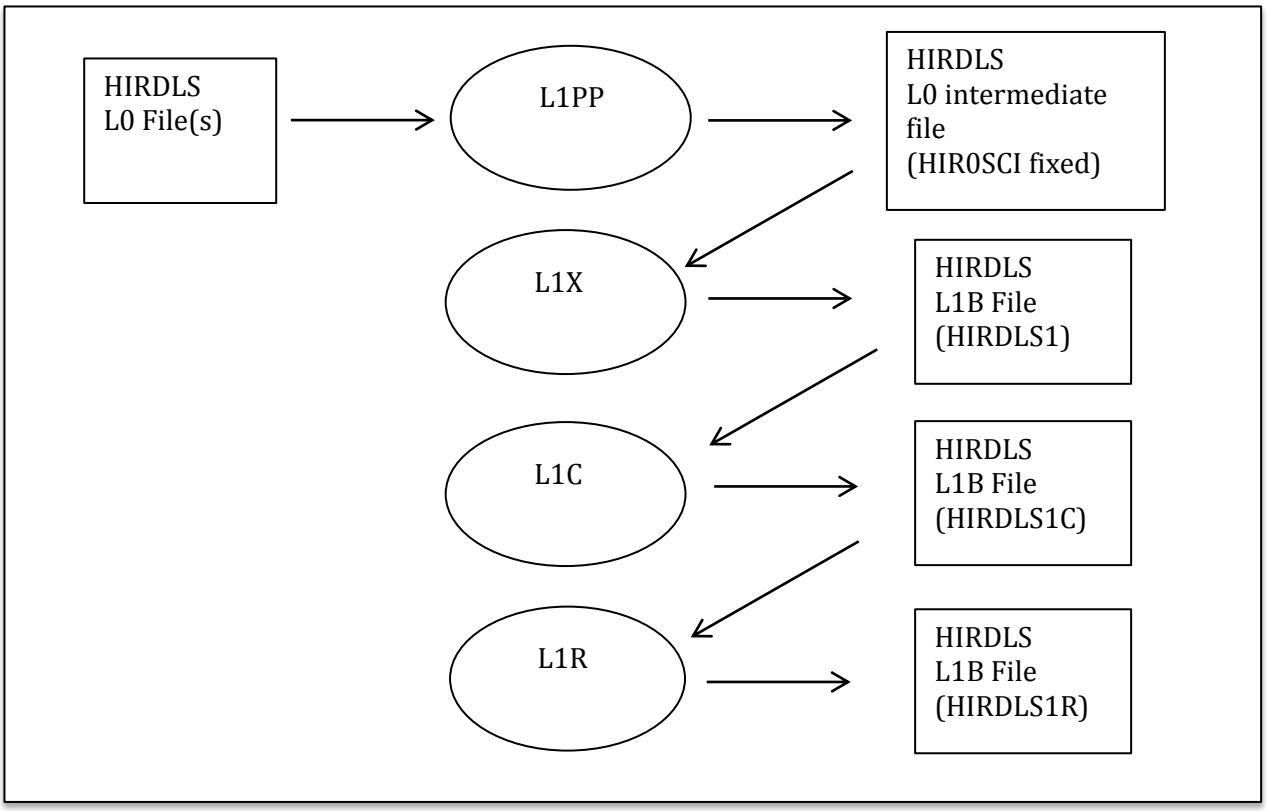

Figure 10. HIRDLS Level 1 Processing Stages

2.7.1 L1PP

The Level One Preprocessor, L1PP, corrects an anomaly in the level 0 data packets, where the spacecraft time is incorrect in a few packets per day. The anomaly and the correction are described in section 3.2.1.2, Spacecraft Time Stamp.

2.7.2 L1X

As introduced in Section 2.8, L1X's task is to generate a time-series of HIRDLS radiance data, as well as any ancillary data that is required by ESDIS or necessary for downstream processing. L1X ingests at least one HIRDLS Level 0 Production Data System (PDS) binary data file, calibrates and geo-locates the radiances contained within these PDS files, and generates an intact time-series of the data into an HDF-EOS file nicknamed HIRDLS1, as shown in Figure 10. HDF-EOS is a file format that up-scales the Hierarchical Data Format (HDF) file type with EOS extensions. Section 3 of this document further details the workings of L1X.

2.7.3 L1C

As introduced in Section 2.8, L1C's task is to correct the time-series of HIRDLS radiance data. L1C ingests one HIRDLS1 file (see Section 2.8.1 for introduction), corrects the radiances within, and generates an exact duplicate of the HIRDLS1 file, with the exception of the corrected radiances replacing the uncorrected radiances, into a HIRDLS1C file, which has the exact same structure as the input HIRDLS1 file, as shown in Figure 10. Section 4 of this document further details the workings of L1C.

2.7.4 L1R

As introduced in Section 2.8, L1R's task is to convert the time-series of HIRDLS data into a series of atmospheric profiles. L1R ingests one HIRDLS1C file (see Section 2.8.2 for introduction), identifies the portions of the data that contain atmospheric scans, converts the data into scans, and generates the intact sequence of atmospheric scans into an HDF-EOS file nicknamed HIRDLS1R, as shown in Figure 10. Section 5 of this document further details the workings of L1R.

3 Generating the Radiance Time Series

This section details the mechanisms employed by HIRDLS to generate an HDF-EOS file of HIRDLS calibrated and geo-located radiance time-series, and ancillary time-series, data. Included in this section are a detailed enumeration of an input Level 0 data file (including a fix for the spacecraft time anomaly), a description of HIRDLS geo-location, a description of HIRDLS radiance calibration, and an introduction to the output HDF-EOS L1B time-series data file.

3.1 Rationale for Generation

As mentioned in Section 2.8, the HIRDLS team is required by NASA to generate an HDF-EOS L1B HIRDLS radiance time-series data file for each day of the Aura mission, concurrent with HIRDLS operating within defined nominal parameters. The HIRDLS team has chosen to retain all data points in the HIRDLS stream, not just those data points that occur within the atmospheric portion of the scan. These additional data points could help diagnose component issues and help improve understanding of those same components under nominal conditions. It is also hoped that analyses of the non-atmospheric portions could illuminate the remote sensing science community regarding instrument behavior vis-à-vis optical, cooling, and motion-sensing (gyroscope) components, as inclusion of these data points in the HIRDLS standard product therefore makes these data points accessible to the public.

3.2 Input Level 0 Data

This section details the format of the Level 0 data that is input to the Level 0 to Level 1 processing software, and details the appropriate conversion algorithms for that input data. Also detailed in this section is the HIRDLS fix to the spacecraft clock anomaly that affected the time stamp of the HIRDLS Level 0 data packets.

The HIRDLS Level 1 processing system ingests two days worth of HIRDLS data acquisitions. One day of HIRDLS data acquisitions is the extent of one HIRDLS Level 0 file, so therefore two of these files are input to the system, to capture the inevitability that a HIRDLS elevation scan will cross a day boundary. The first scan of a day is considered to be the first scan that has at least one data point in that respective day. The last scan of a day is considered to be the last scan that is fully contained within that respective day. In other words, the two data files input to a HIRDLS Level 1 processing run are: 1) the Level 0 file that contains the data for the day to be processed; and 2) the Level 0 file that contains the data for the day previous to the day to be processed.

Every Level 0 data file has, of course, the exact same structure. It is possible for a Level 0 data file to be missing one packet, or more, as there are a myriad of data paths to take for each HIRDLS science packet, and one or more could be lost in those transitions from instrument to data processing center. If a HIRDLS Level 0 file has missing data, it will never be in units smaller than one science packet. When reading the rest of this section, please note that these input HIRDLS Level 0 files are binary, and therefore non-portable. This document details the format of these files on a big-endian machine. The two 8-bit octets that comprise each 16-bit word would need to be swapped to correctly access the data on a little-endian machine.

The acquisition of the HIRDLS Level 0 science data, and therefore the format of that data, is synchronized with the rotation of the optical chopper. One chopper rotation (CR) consists of data from 6 chopper cycles (CC). Each CC consists of two data samples – the photon counts on the back of the chopper blade (or, the chopper closed position), and the photon counts on the detector (or, the chopper open position). Eight CRs make up one science packet or minor frame (MiF). Eight MiFs make up one major frame (MaF). Table 7 describes the relationship between science data timing and chopper revolution. The remainder of this section details the contents and format of the HIRDLS science packet.

Name	Nominal Period (milliseconds)	Nominal Frequency (Hz)	Range (Hz)	Description
Chopper Cycle (CC)	2	500	480 - 520	Corresponds to 1 chopper tooth + gap = 1 cycle of detector signal waveform
Chopper Revolution (CR)	12	83.3	80.00 – 86.67	6 Chopper Cycles; primary telemetry sample rate; sync pulse will be generated by chopper once per revolution
Minor Frame (MiF)	96	10.4	10.000 – 10.833	8 Chopper Revolutions; 1 science data packet is generated every Minor Frame
Major Frame (MaF)	768	1.3	1.250 – 1.354	8 Minor Frames

Table 7. Science Data Timing

3.2.1 GIRD Header

The GIRD (General Interface Requirements Document) Header, shown in Table 8, comprises the first 128 bits of the HIRDLS science data packet. The first 48 bits are considered the GIRD Primary Header, and contain the Application Process Identifier (APID), the packet sequence count, and the packet length. This data can be used to verify that this packet is indeed a HIRDLS science data packet (APID 1632), and verify that this is indeed the next packet in sequence, and verify that this packet is

the correct length (416 words). The next 80 bits are considered the GIRD Secondary Header, and contain spacecraft time stamp information (detailed in Section 3.2.1.2), the primary read head select bits (PRHS) and the secondary read head select bits (SRHS) (both of which detail the method used to acquire the azimuth and elevation encoder data) , and the radiance data sample rate (RDSR – detailed in Section 3.2.1.1).

3.2.1.1 RDSR

The Radiance Data Sample Rate (RDSR), first introduced in Section 3.2.1, encodes the rate at which radiance data is acquired. 1, 2, 3, and 6 are all valid values. An RDSR of 1 is the nominal value, and means data is acquired at the 12-millisecond rate (or once per chopper revolution). An RDSR of 2 means data is acquired twice per chopper revolution). 3 means three times per revolution, and 6 means 6 times per revolution. Since the HIRDLS science packet size is constant, a higher rate of radiance data acquisition means there is not enough room to store data for all channels, and therefore some channels' radiances are not acquired. This will be further detailed in Section 3.2.3.2.
A side effect of acquiring radiance data at different rates is that the scan mirror elevation encoder values must also be acquired at those same different rates, i.e., there must always be one elevation encoder value per radiance data sample. This will be further detailed in Section 3.2.3.3.

Word	**Bit Position**															
Octet	**First Octet**								**Second Octet**							
MSB 0	0	1	2	3	4	5	6	7	0	1	2	3	4	5	6	7
LSB 0	15	14	13	12	11	10	9	8	7	6	5	4	3	2	1	0
GIRD Primary Header																
0	V	V	V	T	H	Application Process ID (APID)										
1	S	S	Packet Sequence Count													
2	Packet Length															
	GIRD Secondary Header															
3	0	Q	R	R	R	R	R	R	1	0	1	0	1	1	1	0
4	0	S/C Leap Seconds							S/C Coarse Time bits 31-24							
5	S/C Coarse Time bits 23-16								S/C Coarse Time bits 15-8							
6	S/C Coarse Time bits 7-0								S/C Fine Time bits 15-8							
7	S/C Fine Time bits 7-0								PRHS		SRHS		0	RDSR		

Table 8. GIRD Header

3.2.1.2 Spacecraft Time Stamp

The spacecraft time stamp, which is the number of seconds passed since Jan 1, 1958 (TAI58) is derived by adding the 24-bit coarse time field with a refactored 16-bit fine time field, via the below equation.

$$time_{spacecraft} = time_{coarse} + (\frac{time_{fine}}{65536}) \qquad (1)$$

However, a bug was found that affected the spacecraft coarse time field, whereby the coarse time occasionally fails to advance correctly. Though the problem is in the spacecraft flight software, a fix to the flight software was deemed too risky, and therefore each Aura instrument team was tasked to implement their own bug fix. The exact nature of the anomaly to fix is that a few times per day, the spacecraft time is in error by exactly one second less than the correct time. The remainder of this section details the anomaly and the HIRDLS fix.

The spacecraft time is a 48-bit field in the header of the science packet. The first 32 bits are the coarse time, in integral seconds. The remaining 16 bits are the fractional part, as a binary fraction. The spacecraft time is provided to the HIRDLS instrument by the Aura spacecraft. The HIRDLS timestamp is an independent 64-bit counter, recording the time from an arbitrary starting point in units of 2.032520325 microseconds. The rollover bug occurs whenever the fractional part of the spacecraft time is exactly zero, something that may happen a few times a day. When the fractional part of the spacecraft time is zero, the integral part will be one second less than it should be. That is, the integral part fails to advance, or "roll over" to the next value until the following packet. There will be a single packet with a spacecraft time that is exactly one second less than it should be. The following sequence illustrates the situation when the coarse time fails to advance correctly. Normally, the spacecraft time will advance by 0.096 seconds for each packet.

100.808
100.904
100.000 ← note error here
101.096
101.192

The third value in this sequence illustrates the bug: the integral part fails to advance when it should.

The EOS Data and Operations System (EDOS) receives the Level 0 science packets and assembles them into 2-hour granules for delivery to the Goddard Space Flight Center (GSFC) Data and Information Services Center (DISC). As part of their processing, EDOS sorts the packets by spacecraft time and removes duplicate packets. Because some packets have the wrong spacecraft time, EDOS will sort them in the wrong sequence. The packets with the incorrect spacecraft time will be moved to an earlier point in the stream, about 10 packets ahead of their proper place. Thus, a few times a day, we have a packet out of sequence and with an incorrect spacecraft time.

Fortunately, the packets contain another time stamp, the HIRDLS time stamp, which is not affected by the bug. Sorting the packets by HIRDLS time restores the proper sequence and provides the information needed to identify the incorrect packets, and correct them by adding one second to the spacecraft time..

Note that packets normally arrive at an interval of 0.096 seconds, but there are situations where the interval may be longer, typically in increments of 0.012 seconds, so we may see intervals of 0.108 or 0.120 seconds between packets. Thus the correction code does not depend on an interval of exactly 0.096 seconds between packets.

The correction is implemented as a small program, the Level One Preprocessor (L1PP), which runs ahead of the L1 processor. It reads the level 0 data files and writes a file where the spacecraft time is corrected and the packets are sorted in the correct order.

3.2.2 Science Packet Header

After the GIRD Header, the Science Packet Header comprises the next 224 bits of the HIRDLS science data packet. As shown in Table 9, these bits contain the 10-bit Science Housekeeping Format Identifier (SHFI), which denotes which housekeeping block offset/conversion table to use (further detailed in Section 3.2.3.7), the 3-bit MiF index into the MaF, the MiF overall counter, the HIRDLS MiF timestamp, and the starting location in the science packet of various HIRDLS telemetry points.

The MiF index into the MaF denotes the position of this science packet (MiF) into the larger MaF. A value of 0 denotes the first MiF; a value of 7 denotes the last MiF.

The MiF overall counter is set to zero at power on (or reset), and increments once per MiF. The 32-bit field should not roll over during the mission.

The HIRDLS MiF timestamp is a 64-bit value integer value that denotes the number of seconds since HIRDLS instrument power-up, relative to the beginning of the MiF (science packet).

Each of the 8-bit telemetry block starting locations (block offsets) denotes the 16-bit word offset (block offset value x 2) into the science packet where the respective data resides. However, a block offset value of 255 (0xFF) denotes no data for that block in the science packet.

3.2.3 Science Data Block

With the GIRD Header comprising the first 8 words of the 416-word science packet, and the Science Packet Header comprising the next 14 words, the remaining 394 words comprise the Science Data Block, which itself is divided into many sub-blocks. These sub-blocks contain radiance, hardware encoder, and various other data, as first shown in Table 9. Not all of the blocks will be represented in each packet, e.g., only one elevation encoder block will be active, as will only one azimuth encoder block, and there might not be a diagnostic block. As first mentioned in Section 3.2.2, the value in the block offset fields will have either a valid offset value (which will need to be multiplied by 2 to derive the 16-bit word offset), or a value of 255 (0xFF) to denote the block is not active. Each of the different types of blocks is discussed further in this section.

Word	Bit Position															
	15	14	13	12	11	10	9	8	7	6	5	4	3	2	1	0
0	Science Housekeeping Format Identifier										Telemetry Pattern			MiF Subcom 0-7, 0=MaF		
1	HIRDLS Minor Frame Counter, Bits 31-16															
2	HIRDLS Minor Frame Counter, Bits 15-0															
3	HIRDLS Timestamp at Beginning of MiF, Bits 63-48															
4	HIRDLS Timestamp at Beginning of MiF, Bits 47-32															
5	HIRDLS Timestamp at Beginning of MiF, Bits 31-16															
6	HIRDLS Timestamp at Beginning of MiF, Bits 15-0															
7	HIRDLS Timestamp Block Offset								Radiance Data Block Offset							
8	Primary Elev Var Encoder Block Offset								Primary Elev 2 Encoder Block Offset							
9	Primary Az Encoder Block Offset								Gyro 0 Data Block Offset							
10	Gyro 1 Data Block Offset								Gyro 2 Data Block Offset							
11	Gyro 3 Data Block Offset								Secondary Elev Var Encoder Block Offset							
12	Secondary Elev 2 Encoder Block Offset								Science Housekeeping Block Offset							
13	Diagnostic Block Offset								Secondary Az Encoder Block Offset							

Table 9. Science Packet Header

3.2.3.1 HIRDLS Timestamp Block

The HIRDLS Timestamp Block comprises 128 bits, and the starting location is denoted by the value of the HIRDLS Timestamp Block Offset value in the Science Packet Header, detailed in Section 3.2.2. The 8 words in this block, when combined with the HIRDLS time stamp in the Science Packet Header, detail the start of each of the 8 chopper revolutions in this MiF, as shown in Table 10.

3.2.3.2 Radiance Block

The Radiance Block comprises, at most, 2720 bits (170 16-bit words), and the starting location is denoted by the value of the Radiance Block Offset value in the Science Packet Header, detailed in Section 3.2.2. The definition of this block allows for a varying block size, depending on the RDSR value. As expected, this block contains the on-board processed, aperture-viewing radiometric signal for all, or a subset of, the 21 detector channels. Also included is a repeat of the RDSR value, and 21 bits that denote channel inclusion (1 = included). Table 11 details the organization of this block.

As originally designed, the HIRDLS instrument is capable of sampling radiance data at a very high vertical resolution, as indicated by the RDSR value. As shown in Table 12, nominal scanning rate (RDSR of 1) samples at 83.3 Hz, with all channels sampled. Other scanning rates sample at higher frequencies, but due to packet size constraints, must limit the number of channels sampled. Once the radiance anomaly (detailed in Section 2.6) was discovered, and the HIRDLS team focused its energy

on overcoming this anomaly, it was determined that keeping the RDSR at nominal was necessary for proper correction of the radiances. No matter the RDSR, the radiance data is packed in channel-major order, meaning there are 8 "chunks" (for all 8 chopper rotations) of channel data. For RDSR of 1, the radiance data for chopper rotation A comprises the first 336 bits, chopper rotation B the next 336 bits, and so on. Each of the 336-bit chunks is organized the same, i.e., channel 1 is the first 16-bit word, channel 2 the second 16-bit word, and so on. Generating radiances from these signal values is detailed in Section 3.4.

Word	Bit Position															
	15	14	13	12	11	10	9	8	7	6	5	4	3	2	1	0
0	16 LS bits of HIRDLS Time, Start of Chopper Rev A															
1	16 LS bits of HIRDLS Time, Start of Chopper Rev B															
2	16 LS bits of HIRDLS Time, Start of Chopper Rev C															
3	16 LS bits of HIRDLS Time, Start of Chopper Rev D															
4	16 LS bits of HIRDLS Time, Start of Chopper Rev E															
5	16 LS bits of HIRDLS Time, Start of Chopper Rev F															
6	16 LS bits of HIRDLS Time, Start of Chopper Rev G															
7	16 LS bits of HIRDLS Time, Start of Chopper Rev H															

Table 10. HIRDLS Timestamp Block

Word	Bit Position															
	15	14	13	12	11	10	9	8	7	6	5	4	3	2	1	0
0	Data Quality Flags								RDSR			Radiance Channel 17-21 Select bit 0= Channel 17 bit 4= Channel 21				
1	Radiance Channel 1-16 Select bit 0= Channel 1 ... Bit 15= channel 16															
2-N	Radiance Data N= ((Number of Radiance Channels Selected)*(8CR/MiF)* RDSR) + 1															

Table 11. Radiance Block

RDSR value	No. of Channels Sampled	Samples/sec (with CR = 83.3 Hz)	Bits per Science pkt	Words per Science pkt
1	All 21	1 per Chopper Rev (nom 83.3 Hz)	2688	168
2	Any 10	2 per Chopper Rev (nom 167 Hz)	2560	160
3	Any 7	3 per Chopper Rev (nom 250 Hz)	2688	168
6	Any 3	6 per Chopper Rev (nom 500 Hz)	2304	144

Table 12. RDSR Sampling

3.2.3.3 Elevation Block

The Elevation Block comprises 192 bits, and the starting location is denoted by the value in one of the four different elevation blocks listed in the Science Packet Header. This could be the Primary Elevation Variable Encoder Block Offset, the Primary Elevation 2 Encoder Block Offset, the Secondary Elevation Variable Encoder Block, or the Secondary Elevation 2 Encoder Block. Only one of these blocks will be in use at a time, and which to use can be determined by inspecting all four offsets, and using the one that does not have a 0xFF value (as mentioned in Section 3.2.3).

The Elevation Block, like the Radiance Block described in Section 3.2.3.2, was defined to allow a block size that varied with RDSR. Since an RDSR of 1 will be the only value used, only that corresponding block definition will be detailed here. The data included in this block represents the elevation encoder value corresponding to the commanded scan mirror Y-axis position, for all eight chopper revolutions in the MiF. The 12 words that comprise this block are detailed further in Table 13. The conversion algorithm from encoder bits to shaft angle degrees is as follows, with OFFSET = 0x9281D and CONVERTER = 4.287e-6:

For CR = 1(A) to 8(H), θ_{CR} = ((unpacked 20-bit encoder value) – OFFSET) x CONVERTER (2)

3.2.3.4 Azimuth Block

The Azimuth Block comprises 192 bits, and the starting location is denoted by the value in one of the two different azimuth blocks listed in the Science Packet Header. This could be the Primary Azimuth Encoder Block Offset or the Secondary Azimuth Encoder Block Offset. Only one of these blocks will be in use at a time, and which to use can be determined by inspecting both offsets, and using the one that does not have a 0xFF value (as first mentioned in Section 3.2.3).

The Azimuth Block, unlike the Elevation or Radiance Block, was not designed to vary with RDSR. Due to the Elevation Block only representing RDSR of 1, the Elevation and Azimuth Blocks have the same definition, but with the Azimuth Block data representing the encoder values corresponding to the commanded scan mirror X-axis position. Table 13 details the 12 words that comprise both types of blocks. Equation 2 details the conversion algorithm of both blocks, but to generate azimuth angles, use an "OFFSET" of 0x77FE0 (instead of 0x9281D used for elevation angles), and use a "CONVERTER" of 6.8598e-5 (instead of 4.287e-6).

Word	Bit Position															
	15	14	13	12	11	10	9	8	7	6	5	4	3	2	1	0
0	Chopper Rev A: Encoder bits 15-0															
1	Chopper Rev B: Encoder bits 15-0															
2	Chopper Rev C: Encoder bits 15-0															
3	Chopper Rev D: Encoder bits 15-0															
4	Chopper Rev E: Encoder bits 15-0															
5	Chopper Rev F: Encoder bits 15-0															
6	Chopper Rev G: Encoder bits 15-0															
7	Chopper Rev H: Encoder bits 15-0															
8	Rev A bits 19-16				Rev B bits 19-16				Rev C bits 19-16				Rev D bits 19-16			
9	Rev E bits 19-16				Rev F bits 19-16				Rev G bits 19-16				Rev H bits 19-16			
10	Rev A Status				Rev B Status				Rev C Status				Rev D Status			
11	Rev E Status				Rev F Status				Rev G Status				Rev H Status			

Table 13. Scan Mirror Encoder Block

3.2.3.5 Gyro Block

The Gyro Block comprises 128 bits, and each of the four HIRDLS gyros has its own block, with the starting locations of each denoted by the values in the Gyro 0 Data Block Offset, the Gyro 1 Data Block Offset, the Gyro 2 Data Block Offset, and the Gyro 3 Data Block Offset. Unlike the Elevation or Azimuth Blocks, all four Gyro Blocks are used at the same time. Table 14 details the contents of the Gyro Block.

As originally designed, HIRDLS necessarily had to make use of its four gyroscopes, as the Aura spacecraft pointing requirements were insufficient for HIRDLS to generate scientifically-valid, high-resolution data. After instrument integration to the spacecraft, testing revealed that the Aura pointing system was far more accurate and stable than specified, and therefore the HIRDLS gyroscope data was not necessary for HIRDLS to meet its requirements. For brevity's sake, this version of the ATBD will not detail the conversion of the gyroscope telemetry to gyroscope rates, as that conversion process requires much more than just the gyroscope telemetry in the Gyro Blocks. Please see Section 3.5.1 of HIRDLS document SW-HIR-168 (the original HIRDLS Level 1 ATBD) for more information on gyro conversion.

3.2.3.6 Diagnostic Block

The Diagnostic Block starting location is denoted by the value in the Diagnostic Block Offset. This block can have many forms, and an enumeration of each here is beyond this document's scope. For more details, please read HIRDLS document SW-LOC-113C, The Instrument Processor Unit (IPU) Software Detailed Design Document, Section 3.5.4.

Word	Bit Position															
	15	14	13	12	11	10	9	8	7	6	5	4	3	2	1	0
0	Chopper Rev A: Gyro N Data bits 15-0															
1	Chopper Rev B: Gyro N Data bits 15-0															
2	Chopper Rev C: Gyro N Data bits 15-0															
3	Chopper Rev D: Gyro N Data bits 15-0															
4	Chopper Rev E: Gyro N Data bits 15-0															
5	Chopper Rev F: Gyro N Data bits 15-0															
6	Chopper Rev G: Gyro N Data bits 15-0															
7	Chopper Rev H: Gyro N Data bits 15-0															

Table 14. Gyro Data Block

3.2.3.7 Housekeeping Block

The Housekeeping Block starting location is denoted by the value in the Science Housekeeping Block Offset. The size and content of this engineering telemetry in this block corresponds to the value of the SHFI value, in the Science Packet Header, as introduced in Section 3.2.2. Only the block corresponding to a SHFI value of 288 will be detailed here, as any other block would not have all the housekeeping data necessary to further process the HIRDLS radiances.

Table 15 enumerates the housekeeping data that are necessary for further processing of HIRDLS data. Column 1 lists the housekeeping value's mnemonic, column 2 is its bit width, column 3 is its bitwise offset into the block, column 4 is its MiF index (more details in the next paragraph), column 5 is its conversion algorithm code (INS means no algorithm, PLY means polynomial), column 6 is its polynomial offset, column 7 is its polynomial function degree, and column 8 are its polynomial coefficients. Those housekeeping values that require polynomial conversion were measured using 500-ohm platinum resistance sensors on a 4-wire AC bridge.

The MiF index listed in column 4 in Table 15 denotes which of the eight MiFs in a Maf contain the respective value. This implies that not all housekeeping values are sampled at the radiance rate, and this is true for all of the hardware sensors of interest. It is important to note that all sensors of interest are sampled at the beginning of each MaF, i.e., every 768 milliseconds. So even though housekeeping values are commuted in different MiFs, they were sampled at the same time.

Mnemonic	Bit Width	Bitwise Offset	MiF Index	Code	Units	Offset	Degree	Coefficients
AZ_HSG_TMP_1	16	544	7	PLY	K	273.15	1	-89.677888 2.716e-3
AZ_HSG_TMP_2	16	1312	2	PLY	K	273.15	1	-89.677888 2.716e-3
CALMIR_TMP1	16	576	3	PLY	K	273.15	1	-89.677888 2.716e-3
CALMIR_TMP3	16	576	5	PLY	K	273.15	1	-89.677888 2.716e-3
CHOP_FREQ	16	832	6	PLY	Hz	0.00	4	2638.41 -1.7776 5.97025e-4 -9.99488e-8 6.67232e-12
CHOP_HSG_TMP3	16	576	2	PLY	K	273.15	2	-66.004572 1.9778575e-3 6.7933264e-10
DOOR_POT	16	464	1	PLY	Degrees	0.00	3	109.12 -0.038156 1.3056e-6 -1.0709e-11
FPA_TMP_A	16	320	0	PLY	K	0.00	3	39.654164 7.21171089e-4 -7.30690562e-9 1.62452343e-12
FPA_TMP_B	16	336	0	PLY	K	0.00	3	40.8340247 7.3162997e-4 -7.34904513e-9 1.63607918e-13
IFCBB_FRPL_TMP	16	608	0	PLY	K	273.15	1	-89.677888 2.716e-03
LNS1_WF_TMP3	16	560	4	PLY	K	273.15	2	-66.004572 1.9778575e-3 6.7933264e-10
LNS2_TMP3	16	560	7	PLY	K	273.15	2	-66.004572 1.9778575e-3 6.7933264e-10
LNSASSY_TMP1	16	592	1	PLY	K	273.15	1	-89.677888 2.716e-3
LNSASSY_TMP2	16	592	2	PLY	K	273.15	1	-89.677888 2.716e-3
M1_TMP3	16	864	0	PLY	K	273.15	2	-66.004572 1.9778575e-3 6.7933264e-10
M2_TMP2	16	576	7	PLY	K	273.15	2	-66.004572 1.9778575e-3 6.7933264e-10
OBA_PLT_TMP	16	592	4	PLY	K	273.15	1	-89.677888 2.716e-3
OBA_TMP_02	16	864	6	PLY	K	273.15	1	-89.677888 2.716e-3
OBA_TMP_06	16	880	2	PLY	K	273.15	1	-89.677888 2.716e-3
OBA_TMP_07	16	880	3	PLY	K	273.15	1	-89.677888 2.716e-3
SAIL_SHM_256	32	64	0	INS	n/a			
SAIL_SHM_264	32	224	5	INS	n/a			

Table 15. Housekeeping Data Enumeration

Mnemonic	Bit Width	Bitwise Offset	MiF Index	Code	Units	Offset	Degree	Coefficients
SM_TMP3	16	544	6	PLY	K	273.15	2	-66.004572 1.9778575e-3 6.7933264e-10
SMA_MTRING_TMP	16	592	0	PLY	K	273.15	1	-89.677888 2.716e-3
SPU_CH_01_ZERO	16	624	6	INS	counts			
SPU_CH_02_ZERO	16	624	7	INS	counts			
SPU_CH_03_ZERO	16	640	0	INS	counts			
SPU_CH_04_ZERO	16	640	1	INS	counts			
SPU_CH_05_ZERO	16	640	2	INS	counts			
SPU_CH_06_ZERO	16	640	3	INS	counts			
SPU_CH_07_ZERO	16	640	4	INS	counts			
SPU_CH_08_ZERO	16	640	5	INS	counts			
SPU_CH_09_ZERO	16	640	6	INS	counts			
SPU_CH_10_ZERO	16	640	7	INS	counts			
SPU_CH_11_ZERO	16	656	0	INS	counts			
SPU_CH_12_ZERO	16	656	1	INS	counts			
SPU_CH_13_ZERO	16	656	2	INS	counts			
SPU_CH_14_ZERO	16	656	3	INS	counts			
SPU_CH_15_ZERO	16	656	4	INS	counts			
SPU_CH_16_ZERO	16	656	5	INS	counts			
SPU_CH_17_ZERO	16	656	6	INS	counts			
SPU_CH_18_ZERO	16	656	7	INS	counts			
SPU_CH_19_ZERO	16	672	0	INS	counts			
SPU_CH_20_ZERO	16	672	1	INS	counts			
SPU_CH_21_ZERO	16	672	2	INS	counts			
SPVUMIR_TMP3	16	864	3	PLY	K	273.15	2	-66.004572 1.9778575e-3 6.7933264e-10
SSH_APL_TMP	16	454	5	PLY	K	273.15	1	-89.677888 2.716e-3
SSH_DOOR_TMP	16	1152	7	PLY	K	273.15	1	-89.677888 2.716e-3
SSH_DORMOT_TMP	16	464	4	PLY	K	273.15	1	-61.280448 3.136e-3
SSH_HWA_TMP	16	464	3	PLY	K	273.15	1	-61.280448 3.136e-3
SSH_NZSURF_TMP	16	464	7	PLY	K	273.15	1	-89.677888 2.716e-3
SSH_PZSURF_TMP	16	464	6	PLY	K	273.15	1	-89.677888 2.716e-3
SUNSEN1_TMP	16	448	6	PLY	K	273.15	3	12485.71091 -0.9382890944 2.36608e-5 -2.0e-10
SUNSEN2_TMP	16	448	6	PLY	K	273.15	3	12485.71091 -0.9382890944 2.36608e-5 -2.0e-10
SUNSEN3_TMP	16	448	6	PLY	K	273.15	3	12485.71091 -0.9382890944 2.36608e-5 -2.0e-10
TSW_CTL_INDEX	16	912	2	INS				

Table 15. Housekeeping Data Enumeration (cont.)

3.3 Geo-Location

Geo-location of HIRDLS radiometric data is necessary so that downstream processors can accurately tag the location of HIRDLS temperature and volume mixing ratio profiles. A subset of the geo-location data is also necessary for correction of the radiance anomaly effects.

Please note that atmospheric refraction due to air and water vapor are very significant for limb sounding, particularly below 30km tangent altitude. The calculations performed at Level-1 are specified not to include any correction for refraction, since it can only be adequately accounted for at Level-2. Hence geo-locations assume no refraction, i.e. are as if no atmosphere is present. Also note that the WGS84 ellipsoid model is to be used for all appropriate geo-location data retrievals.

3.3.1 Spacecraft Location

The spacecraft location data of interest to HIRDLS is the sub-spacecraft latitude and longitude, the spacecraft's height, and the spacecraft's velocity and position vectors. These data points are the most straightforward to acquire, and require only the appropriately formatted time stamp of the data point of interest. The first three data points can be obtained from calling the Science Data Processing (SDP) Toolkit routine PGS_CSC_SubSatPoint, and the vectors can be obtained by calling the SDP Toolkit routine PGS_EPH_EphemAttit. Note that the latter routine returns the vectors in the Earth-Centered Inertial (ECI) coordinate frame.

3.3.2 Field-of-View Coordinate Transformation

For every chopper rotation, an operator **L** will be generated which rotates a vector in the Telescope Reference Coordinate Frame (TRCF) entering and incident on the primary mirror to the corresponding line of sight direction in the ECI-Spacecraft (ECIS) frame incident upon the instrument. The ECIS frame is identical to the ECI frame except that it is instantaneously moving at the spacecraft velocity (the distinction is necessary to allow for aberration). Note that with the scan mirror in the nominal position and perfect geometry, the TRCF axes are parallel to the Spacecraft Reference Frame (SCRF) axes, and that all rotation matrices denoted are unit matrices. The two components of **L** are the mirror reflection operator **R** and the spacecraft quaternion **Q**, both of which are discussed further in this section. Those two matrices are multiplied together to form **L**, i.e., **L** = **QR**.

3.3.2.1 Mirror Reflection Operator

The original plan for HIRDLS was to incorporate its gyroscope data to generate more accurate pointing data than that provided by the combination of spacecraft attitude data and rigid body geometry. A set of four rate-integrated gyroscopes was mounted on the HIRDLS optical bench to continuously measure its orientation, thereby compensating for the small time-varying distortions between the optical bench and the instrument baseplate, and between the instrument baseplate and the spacecraft altitude measuring system. After Aura launch, further testing revealed the pointing data to be much better than thought, and the HIRDLS gyroscope data was not needed to generate accurate pointing information. The calculation of the mirror reflection operator **R** was then simplified to require only the data point-specific hardware angles of the scan mirror.

This calculation begins with constructing a mirror direction vector **D** that defines the direction of the mirror normal in the telescope reference frame. This is done by multiplying the azimuth directional

matrix **A** with the elevation directional matrix **E**, and then multiplying this by the –velocity unit vector **N** [-1, 0, 0], since HIRDLS looks directly out the back of the Aura spacecraft, in the –velocity direction. That gives an equation of **D** = **AEN**. The equations of **A** and **E** are below, with each taking their corresponding scan mirror hardware angle, in radians.

$$\mathbf{A} = \begin{pmatrix} \cos(rad) & -\sin(rad) & 0 \\ \sin(rad) & \cos(rad) & 0 \\ 0 & 0 & 1 \end{pmatrix} \qquad (3)$$

$$\mathbf{E} = \begin{pmatrix} \cos(rad) & 0 & \sin(rad) \\ 0 & 1 & 0 \\ -\sin(rad) & 0 & \cos(rad) \end{pmatrix} \qquad (4)$$

The next step is to use the mirror direction vector **D** to generate azimuth (yaw) **Y** and elevation (pitch) **P** reflection matrices, shown below.

$$\mathbf{Y} = \begin{pmatrix} \cos(rad) & \sin(rad) & 0 \\ -\sin(rad) & \cos(rad) & 0 \\ 0 & 0 & 1 \end{pmatrix}, \text{ with rad = atan2 (-}\mathbf{D}[2], -\mathbf{D}[1]) \qquad (5)$$

$$\mathbf{P} = \begin{pmatrix} \mathbf{D}[3] & 0 & \sin(rad) \\ 0 & 1 & 0 \\ -\sin(rad) & 0 & \mathbf{D}[3] \end{pmatrix}, \text{ with rad = } \cos^{-1}(\mathbf{D}[3]) \qquad (6)$$

The final step before generating **R** is to generate the roll reflection matrix **Z** in clockwise space. The equation for this is $\mathbf{Z} = (\mathbf{YP})^{T}\mathbf{Z_I}$, with the inverted Z space identity matrix $\mathbf{Z_I}$ show below.

$$\mathbf{Z_I} = \begin{pmatrix} 1 & 0 & 0 \\ 0 & 1 & 0 \\ 0 & 0 & -1 \end{pmatrix} \qquad (7)$$

R is now generated with the equation **R** = **YPZ**.

3.3.2.2 Spacecraft Quaternion

The initial spacecraft quaternion is obtained by calling the SDP Toolkit routine PGS_EPH_EphemAttit. The returned 4-element spacecraft to ECI rotation quaternion vector needs to be converted to a 9-element orthogonal matrix **W**, and is done so with the below listed formula, assuming the unit quaternion z = a + b*i* +c*j* + d*k* (with |z| = 1).

$$\mathbf{W} = \begin{pmatrix} a^2 + b^2 - c^2 - d^2 & 2bc - 2ad & 2bd + 2ac \\ 2bc + 2ad & a^2 - b^2 + c^2 - d^2 & 2cd - 2ab \\ 2bd - 2ac & 2cd + 2ab & a^2 - b^2 - c^2 + d^2 \end{pmatrix} \qquad (8)$$

After conversion, the matrix needs to be altered by the HIRDLS alignment cosine directional matrices in all three directions: yaw **X**, pitch **Y**, and roll **Z**, giving the final equation of the spacecraft quaternion **Q** as **Q** = **W(XYZ)**. Ideally, with no misalignment, these three cosine matrices (shown below) would have been identity matrices, but post-installation calibration determined that HIRDLS was misaligned on the spacecraft in the pitch axis and roll axis, with both axes misaligned by 4.97622e-4 radians.

$$\mathbf{X} = \begin{pmatrix} \cos(rad) & -\sin(rad) & 0 \\ \sin(rad) & \cos(rad) & 0 \\ 0 & 0 & 1 \end{pmatrix}, \text{ with rad = yaw misalignment} \qquad (9)$$

$$\mathbf{Y} = \begin{pmatrix} \cos(rad) & 0 & \sin(rad) \\ 0 & 1 & 0 \\ -\sin(rad) & 0 & \cos(rad) \end{pmatrix}, \text{ with rad = pitch misalignment} \qquad (10)$$

$$\mathbf{Z} = \begin{pmatrix} 1 & 0 & 0 \\ 0 & \cos(rad) & -\sin(rad) \\ 0 & \sin(rad) & \cos(rad) \end{pmatrix}, \text{ with rad = roll misalignment} \qquad (11)$$

3.3.3 Tangent Point Location

So that the Level 1-2 processor can re-construct the accurate tangent point location (latitude, longitude and altitude) of each of the 21 detector elements, it is necessary to include very precise information about the boresight vector and the rotation of the instrument field-of-view (IFOV) about the boresight in the Level 1 file. Further, the tangent point altitude of each detector element needs to be calculated for the Level 0-1 processor to decide if a view is a valid "space" view. Much less precision is required for this calculation. The SDP Toolkit routine PGS_CSC_GrazingRay will be used to determine the boresight tangent point and then constant altitude offsets for each row will be applied to this value. The tangent point location appropriate to each detector element will be determined using tabulated angular differences between the boresight and each detector.

Please note that the boresight tangent point will pass below the Earth surface as part of the proper operation of the instrument (in order that detector elements in the top part of the array can view the lowest part of the atmosphere). The returned geolocation will be in accord with the specification of PGS_CSC_GrazingRay, which is to return the mid point of the ray within the Earth.

3.3.4 Celestial Bodies

The moon and some bright planets and stars can enter both the atmospheric field of view of HIRDLS and also the field of view of the chopper reference port. (The orbital geometry of HIRDLS is such that contamination of the chopper reference by the moon will be a moderate frequency event.). All radiance measurements affected by celestial body contamination will be flagged as invalid. The SDP Toolkit routine PGS_CBP_body_inFOV, given the data point time stamp and rotation operator **L** (detailed in section 4.2), is the appropriate routine to determine which radiances are affected.

3.4 Radiometric Calibration

This section details the 2-point (cold target, warm target) calibration technique used by HIRDLS, and the adaptation to that technique that was made necessary by the radiance anomaly (discussed in Section 2.6). Also necessary for calibration of HIRDLS radiances is an out-of-field effect correction, and that too is detailed in this section.

3.4.1 Original Calculation

The HIRDLS flight instrument measures channel radiance L (in units of W m^{-2} sr^{-1}) emitted by the atmosphere, averaged over the spectral and instantaneous fields of view for a given HIRDLS channel:

$$L(\nu) = \int F(\nu, n)\, L_{mc}(\nu, n)\, dQ\, d\nu \qquad (12)$$

Here, $F(\nu, n)$ is the HIRDLS averaging function, which depends on the wavenumber ν of the differential bandwidth $d\nu$, and the unit vector n, which defines the direction at the entrance pupil of the differential solid angle $d\phi$. $L_{mc}(\nu, n)$ is the incident spectral radiance at the pupil of HIRDLS, with the same independent variables as those of $F(\nu, n)$. Effects from polarization are presumed to be inconsequential for a HIRDLS channel radiance measurement, and therefore are not included in (12). Certainly, the blackbody targets used in this calibration exercise were not polarized, while on-orbit spectral radiance measurements of the atmosphere, are, at most, only slightly polarized.

During calibration, a large blackbody cavity was used as a full field-of-view atmospheric target for characterizing the radiometric response of the HIRDLS flight instrument. The blackbody provided incident radiation that was spatially and spectrally uniform. This point is important because it allows for $F(\nu,n)$ in (12) to be factorized into components which describe the instrument spectral and geometric responses:

$$F(\nu, n) = F_{fov}(n)\, F_{spec}(\nu) \qquad (13)$$

Here the field-of-view function, $F_{fov}(\square)$, and the spectral response function, $F_{spec}\square\nu)$, are separately normalized to unity. The approximation in (13) allows for a separate determination of each of these functions during calibration. The absolute scaling of $F(\nu,n)$ then represents the radiometric response. During calibration, this scaling was achieved by using a full field-of-view blackbody, which provided a spatially uniform radiance target that could be imaged over the entire focal plane. Introducing the approximation in (13), the channel radiance (or measured flux) L can be represented as:

$$L = \int F_{spec}(\nu)\, B(\nu, T)\, d\nu \qquad (14)$$

Here, $B(\nu, T)$ is the Planck function at temperature T. In orbit, the HIRDLS flight instrument must convert channel signals into radiances, while also having the capability of performing an on-orbit radiometric calibration, hence, being a self-calibrating instrument. To achieve these goals, an in-flight calibrator (IFC) was used to provide a spatially uniform, thermally stable warm blackbody target. Effectively, a view to the IFC at a temperature T provides a measured flux L_{ifc}, which comes from (14), and an associated digitized signal S_{ifc}. The conversion of any atmospheric channel signal S to radiance L can thus be accomplished the following way:

$$L = L_{ifc}\, \frac{S}{S_{ifc}} \qquad (15)$$

It should be noted at this time that during calibration, a thermometric test between the IFC and the warm atmospheric blackbody (HBB) was performed, where the results showed that when $T_{ifc} = T_{hbb}$, then $S_{ifc} = S_{hbb}$, to within the radiometric noise of each channel.

Equation 4 is not yet complete for two main reasons. First, for low or moderate count levels, (15) is a good representation of the measured flux; however, as will be observed later, larger signal levels up to a value of 2^{16} (= 65536) counts, reveals a small non-linearity in the behavior of L for each channel. Because this non-linearity was predicted to be small (< 3%), a reasonable approximation for L is then:

$$L = L_{ifc} \frac{S\,(1+kS)}{S_{ifc}\,(1+kS_{ifc})} \qquad (16)$$

Here, k is the measured detector non-linearity (in units of counts^{-1}), and was solely determined from this calibration. The second point originates from the notion that the signal in HIRDLS is a chopped signal, and that the "true" radiance as perceived by the instrument is the difference between the atmospheric-view and the space-view (S_o) signals. Taking this point into account, the radiometric conversion equation is now given fully as:

$$L = L_{ifc} \frac{(S - S_o)\,(1+k\,(S - S_o))}{(S_{ifc} - S_o)\,(1+k\,(S_{ifc} - S_o))} \qquad (17)$$

When $S = S_o$ in (17), the low radiance (L_o) point in the two-point radiometric calibration algorithm is known. Thus, under the planned operating conditions the only quantity that would be needed from the pre-launch calibration would be the non-linearity parameter k. Table 16 enumerates parameter k for all 21 HIRDLS channels.

However, as was discussed in Section 2.6, a detrimental blockage problem occurred during launch, which precluded any use of the on-board IFC for calibration purposes. Furthermore, an unobstructed view outside the instrument to attain a useful S_o was also impossible. The following two subsections will detail the revised algorithms used to calibrate HIRDLS radiances.

3.4.1.1 Revised Gain Calculation

Due to the aforementioned blockage problem, HIRDLS was not able to perform an on-board determination of radiometric gain. Therefore, in-orbit radiometric conversion is done by utilizing Equation 17 in Section 3.4.1, which requires knowledge of the detector gain G determined during calibration. As with any space borne cryogenic photoconductive detector system, there is a high probability for a long term, slow degradation of the channel gains while in orbit, whether it be from the detectors, electronics, or optical degradation (*e.g.*, mirror surfaces become less reflective). To a high degree, the channel gains have not changed noticeably since launch. The following three paragraphs discuss the support of this statement. The gains used for calibration are enumerated in Table 16.

The cryogenic cooler has been operating near flawlessly since launch, and has kept the FPA (Focal Plane Array) cooled to (61.616° ± 0.002°) K. This value is nearly identical to the average FPA temperature for the 61° K pre-launch calibration data point, which was 61.632° K. Incidentally, it was determined that the difference in FPA temperature between the in-orbit and pre-launch values provide a negligible change in gain for all channels.

The time series of HIRDLS zonal mean radiances in the tropics has been continuously monitored, and appears to repeat from year to year.

The photoconductive detector substrate HgCdTe is of the same type and manufacturer that is currently being used in the Aqua Atmospheric Infrared Sounder (AIRS) instrument, and the gains of the AIRS detectors have stayed constant to 0.25% over a greater than five year period since launch.

3.4.1.2 Revised Offset Calculation

The need to establish a usable space-view signal S_o is necessary in Equation 17 in Section 3.4.1, where a channel signal in counts is converted to a radiance (in units of W m^{-2} sr^{-1}). To successfully produce a reasonable orbital space-view signal, both in-orbit and calibration data must be utilized. During normal science data taking, in-orbit or on the ground, the space-view image plane provides views of cold space through the space-view aperture. Views of this image are reflected off the backside of the chopper (closed position), transmitted to the FPA, and are differenced with its scan mirror accessible atmospheric component (chopper open) in the signal-processing unit. Of course, this space-view signal alone is not available to replace S_o in Equation 6, but it can provide useful information concerning S_o with a scan mirror viewing a cold space-view blackbody, which was the case during the pre-launch radiometric calibration.

During calibration, a liquid nitrogen target was used at the space-view aperture, and a large external blackbody fixed at ~90° K was used as a space-view reference target accessed by the scan-mirror. For various experimental conditions, a usable in-orbit S_o can be obtained by making use of scan mirror views of this cold-space blackbody target during calibration. A HIRDLS channel radiometric signal (in counts) is just the difference between the atmospheric and space-view image signals, and can be represented the following way:

$$S_o = E_o + G\left((\varepsilon_{SM} B_{SM} + \varepsilon_{M1} B_{M1}) - (\varepsilon_{CH} B_{CH} + \varepsilon_{SVA} B_{SVA})\right) \qquad (18)$$

Here, ε is a mirror emissivity and B is a blackbody-equivalent measured flux for unlike components in each optical chain, where E_o is the electronic offset, G is the gain, and the subscripts "SM," "M1," "CH," and "SVA" refer to the scan mirror, M1 primary mirror, reflective backside of the chopper, and space-view aperture, respectively. Temperature sensors are located on, or near, each of these hardware elements. If the electronic offset, gain and mirror emissivities are known, then S_o can be computed. Emissivities were not known for these elements, but measurements were performed on the full aperture, concave calibration mirror (CM) during pre-launch calibration.

To proceed, the following assumption was made: $\varepsilon_{SM} = \varepsilon_{M1} = \varepsilon_{SVA} \equiv \varepsilon_{CM}$. This assumption seems reasonable because these surfaces are very similar to that of the CM, and therefore the emissivity of the CM can be substituted in for the respective emissivities in (18). The chopper backside reflective surface, however, is not similar to that of the CM, and the surface's emissivity had to be derived from calibration data, noting that this is valid due to the launch-time blockage not affecting the chopper area. ε_{CH} was derived from four different calibration data sets, and the error in ε_{CH} was computed, via a typical 24-hour portion of in-orbit data, to be about the level of the radiometric noise. Table 16 enumerates both ε_{CM} and ε_{CH} for all 21 HIRDLS channels.

Channel	k	G	ε_{CM}	ε_{CH}
1	3.748e-8	5.1057e-5	0.0109	0.0182
2	4.527e-7	4.2801e-5	0.0109	0.0164
3	8.253 e-7	6.8616e-5	0.0109	0.0149
4	6.749 e-7	6.6753e-5	0.0110	0.0140
5	6.718 e-7	7.4500e-5	0.0110	0.0136
6	2.989 e-7	4.9818e-5	0.0115	0.0099
7	5.196 e-7	5.2129e-5	0.0115	0.0111
8	1.556 e-6	1.1402e-5	0.0114	0.0086
9	4.491 e-7	4.6018e-5	0.0116	0.0070
10	6.385 e-7	3.7341e-5	0.0117	0.0054
11	8.846 e-7	6.1680e-5	0.0117	0.0053
12	5.503 e-7	3.0953e-5	0.0119	0.0051
13	8.598 e-7	2.4334e-5	0.0120	0.0048
14	1.125 e-7	3.3064e-5	0.0120	0.0050
15	5.719 e-7	2.4676e-5	0.0121	0.0052
16	6.378 e-7	2.1001e-5	0.0121	0.0057
17	1.074 e-6	3.4070e-5	0.0120	0.0101
18	2.972 e-7	3.4730e-5	0.0122	0.0163
19	1.939 e-7	1.0360e-5	0.0123	0.0164
20	4.395 e-7	5.8477e-5	0.0123	0.0171
21	2.819 e-7	2.1008e-5	0.0125	0.0179

Table 16. Radiometric Calibration Parameters

3.4.2 Out-of-Field Correction

Field-of-view measurements made during HIRDLS calibration determined that some of the 21 channels are affected by incident radiation, whose source is a reflection of incoming radiation off a channel adjacent in the focal plane. Figure 11 shows the mechanism of this radiometric contamination. Radiation at channel 9's wavelength (i.e., in-field) passes through channel 9's cold filter and is blocked by channel 6's cold filter (i.e., out-of-field). However, after passing through the filter, some of channel 9's radiation reflects off the beveled edge of the detector, and again off the underside of the cold filter, and onto channel 6's detector. Fortunately, this contamination can be measured, and therefore its effect can be corrected.

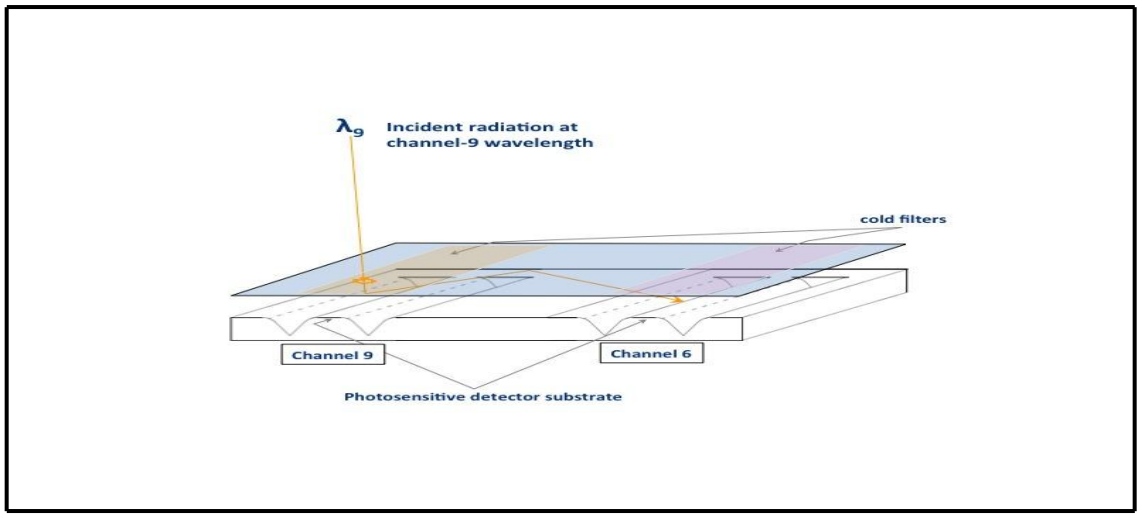

Figure 11. Out-of-Field Contamination Mechanism

Measurements of out-of-field contamination were made during instrument calibration, with an external blackbody target. These measurements determined that the total integrated counts due to any out-of-field response could be expressed as a fraction of the total integrated counts of the in-field response. Of the 21 x 20 sets of measurements taken (each of the 21 channels' effect on the other 20 channels), those channel pairs that had an out-of-field contribution of over 1 noise-equivalent radiance of the affected channel, when compared to a model atmosphere, were considered important and needing correction. Table 17 enumerates those channel pairs and the weighting of the out-of-field contribution. The correction applied to the affected channels is to remove, from every data point in the affected channel, a portion of the contributing channel's simultaneous signal, as specified by the weighting. This is expressed via the following equation:

$$S_{affected} = S_{affected} - (W\, S_{contributing}) \qquad (19)$$

As listed in Table 17, the radiances in channel 4 are affected by radiances from channels 3 and 5, and therefore both of these channels' effects must be removed.

Affected Channel	***Contributing Channel***	***Weight***
2	3	.001604
3	4	.000648
4	3	.001713
4	5	.002606
5	4	.000929
6	9	.003173
7	8	.003728
10	11	.000871
12	11	.001168
15	14	.001758
19	18	.004456
19	20	.005246

Table 17. Out-of-Field Channel Pairs and Weightings

3.4.3 Error Estimation

As originally designed, the independent variables that go into the calculation of radiance R are the measured signal S, the space-view (offset) signal S_0, the IFC (gain) signal S_B, and the IFC radiance V, expressed as:

$$R = V \frac{S - S_0}{S_B - S_0} \qquad (20)$$

Giving partial derivatives:

$$\frac{\partial R}{\partial S} = \frac{V}{S_B - S_0} \qquad (21)$$

$$\frac{\partial R}{\partial S_0} = \frac{R - V}{S_B - S_0} \qquad (22)$$

$$\frac{\partial R}{\partial S_B} = \frac{-R}{S_B - S_0} \qquad (23)$$

$$\frac{\partial R}{\partial V} = \frac{R}{V} \qquad (24)$$

And an error variance of the calibrated radiances sR^2 of:

$$sR^2 = \frac{V^2 s^2 + s0^2 (R - V)^2 + R^2 sB^2}{(S_B - S_0)^2 + \frac{R^2 sV^2}{V^2}} \qquad (25)$$

where s^2, $s0^2$, sB^2 and sV^2 are the error variances of S, S_0, S_B and V, respectively. Detector noise sD is monitored by examination of the differences between signals from pairs of consecutive views of the same target. The time interval between these consecutive views (12 milliseconds) is so short as to render all instrument temperatures as effectively constant. Each one difference provides a poor estimate of the variance, but by meaning many such values, the estimate improves, giving an error estimation sD^2 of:

$$sD^2 = \frac{\sum_{i=1}^{k} (S_i - S_{i+1})^2}{2k} \qquad (26)$$

Due to the radiance anomaly (discussed in Section 2.6), these error estimations were derived from space-view scans, with the scan mirror at a fixed position (i.e., not moving).

3.5 Output Level 1 Time Series Data

The HIRDLS Level 1 processing system is required to generate one output HIRDLS Level 1 data product for each calendar day in the Aura mission, excluding unforeseen events. That data product is a collection of time-series. As stated previously in this document, the radiances, scan mirror hardware angles, and geo-location values are all stored at the data acquisition rate, which generates roughly 7.2 million data points per day. Instrument temperatures are stored at their acquisition rate, which is once every eight science packets, or roughly 112,500 times per day. Other information, such as science table and orbit number, are stored at their acquisition rate, which is once per science

packet, or roughly 900,000 times per day. The exact definition of the data format of the Level 1 data product is left for discussion in the Level 1 processing system requirements document (SW-HIR-2000), and will not be duplicated here.

As intimated in the previous paragraph, the size of the output data file is considerable. Considering all that was previously mentioned, the output file contains over 100 bytes per data point, or over 720 million bytes per day. Data compression was used to lessen the final file size, which is roughly 750 Mbytes. Data product storage considerations of both input and output files are discussed further in Section 6.4.

This output Level 1 data file is not the file that is further processed by the HIRDLS Level 2 software. This file is input to the HIRDLS L1 Radiance Correction processor, which is discussed in Section 4.

4 Correcting the Radiance Time Series

This section details the mechanisms employed by HIRDLS to correct for the radiance anomaly that affected HIRDLS at launch (see Section 2.6 for more details). Included in this section are detailed discussions on the three different corrections applied, and how the output file of this processing system differs from its input file.

4.1 Rationale for Correction

As referenced previously, a catastrophic anomaly affected the HIRDLS instrument during launch, causing about 80% of the HIRDLS Earth-view aperture to be obstructed, and also causing the internal warm target in-flight calibrator to be obstructed from viewing. Via the efforts of the HIRDLS team over a span of months, it was shown that the radiometric effects of the obscuration could be characterized off-line and modeled in-flight. Certain channels, specifically the longer wave channels, could be "corrected" to a very high degree. Other channels, specifically the short wave channels, showed promise, but would require more work. NASA gave the go-ahead to the HIRDLS team to implement the correction algorithms already developed, and continue to revise the algorithms for greater efficacy.

4.2 Input Level 1 Time Series

The input to the HIRDLS Level 1 Correction Processor is the same as the output of the HIRDLS Level 1 Processor, and that is detailed in Section 3.5.

4.3 Oscillation Effect Correction

The oscillations are attributed to the material contact between the loosened Kapton® sheet and the elevation scan mirror, which sets the Kapton® into forced harmonic motion at every scan cycle. The remainder of this section provides an introduction to the correction methodology, and a detailed discussion of the characterization of the oscillation and the method used to fit the correction Eigenvectors.

4.3.1 Methodology of Correction

The main trigger point of the oscillation lies at a scan elevation of about 0.0 degrees. The amplitude of oscillations is about 0.03% of the background Kapton® radiance, or in the range of 1 to 10 times 10^{-4} watt/m^2/sr. For its characterization, the oscillation effect is isolated from the background Kapton® emission by applying a high pass filter (HPF) to observed radiance profiles (see Figure 18), expressed via the equation:

$$R_{OSC}(\theta) = HPF\{R(\theta)\} = R(\theta) - LPF\{R(\theta)\} \qquad (27)$$

The low pass filter (LPF) is a moving average triangular filter with a period of 87 samples with a fixed sampling rate of 83.3 samples/sec. The high pass filter separates the high spatial frequencies of the oscillation effect from the low spatial frequencies of the background Kapton® emission, collecting radiance features with length scales ≤44 samples or limb height scales ≤ 9 km, assuming a scan speed of 0.1554 degrees/sec for scan table 23 (see Section 2.7.2.4) and a limb geometric factor of about 54 km/deg. For reference, a scan elevation angle of 0.1 degrees translates into ~11 km at the atmospheric limb, taking into account a factor of two in the conversion from scan mirror angle to LOS angle.

Figure 12 shows, in the left-most column, an orbit's worth of radiances for channel 18, segregated by scan direction (up and down), during a spacecraft pitch-down maneuver (and therefore an instrument pitch-up maneuver). The middle column shows the high-pass filtered oscillations before the correction, while the right-most column shows the high-pass filtered oscillations after the correction. As opposed to simply smoothing the observed radiance profiles, the de-oscillation method removes oscillations from the high pass filtered profiles without loss of atmospheric structure. The algorithm 1) characterizes the oscillations in pitch-up (atmosphere-free) profiles by means of eigenvectors, 2) fits those eigenvectors to channel 18 radiances over space-view windows and uses the fit coefficients to extrapolate over the atmospheric range. The fit coefficients for channel 18 are 3) scaled to other channels using inter-channel oscillation ratios. The algorithm handles all of the baseline scan tables separately, both for up-scan and down-scan modes

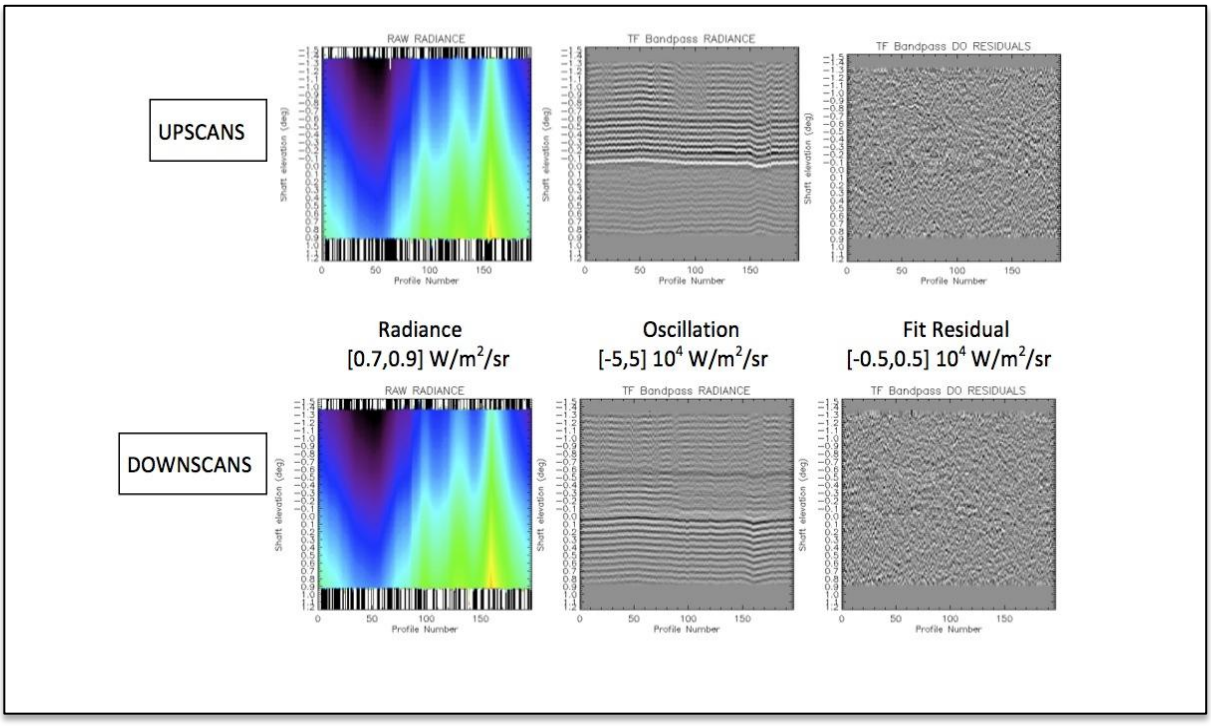

Figure 12. Observed Radiance Profiles and their Oscillation

4.3.2 Oscillation Characterization

The oscillation effect in radiance profiles has been characterized during pitch-up maneuvers using spectral methods and Singular Value Decomposition (SVD) for up-scan and down-scan modes and the different science data scan tables (23, 13 and 30). The power spectra of the pitch-up oscillation profiles show a primary oscillation beat centered about 2Hz, a secondary beat centered about 4Hz that proves stronger in down-scans, and a tertiary double beat centered about 6 Hz. Figure 13 shows the power spectra for scan table 23, channel 18 up-scans and down-scans, for six different instrument pitch-up maneuvers.

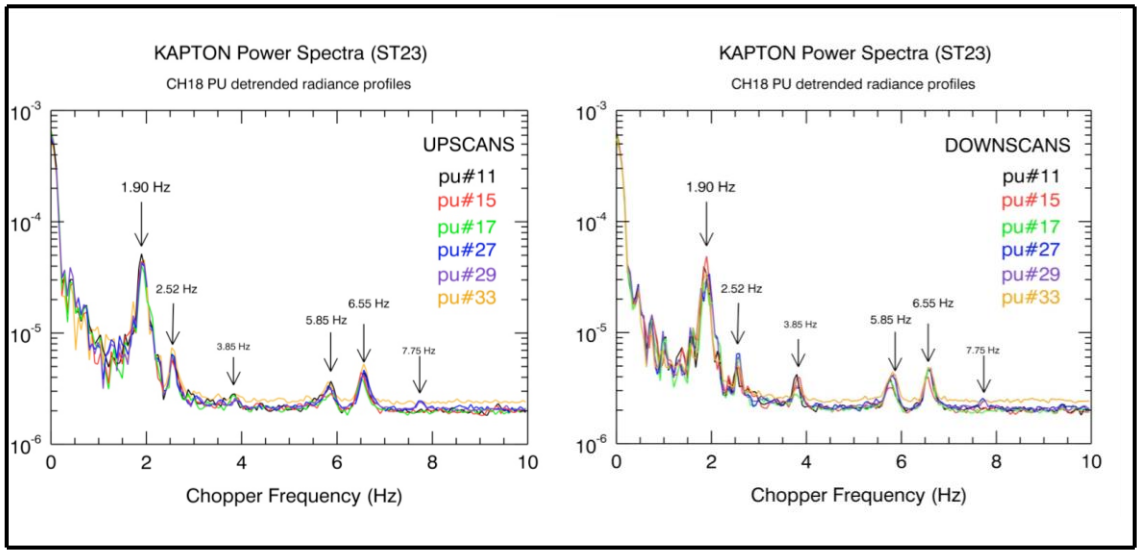

Figure 13. Channel 18 Power Spectra

A reduced number of Empirical Orthogonal Functions (EOFs or eigenvectors), those with the largest eigenvalues, are selected as representative of the main variability modes within three spatial bandpasses: 16 eigenvectors from 0 to 3.25 Hz (BP1), 2 eigenvectors from 3.25 to 4.25 Hz (BP2), and 7 eigenvectors from 5.3 to 7.2 Hz (BP3). A sample of results for scan table 23, channel 18 is shown in Figure 14. This spectrally selective procedure is effective at reducing the amount of instrument noise passed on to the predictive eigenvectors and is done separately for up-scans and down-scans, and scan tables 23, 13, and 30.

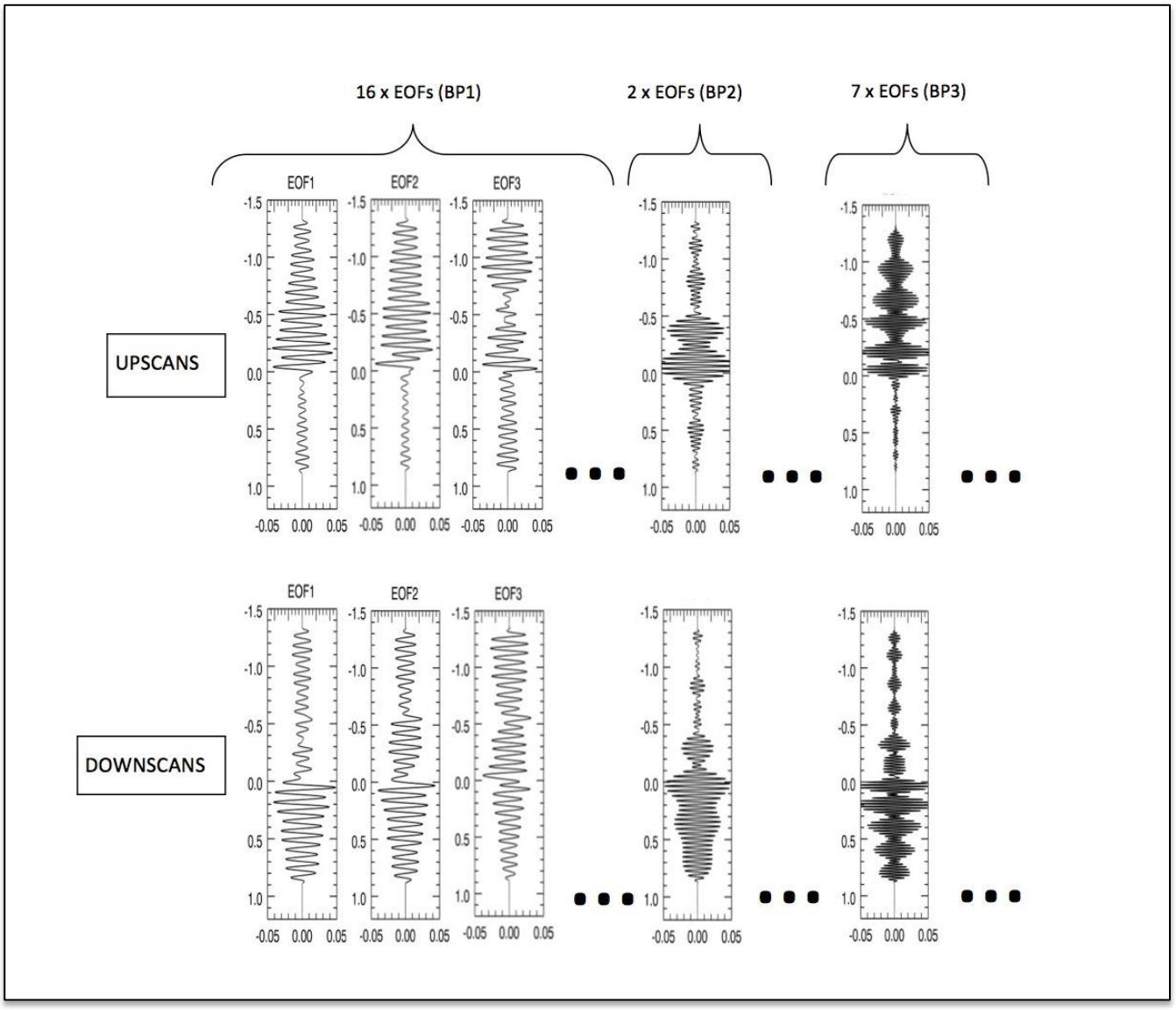

Figure 14. Channel 18 Eigenvectors for Scan Table 23

4.3.3 Eigenvector Fitting

Only the high-pass portion of the observed radiance is subject to the de-oscillation procedure. The de-oscillation operates on channel 18 because this is the channel with the largest available space view. The de-oscillation coefficients are then scaled to all the other channels using known inter-channel oscillation ratios (see Section 4.3.4). The de-oscillation algorithm fits the selected 25 eigenvectors (Y_{EOF}) to oscillation profiles (Y) over 5 adjacent regression windows above the "top of the atmosphere" (TOA) in channel 18. The scan elevation angles for the boundaries of the regression windows are shown in Figure 15. A separate full window regression from -1.0 to TOA is used to predict/extrapolate the oscillation into the atmospheric region.

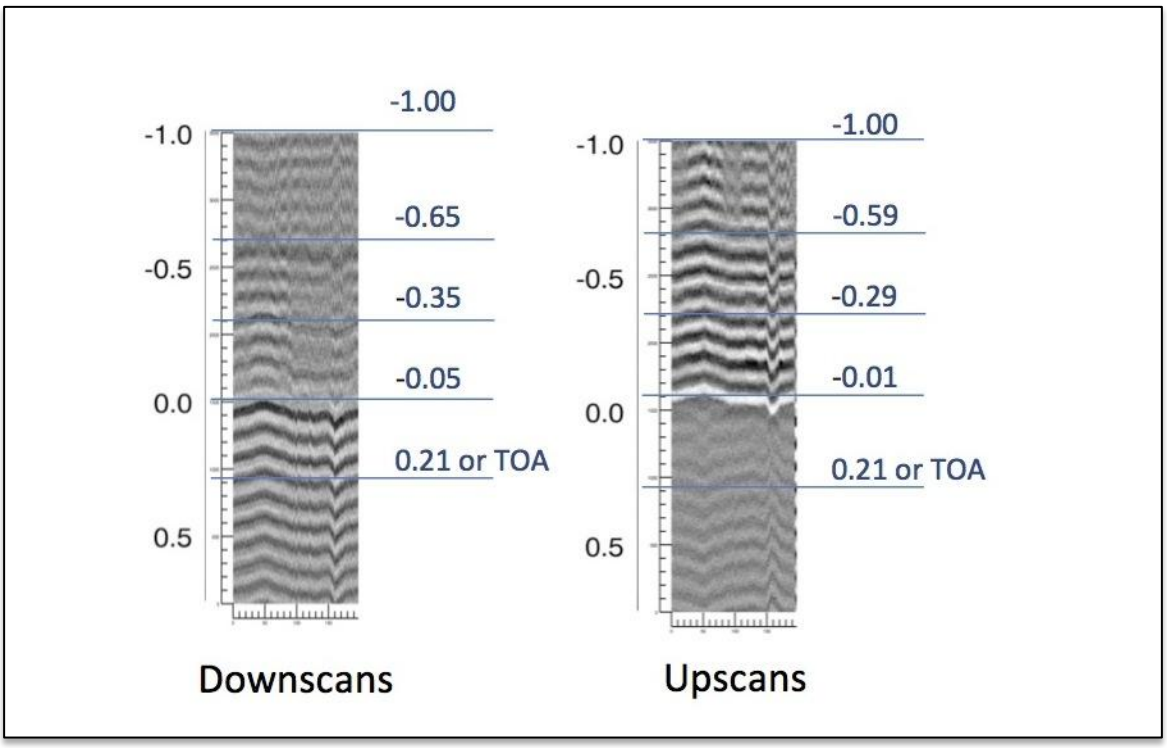

Figure 15. Scan Elevation Angle Regression Windows

To obtain the EOF coefficients (C_i) within the difference regression windows, assume:

$$Y = \sum_{i=1}^{25} C_i \cdot Y_{EOF_i} \qquad (28)$$

Then project the observed profile subsets onto orthogonalized bases of oscillation eigenvectors:

$$Y \cdot Y_{EOF_i} = \sum_j C_j Y_{EOF_j} \cdot Y_{EOF_i} = \sum_j C_j B_{ji} \qquad (29)$$

To obtain the fit coefficients:

$$C_j = \sum_j Y \cdot Y_{EOF_i} B_{ji}^{-1} \qquad (30)$$

The oscillation correction is formed as:

$$Y_c = \sum_{i=1}^{25} C_i \cdot Y_{EOF_i} \qquad (31)$$

And the fit residuals become:

$$\Delta_{osc} = Y - Y_c \qquad (32)$$

The fit residuals over the space view range are of the order of the radiometric noise. The presence of systematic errors at this stage can be only exposed after accumulating residuals from a number of adjacent profiles (e.g. using daily zonal means).

4.3.4 Scaling to Other Channels

Because the oscillation fields across channels are very highly correlated, as shown in Figure 16's comparison of channels 8 and 18, it is possible to export the oscillation correction obtained for one channel (the channel with the largest space view, i.e., channel 18) to all other channels. The scaling is effected as:

$$Y_c(\theta, channel) = Scalefactor(\theta, channel) \cdot Y_c(\theta, channel\ 18) \qquad (33)$$

The scale factor is calculated using pitch-up data as a function of channel and elevation angle. The scale factor arises from the ratio of 2Hz oscillation amplitudes relative to channel 18 and averaged over an entire orbit. The resulting scale factor profiles are shown in Figure 17.

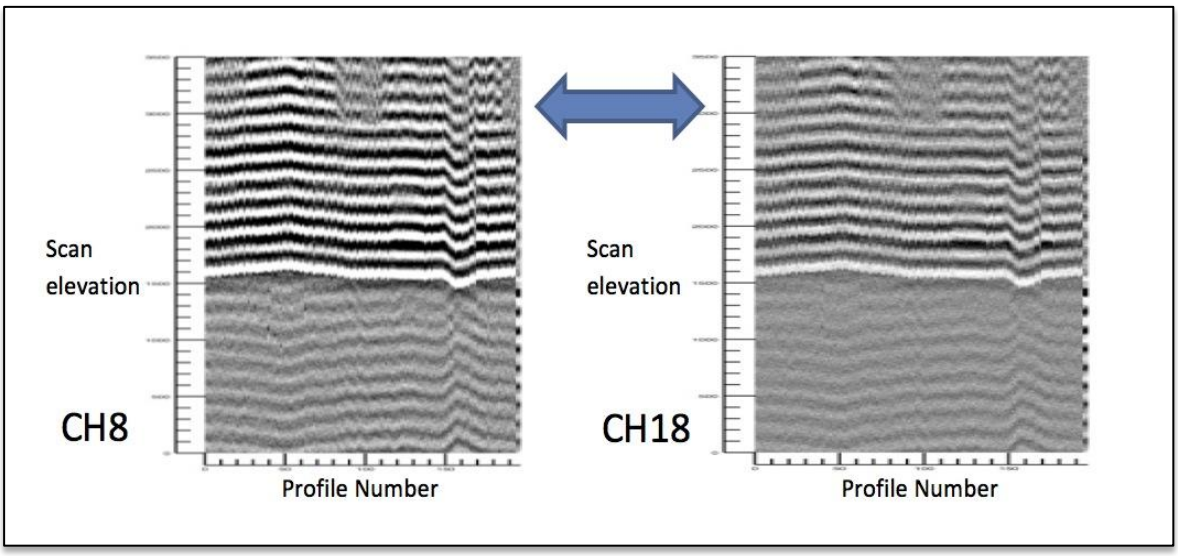

Figure 16. Oscillation Correlation

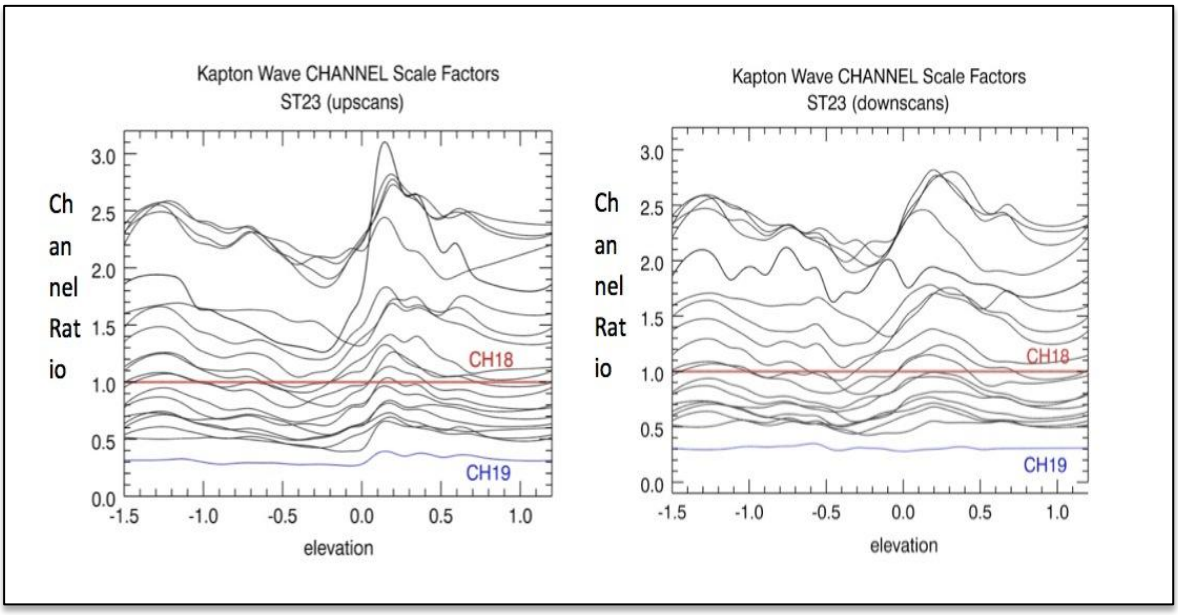

Figure 17. Oscillation Channel Scale Factors

4.4 Kapton® Emission Correction

As stated in Section 2.6, the emission from the Kapton® plastic overwhelms the atmospheric signal as measured by HIRDLS. Successful recovery requires the ability to dynamically model the Kapton emission operationally. The remainder of this section provides an introduction to the signal contribution of the Kapton®, as well as the correction methodology used to characterize the Kapton® emission during nominal HIRDLS science scanning.

4.4.1 Contribution to HIRDLS Science Scan Radiances

Each HIRDLS science limb scan contains a radiance contribution from both the Kapton obstruction and the atmosphere. Specifically, the "spaceview" portion of each scan is directed above the atmosphere and therefore measures radiance from the obstruction. In contrast, the "Earthview" portion of the scan, directed through the atmosphere, contains a signal equal to the sum of the atmospheric emission and the radiance from the obstruction, as shown in Figure 18.

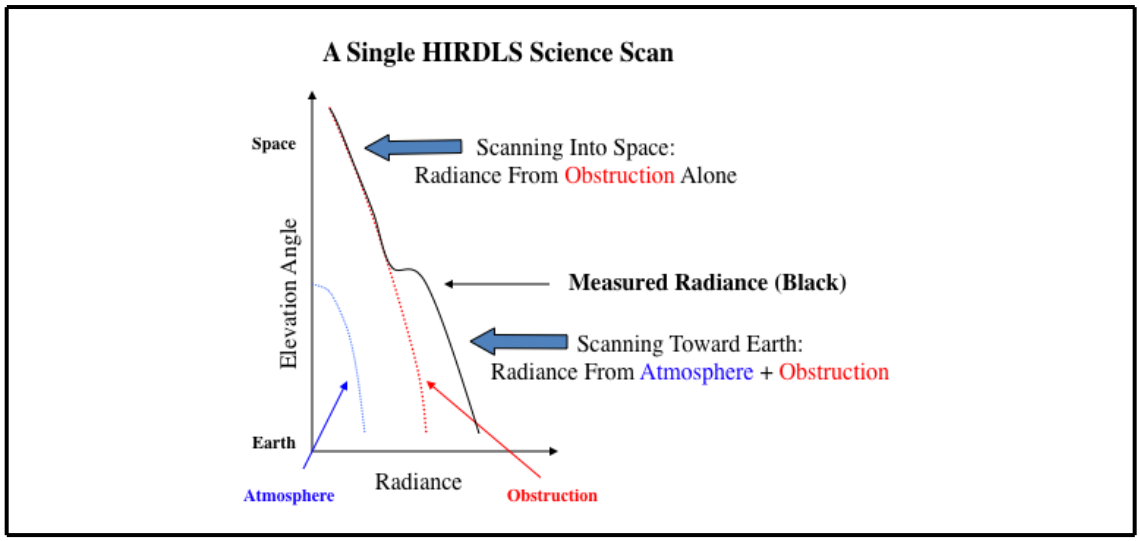

Figure 18. Scan Radiance Contributions

During an Aura pitch-down (HIRDLS pitch-up), HIRDLS elevation scans do not enter the atmosphere. The measurements obtained in this instrument configuration give a portrait of the obstruction radiance alone, as a function of time, at all elevation angles. Figure 19 shows a typical obstruction radiance measured during a pitchup, for channel 2, over a full orbit. These data are shown in two ways: as a surface plot and as individual scans.

4.4.2 Operational Modeling

The basic strategy for operationally modeling the obstruction radiance in each science scan involves two steps, and is summarized as follows: First, an offline calculation carries out an EOF decomposition of the obstruction radiance using data from a specific pitchup. A full orbit of pitchup data is used. Second, the pre-computed EOF description is used operationally to rapidly estimate the contribution of the obstruction radiance to each measured science scan. This obstruction estimate will vary from scan to scan, and will require a least-squares fit of the EOF coefficients to model this estimate. The remainder of this section describes these modeling aspects.

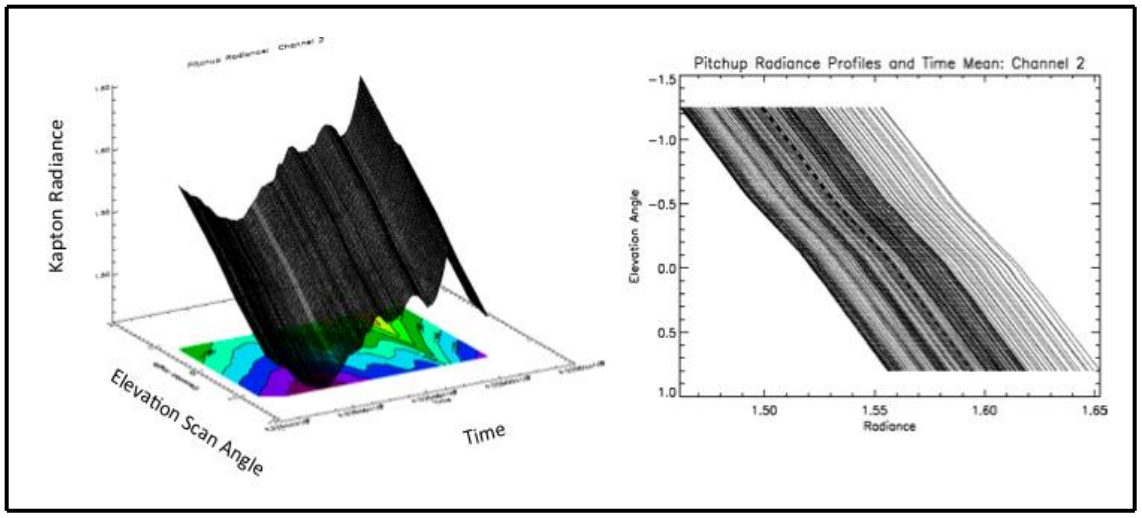

Figure 19. HIRDLS Pitch-Up Radiances

4.4.2.1 Empirical Orthogonal Functions

The EOF eigenvectors are obtained from the covariance matrix of the HIRDLS pitch-up radiances. An important numerical simplification arises from the fact that the corresponding eigenvalues of the EOF modes decrease rapidly in magnitude. Therefore, only two or three leading-order modes are needed to capture the variability of the obstruction radiance, depending on channel. Higher-order modes have variability comparable to, or smaller than, typical channel noise levels and are therefore not needed. Figure 20 shows an example of the decrease in eigenvalue magnitude for channel 2, based on a typical orbit of HIRDLS pitch-up radiance data. In this figure, the first eigenvalue is about 0.1 while the fourth eigenvalue is roughly 0.000001, five orders of magnitude smaller. The standard deviation of Mode 4 is therefore about 0.0003, comparable to the radiometric noise in Channel 2. This indicates we may safely ignore variability from modes of fourth and higher order, truncating our EOF expansions to third order. Similar calculations for the other channels indicate that three, or even two, modes can be used operationally.

As a numerical consistency and accuracy check, a given pitchup dataset can be reconstructed using the leading EOF modes derived from it. In this test, the least squares fit is done over the entire elevation range because, in this case, all elevations measure only the obstruction signal. The resulting fitting coefficients (termed "exact") are denoted $\{A_1, A_2, A_3\}$ for a third-order fit. The fitting residual is very small in these calculations, typically at least an order of magnitude smaller than the channel noise.

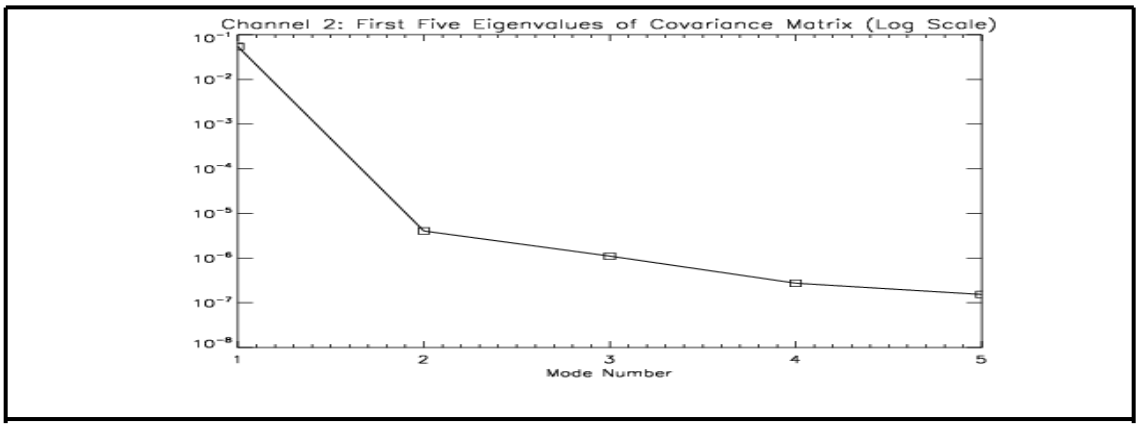

Figure 20. Channel 2 Eigenvalues of Covariance Matrix

4.4.2.2 Least-Squares Fitting Coefficients

To estimate the Kapton® emission in a science scan, we fit the eigenvectors only over the spaceview region, since this region contains the information about the obstruction. We term the resulting least-squares fitting coefficients $\{D_1, D_2\}$ or $\{D_1, D_2, D_3\}$.

Ideally, the obstruction emission is observable over a large vertical space view range, resulting in a robust regression fit. In fact, the goodness-of-fit is determined by how good the correlation is over a full orbit of profiles, between the D coefficients (Ds, fitted over the limited space view range) and the A coefficients (As, fitted over the full vertical range). The calculation of As, and hence this comparison, is only possible at HIRDLS pitch-up orientation.

During operational observations, at normal orientation, for some channels the space view, and hence the obstruction emission, is observable over a vertical range which is very limited. This vertical range is determined by the optical thickness of the emission and the position on the detector of the channel in question. For channels at the top of the detector measuring optically thick emissions such as, but not limited to, the temperature channels (2-5), the fitted Ds are sub-optimal, with the result that the Ds are not robust and correlate poorly with the optimal As (when compared during pitch-up). This can be severe enough to produce an inaccurate estimation of the Kapton obstruction emission. Indeed, for any channel, pitch-up radiance reconstructions based on the Ds have precisions that are typically five to ten times larger than reconstructions based on the As. The solution to this problem is to use scaled Ds of other channels as proxies for the poorly performing channels. The optimal channel substitution and scaling factor can be determined off-line using measured pitch-up emissions. This is done by calculating for one orbit the As for a particular channel, as well as the Ds for all channels, using their individual limited space-view ranges. One can then determine the correlation coefficient of the As with each set of Ds. Cases where substitution is deemed to be warranted are those cases where the correlation to the As is significantly higher for the Ds of another channel compared with the correlation of Ds of the channel itself. The scaling factor is determined by doing a simple linear regression of the Ds of the substitution channel to fit the As. Operationally, the substituted channels will use the scaled D coefficient of the substitution channel to calculate the obstruction emission. Figure 21 shows the effect of coefficient substitution in channel 5's $A_2 \sim D_2$ correlation.

Under no circumstances and for no channel was it found that the D coefficients corresponding to the first EOF required substitution. It was found that the D coefficients corresponding to the second EOF required substitution for several channels, especially among the temperature and ozone channels. The D coefficients corresponding to the third EOF, had they been used (they were not), would have required substitutions for most channels.

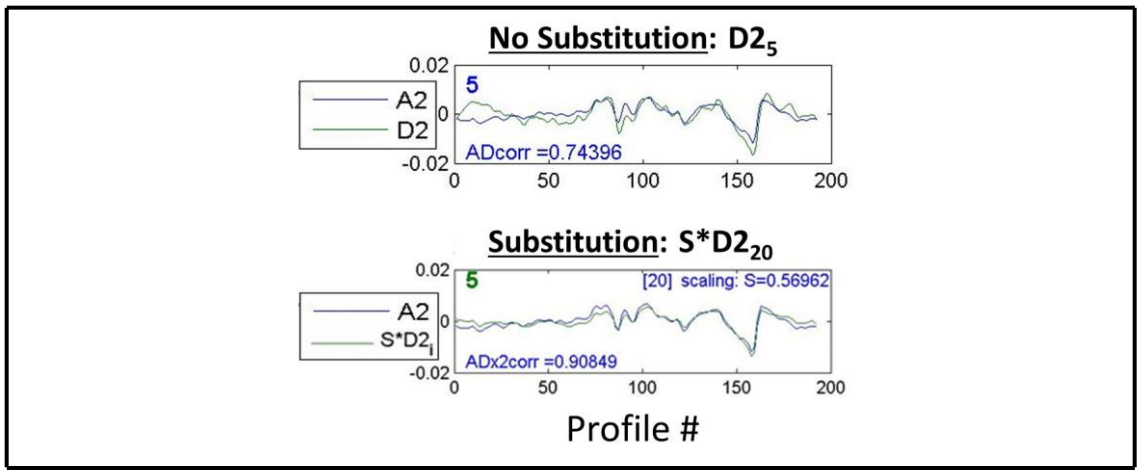

Figure 21. Channel 5 Coefficient Substitution Effect

4.4.2.3 Operational Algorithm

Kapton emission modeling is done for each of the 21 HIRDLS channels, on a per-orbit basis, and is as follows:

Calculate orbital mean of measured limb radiance, $\bar{R}(\theta)$, a function of elevation angle θ.

Rigidly translate $\bar{R}(\theta)$ to match the pitchup time-mean in the space-view. The "match" is chosen by minimizing the root mean square (RMS) spaceview difference of the two profiles. Call this translation $\overline{R_T}(\theta)$.

For each measured limb scan $R(\theta, t)$ in this orbit of data:

Compute radiance departure from the time-mean: $R_D(\theta, t) = R(\theta, t) - \bar{R}(\theta)$

Fit the spaceview radiance portion of $R_D(\theta, t)$ to the spaceview portion of the EOF eigenvectors via a linear least-squares fit. Call the fitting coefficients $\{D_1(t), D_2(t)\}$ or $\{D_1(t), D_2(t), D_3(t)\}$, depending on whether two or three fitting coefficients are computed in the given channel.

Apply the "D-substitution" algorithm described above to $D_2(t)$ or $\{D_2(t), D_3(t)\}$.

Recompute $D_1(t)$ (via the Normal Equations) to make it consistent with the modified $D_2(t)$ and/or $\{D_2(t), D_3(t)\}$

Calculate the Kapton emission correction $R_K(\theta, t)$ for the current scan, as follows:
$R_K(\theta, t) = \overline{R_T}(\theta) + D_1(t) \cdot EOF_1(\theta) + D_2(t) \cdot EOF_2(\theta) \ldots (+ D_3(t) \cdot EOF_3(\theta))$

End measured limb scan loop

4.5 Aperture Obscuration Correction

The last of the three applied radiometric corrections is the correction for the partial blockage of the view through the aperture. As stated previously, the blockage was apparent in the first observations that were made, showing much higher signals than expected from the atmosphere. Azimuthal scans at different elevation angles indicated a general shape of the blockage, covering more of the aperture at earthward angles and covering less in the space direction. This is shown conceptually in Figure 22. Correction of the radiances to what they would have been in the absence of this blockage requires that we have a quantitative estimate of the open area fraction (OAF) as a function of elevation angle for each channel. In the remainder of this section, the determination of these functions is outlined.

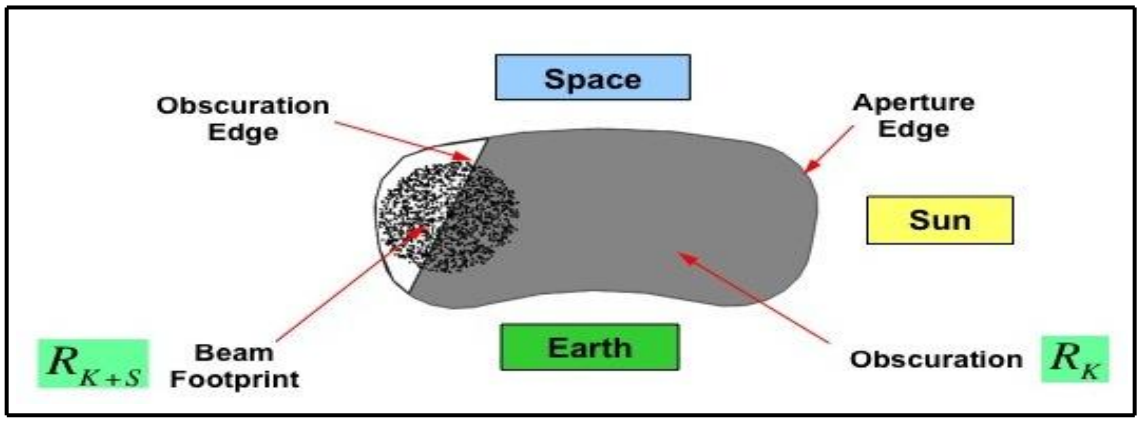

Figure 22. HIRDLS Aperture Blockage Conceptualization

4.5.1 Initial Scanning Efforts

Initial efforts to determine the blockage extent were straightforward, based on azimuth (horizontal) scanning at a number of elevation angles. As expected, the radiative signal was fairly constant when the detectors were estimated to be receiving signals from the blockage, at smaller negative azimuth angles relative to the orbital plane. As the azimuth angle became more negative, to its limit at an encoder angle of -24.5°, the radiometric signal decreased, reflecting the detectors seeing more of space or atmosphere beyond the edge of the blockage. The most straightforward approach is to locate the azimuth angle at which the signal begins to drop, and use that to estimate the OAF.

In normal orientation, the signal from beyond the blockage is space at the more spaceward lines-of-sight (LOS), but the atmosphere or earth at earthward LOS. These latter provide a variable signal that makes it very difficult to determine the OAF. For this reason the HIRDLS team requested that the Aura S/C be pitched down such that the HIRDLS LOS's were raised 5.25°, so that all detectors were viewing above the atmosphere for all elevation angles. Such pitch maneuvers were made several times during the HIRDLS mission, for up to 4 orbits.

The results of the raster scans, described above, during a pitch maneuver, showed the expected variation from channel to channel, based on their positions on the focal plane (see Figure 2, on page 6). However, because the beam feeding the detectors is not in focus at this location, it is quite large, and the point at which this beam moves off the blockage is not distinct, but is a wide, rounded curve. It was concluded that the error bars on the results were too large to provide useful final results.

4.5.2 Radiometric Modeling

It was found in the course of other studies that the variation of the signal around an orbit contained much useful information. Figure 23 shows the orbital variation for (left) Channel 8, the most covered, and (right) Channel 18, the least covered, under 2 conditions during a pitch maneuver. The red shows the variation at an elevation angle of -0.25°, viewing at an azimuth encoder angle of -14°, i.e. entirely viewing the blockage, while the green gives the variation at the same elevation angle when looking at an azimuth encoder angle of -23.5°, the standard angle for taking science data, where a combination of blockage and space is viewed. The vertical line indicates the terminator, the upper intersection with the radiometric curve is the sunset position, and the lower one the sunrise. Portions of the curve to the right of the terminator line are during S/C night. With the temperatures nearly the same for the 2 scan angles, the difference between the green and red curves tells us something about how much of the beam is not blocked, but is viewing space.

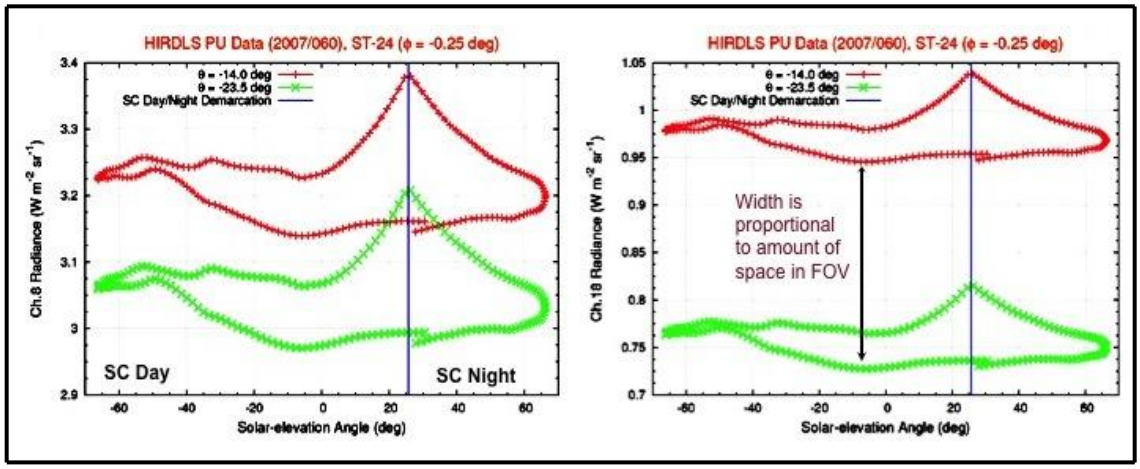

Figure 23. Orbital Radiance Variations in Channels 8 and 18

It
was found that when viewing the blockage, the signal could be estimated from a linear combination of blackbody radiances based on several temperature sensors. These included the sunshield door (SSH) temperature, whose upward temperature spike at sunset was crucial to fitting the signal at that time. Three temperatures came within a few percent of fitting the signal during the entire orbit, as given by the equation

$$R(\phi) = \sum_{i=1}^{n} \alpha_i \, B_i(\phi) \qquad (34)$$

where α_i are the fitting coefficients, and B is the vector of instrument temperature blackbody radiances. The addition of more temperature sensors did not consistently improve the ability to represent the signal. The best set of temperature sensors is: the sunshield door (SSH_DOOR), the optical bench assembly temperature (OBA_TMP) and the scan-mirror mounting ring (SM_MTRING). The sum of the fitting coefficients in (34) is within a few percent of 1, as should be. If the same fit is done for the signals at -23.5°, the sum of the fitting coefficients is < 1. The OAF is then taken as

$$OAF(-23.5°, \phi) = \sum_{i=1}^{n} \alpha_i^{Kapton} - \sum_{i=1}^{n} \alpha_i^{Kapton+space} \qquad (35)$$

More repeatable results are obtained if only the nighttime portion of the curve is used. Examples of the scans and fits are presented in Figures 24 and 25, with 24 showing the fit for Channel 8 and the scans on the Kapton® only, and 25 showing the fit at the science azimuth.

There are a number of complications, including the fact that some temperatures continued to rise for a short period after the instrument entered night time, and on occasion some showed anomalous behavior just before sunrise. It was decided to include these segments because they led to better fits to the data. Examples for the 4 corner channels are given in Figure 26, in which the red curves include all nighttime (NT) scans, and the green show the results when those scans are omitted.

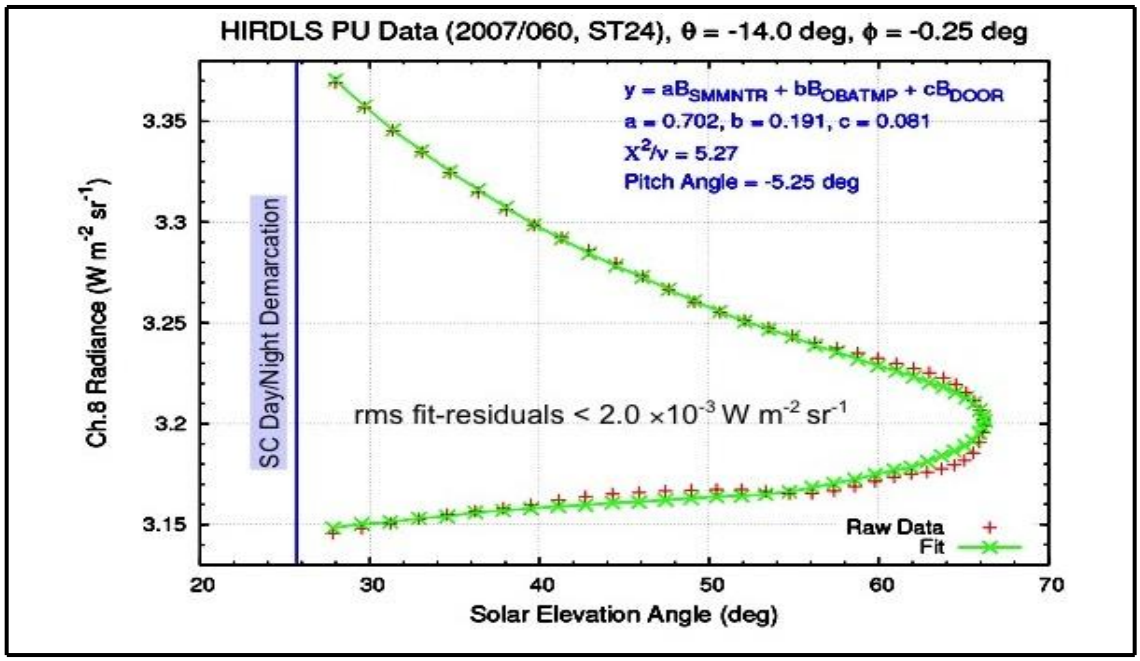

Figure 24. Channel 8 Nighttime Kapton®-Only Scans

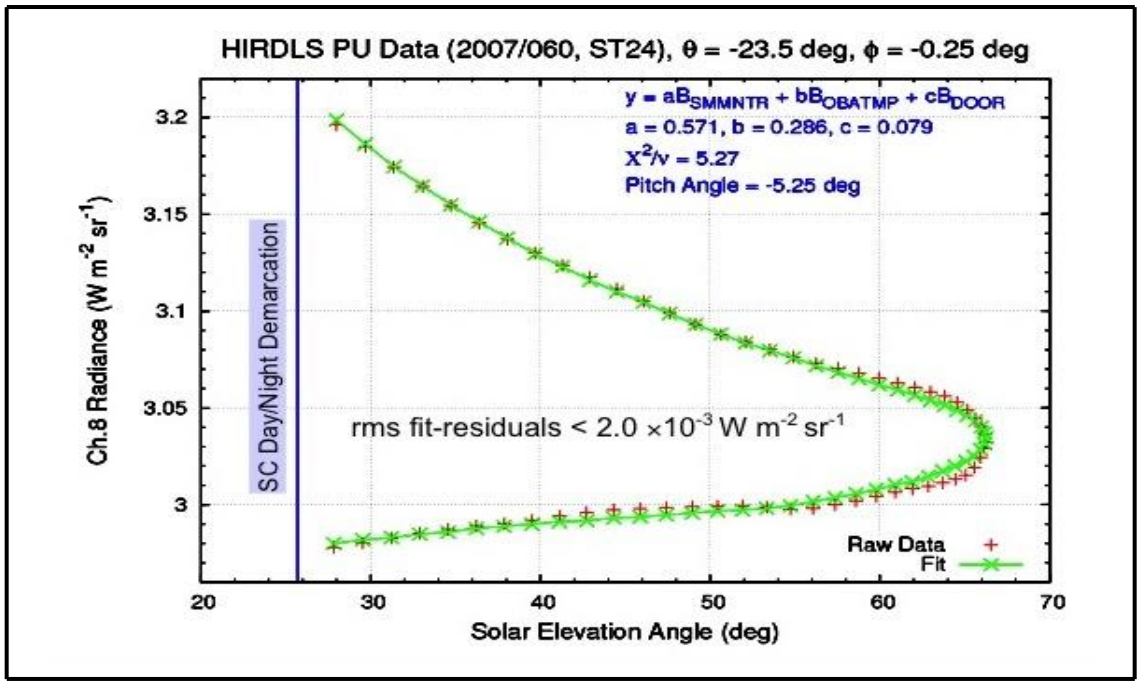

Figure 25. Channel 8 Nighttime Science Scans

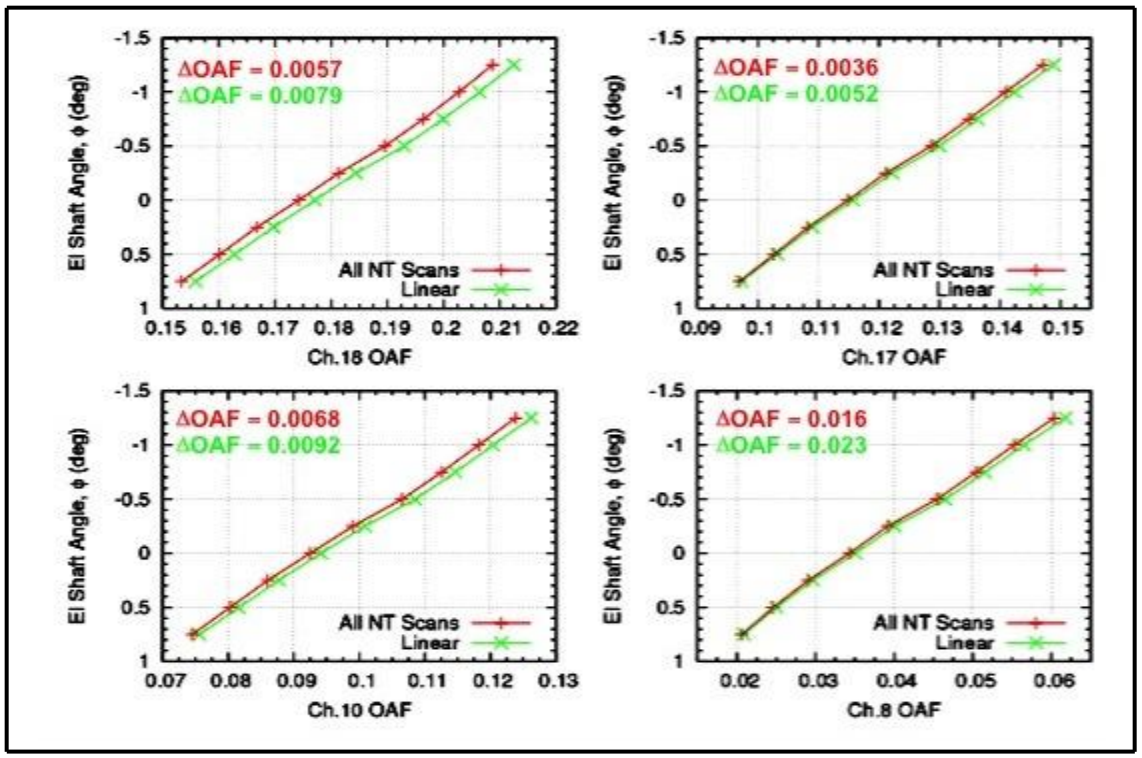

Figure 26. OAF Curves With and Without Anomalous Segments

Similarly, not all pitch maneuvers led to exactly the same results, nor did the different scan sequences. Figure 27 shows the resulting OAF curves for four sample channels, for four pitch / scan sequence scenarios. The final pitch maneuvers used were on 2007 day 060 (green) and 2007 day 310 (blue).

Finally, the scans on the blockage were fit with a first order polynomial, nullifying any influence from blockage defects in the modeling of the orbital radiances. Final results for all channels are shown in Figures 28 (leftmost column of detector array), 29 (center column) and 30 (rightmost column). Because of the possibility of systematic errors in the OAF, the capability to adjust the final radiances was added to the HIRDLS L1 Conditioning Processor (detailed in Section 5).

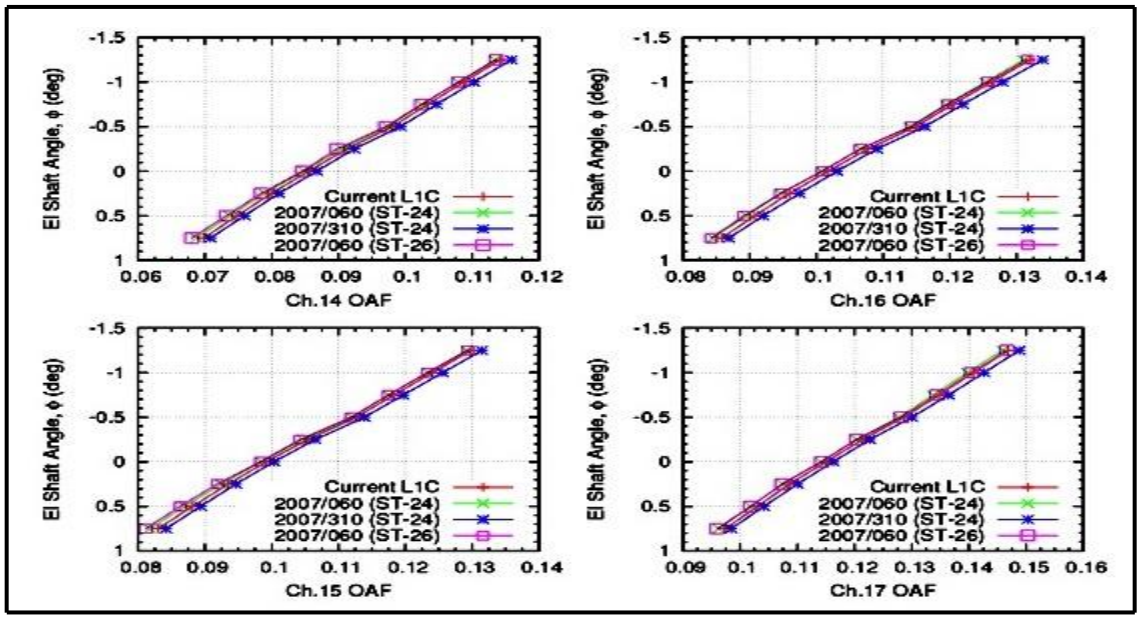

Figure 27. Four Pitch / Scan Sequence Scenario Curves

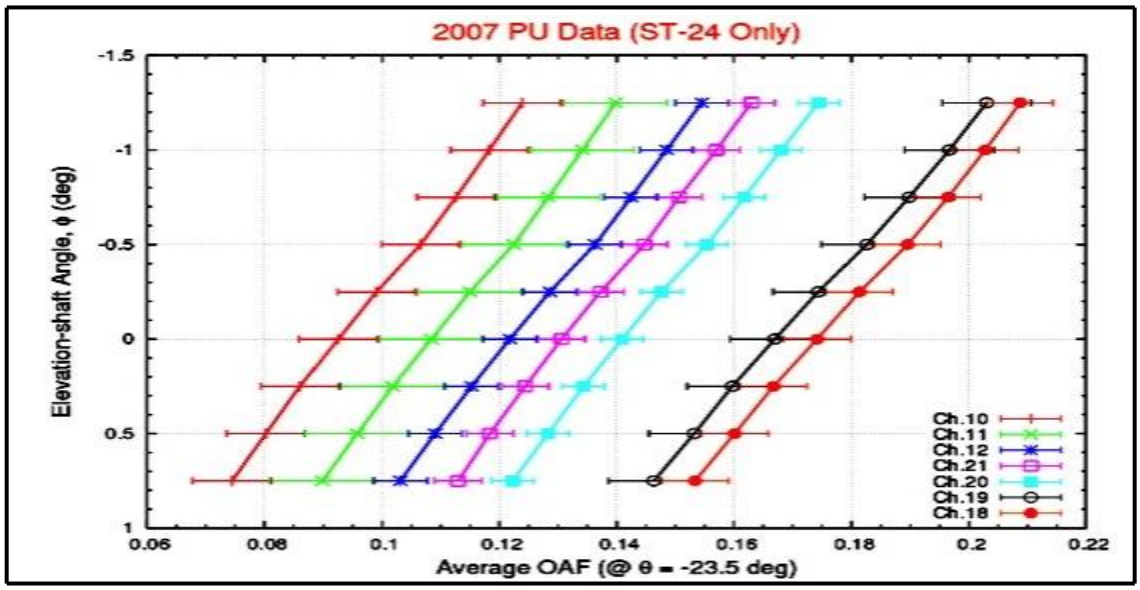

Figure 28. Left Column OAF Curves

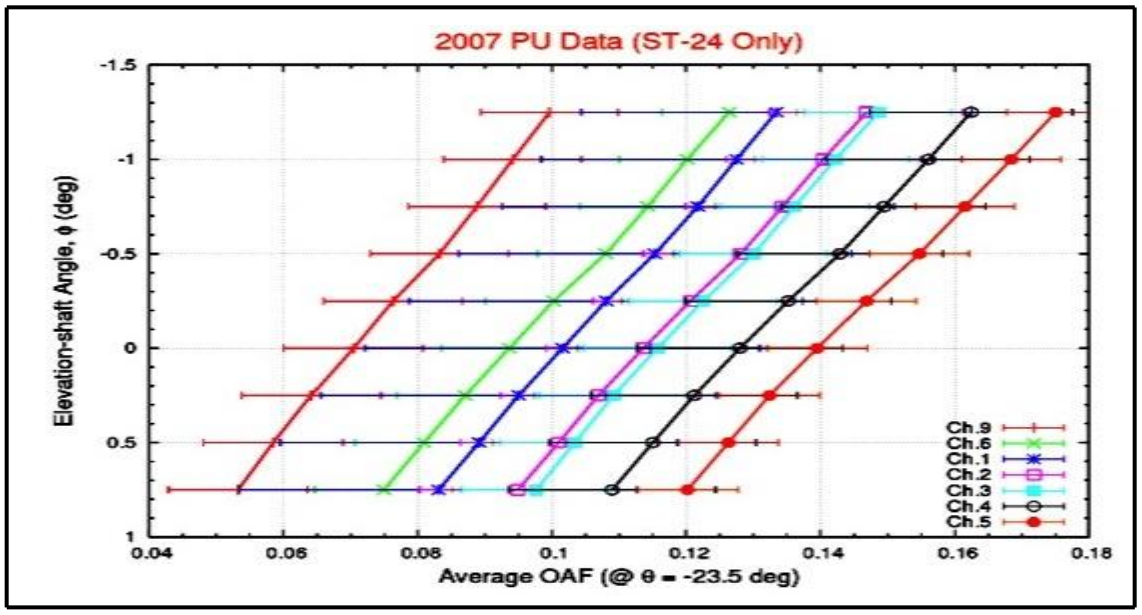

Figure 29. Center Column OAF Curves

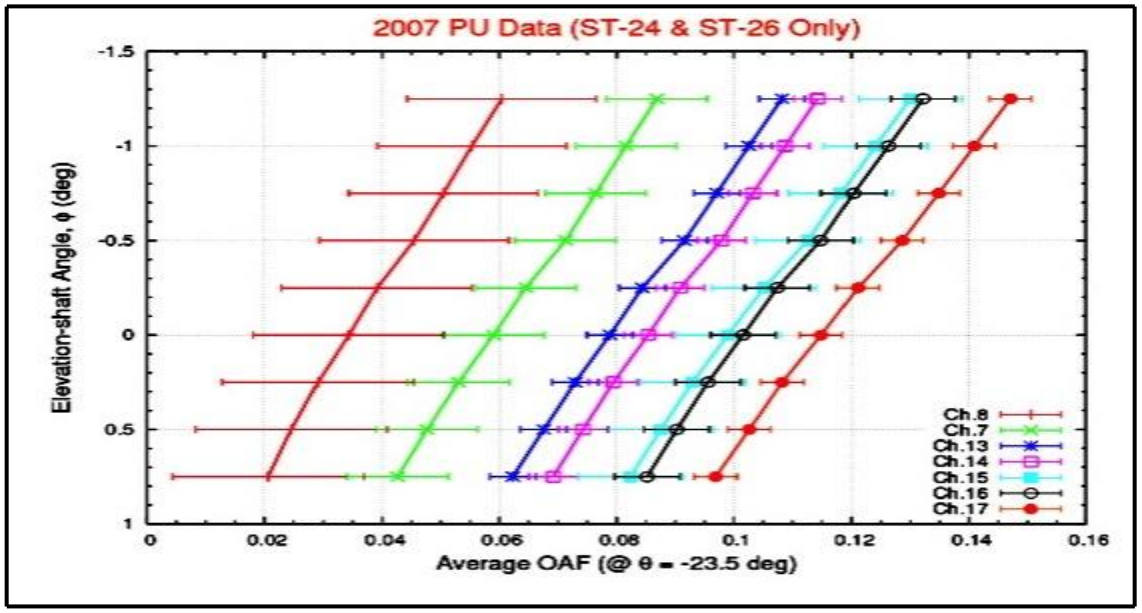

Figure 30. Right Column OAF Curves

4.6 Output Level 1 Corrected Time Series Data

The output file of the Level 1 Correction Processor is exactly the same, in format, as the input file of this processor. The data differences are limited to the fields containing radiometric information, such as the respective channels' radiance and radiance error fields, and the radiometric scale offsets and scale factors. The data differences are also limited to those data points that are sampled during

the entire extent of the nominal science scans. The Flags field could, potentially, changed during this processing step. If one of the three correction components fails to work correctly during a science scan, that scan is further removed from processing by altering the scan's Flags field values to indicate the scan is not to be further processed.

5 Converting to Atmospheric Profiles

This section details the mechanisms employed by HIRDLS to convert the Level 1 corrected time series data to atmospheric profiles, which are the input to the HIRDLS Level 1 to 2 processing system. This processing stage is known internally to HIRDLS as the Level 1 Radiance Conversion (L1R) stage. Included in this section are detailed discussions on the conversion process, including altitude alignment and radiance conditioning, and on the format of the output file.

5.1 Rationale for Conversion

HIRDLS is on contract to deliver L1B and L2 files to NASA. The generation of the L1B files is discussed in Sections 3 and 4 of this document. The generation of the L2 files is out of scope of this document, but is detailed in both the original HIRDLS L2 ATBD, SW-HIR-339, and the post-launch updated HIRDLS L2 ATBD, SW-HIR-2047. The format of the L1B files is not optimal for ingestion into Level 1 to 2 processing, and therefore the HIRDLS team decided to create an "intermediate" internal file that more optimally presents HIRDLS atmospheric radiances. While the non-atmospheric radiances are of great interest to HIRDLS team members, they are not science-mode, and therefore they do not lead to atmospheric profiles of volume mixing ratios, and therefore are not to be passed to the Level 1 to 2 processing system. Another important reason to provide this intermediate step is to further condition the radiances in hardware-space (i.e., while the radiances are still aligned with hardware angles). The hardware units are intrinsic to Level 1 processing, but are not necessary for Level 2 processing, and their inclusion in L2 processing would create an unbalanced processing approach. The conditioning of the radiances includes filtering in angle-space and splining to altitude-space. These conditioning steps are discussed further in Section 5.3 and 5.4.

5.2 Input Level 1 Corrected Time Series Data

The input to the HIRDLS Level 1 Radiance Conditioning processing stage is the same as the output of the Level 1 Correction Processor, and that is detailed in Section 4.6.

5.3 Filtering Radiances

Radiance filtering is the first step in the HIRDLS L1 Radiance Conditioning processor. The goal of this step is the remove the spatial response from the measured limb radiance profile, and the process requires knowledge of HIRDLS hardware space. This "deconvolution" step can be implemented efficiently using a Fast Fourier Transform (FFT) technique, but first the measured limb radiances must be reformed onto a uniform hardware-space grid. The scan-specific hardware angles must be retained though, because the filtered radiances must then be reformed back onto their original scan-specific angles. The reforming, both before and after the FFT, are to be done with splines.

5.3.1 Splining to Uniform Grid

As mentioned in the previous section, all scan filtering is done on a common, uniform grid. Grid spacing and extent is designed to mimic the spacing of the most common scan table (ST 23), yet capably represent all other scan tables. With that in mind, the grid Δ is 0.0018647°, and the extent is -1.51° to 1.51°. A cubic spline is to be used to reform scan radiances onto this grid before FFT deconvolution, and then back to the original grid after FFT deconvolution.

5.3.2 Fast Fourier Transform

A Fast Fourier Transform (FFT) has been chosen to perform a deconvolution of the FOV response with the measured limb radiances. This section discusses background history of convolution and deconvolution principles, and an introduction to both methodologies, as well as HIRDLS-specific applicability of the FFT.

5.3.2.1 Background

The effect of instrument spatial response on the information content of measured limb radiances has been discuss previously by Gille and Bailey (1978) and Peckham (1995). Removing the spatial response from the measured limb radiance profile by a deconvolution process before inversion has the potential advantage of computational efficiency and has been successfully used on previous limb experiments [*Bailey and Gille* (1986)]. The deconvolution can be implemented efficiently using a fast Fourier transform technique and performed only once during the pre-processing step. An alternate and more direct approach is to apply the measured FOV response to simulated radiances produced by the forward model. The vertical spacing required for the convolution or deconvolution will depend upon the expected scale of vertical variations in the limb profile and small-scale variations in FOV response. A concern with inclusion of the FOV effect in the forward radiance model is the additional computational burden that may result if several iterations of the retrieval process are necessary and if fine tangent height spacing is necessary.

5.3.2.2 Convolution

Small-scale vertical features in the radiance profile, produced by variations in temperature and constituent concentrations, are smoothed by the detector FOV as it is scanned across the limb. This smoothing reduces the amplitudes of high spatial frequency components and must be carefully modeled or the effect removed to achieve the high vertical resolution requirements for HIRDLS observations.

Smoothing by the detector FOV can be expressed as a convolution of the FOV response with the limb radiance profile, assuming the FOV response is invariant with vertical scan position. This is a reasonable assumption for vertical scans near zero degrees in azimuth. Corrections for vertical scans at the extreme azimuth positions, where there may be small variations, were not made. Mathematically, the convolution integral is,

$$g(\theta) = \int_{-\infty}^{\infty} h(\theta - \xi) f(\xi)\, d\xi \qquad (36)$$

where $h(\theta)$ represents the vertical response function of a detector channel as a function of relative line-of-sight elevation angle, θ , and $f(\xi)$ is the limb radiance profile specified on the same relative angle scale.

The vertical response function is defined as the horizontally integrated spatial response of a spectral channel to incident radiation. For the HIRDLS detectors, the vertical response is determined by the finite FOV of a detector, and to a lesser extent by diffraction, aberrations and electronic response. An example of the FOV response for HIRDLS channel 10, calculated assuming a 1 km FOV for the detector and the effect of diffraction, is shown in Figure 31, as the 0° curve. Measured FOV responses are used in the following calculations.

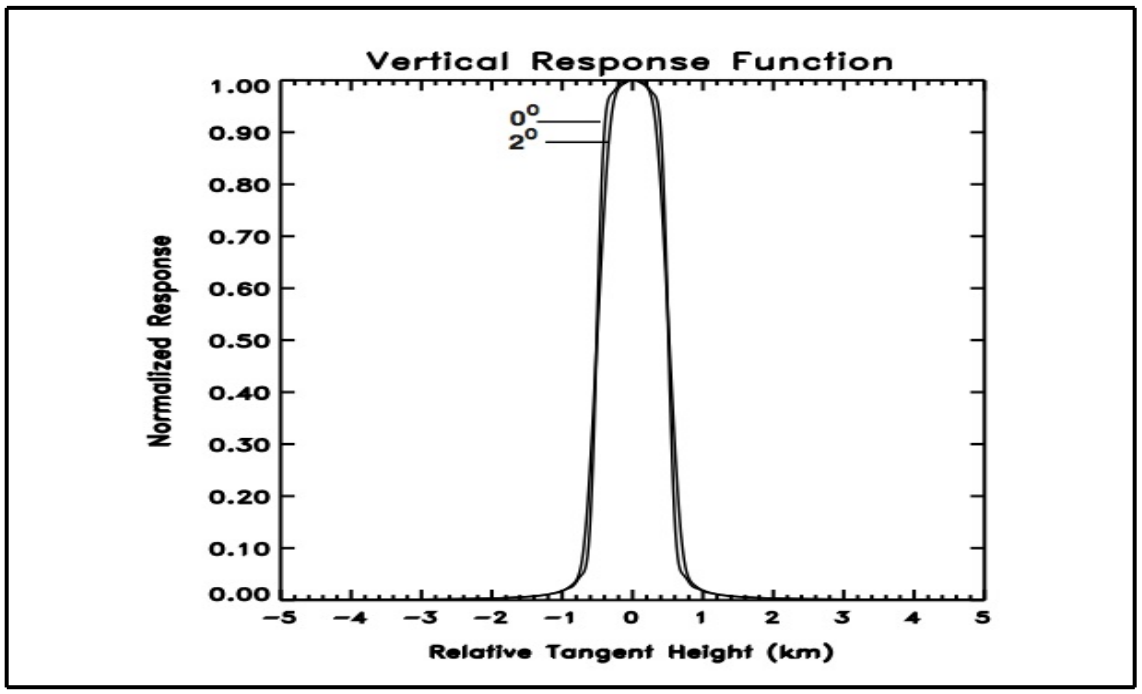

Figure 31. Channel 10 Vertical Response Function

The vertical response function is affected by a rotation of the FOV, which can be caused by spacecraft attitude (expected to be 2 degrees or less) or by the scan mirror geometry. Rotation caused by spacecraft roll will be defined by a field rotation angle calculated during Level 1 processing. The rotation due to scan mirror geometry is well characterized by $\alpha = 2\epsilon_m \, sin\phi_m$, where ϵ_m and ϕ_m are the elevation and azimuth mirror position angles, respectively. For the extreme elevation and azimuth position, a = 1.5 degrees.

The convolution integral can be equivalently expressed in the Fourier domain as

$$G(s) = H(s)F(s) \qquad (37)$$

The Fourier spectra of the actual and measured limb radiances are $F(s)$ and $G(s)$, respectively. $H(s)$ Represents the Fourier transform of the vertical response function, which is often referred to as the system modulation transfer function (MTF). For all of the HIRDLS spectral channels, $H(s)$ rolls off smoothly with increasing spatial frequency, approaching zero at the detector cut-off, i.e., 1 km^{-1} in object space, as shown in Figure 32. Spatial frequency components beyond the detector cut-off will have been attenuated below the expected radiometric noise level, and therefore cannot be reconstructed from the measured limb profiles. This sets a practical upper limit on the smallest distinguishable vertical scale that can be recovered from HIRDLS observations.

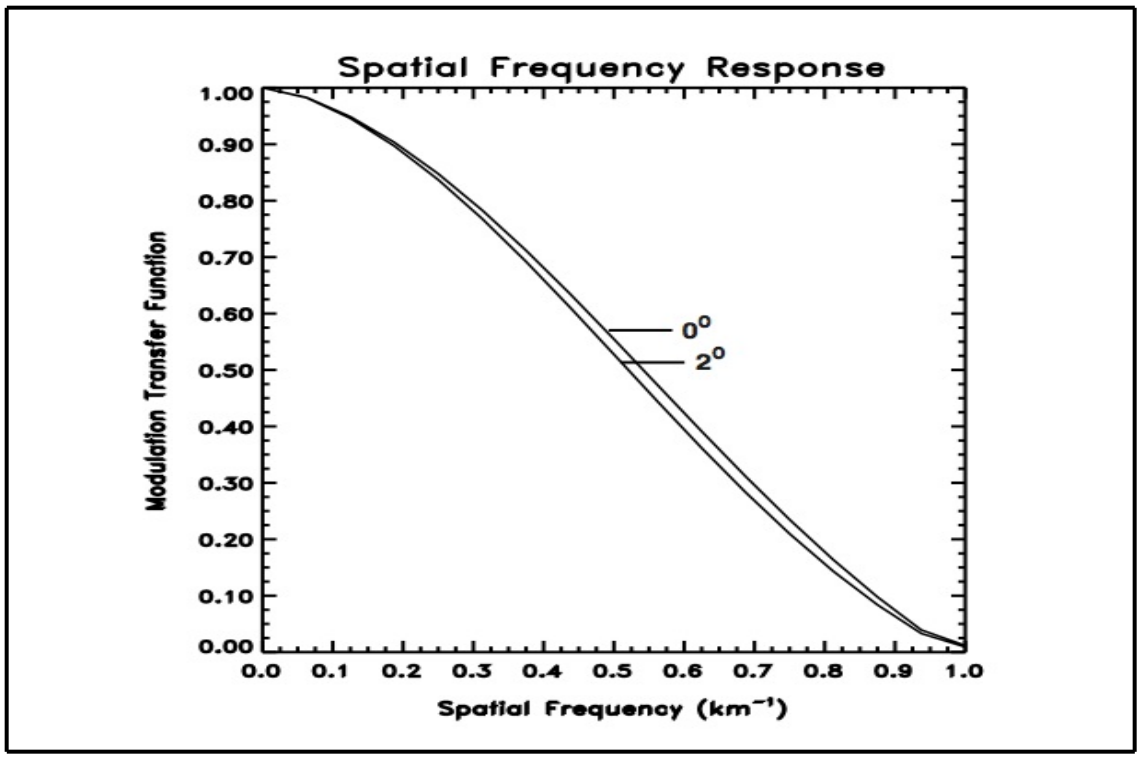

Figure 32. Channel 10 Spatial Frequency Response

5.3.2.3 Deconvolution

An alternative to modeling the FOV convolution in the forward radiance calculation is to remove the effect before inversion of the radiance profiles. To recover the original limb spectrum, Equation 2 in Section 5.3.2.2 may be directly inverted ([*Brault and White* (1971)]),

$$F(s) = H(s)^{-1} G(s) \qquad (38)$$

and the deconvolved radiance profile reconstructed from $F(s)$ by an inverse Fourier transform. The inverse MTF restores the amplitudes of high spatial frequency components attenuated by the instrument MTF. Note that this is a restoration process seeking to preserve the original signal spectrum and is not an enhancement process. The direct inversion method is problematic because in the presence of measurement noise, the solution becomes unbounded as $H(s)$ approaches the detector cutoff frequency due to the of amplification of high frequency noise components. Regularization techniques are commonly used to condition the problem, and to produce stable and meaningful solutions by applying some form of smoothing ([*Andrews* (1974)], [*Banham and Katsaggelos* (1977)]), e.g.,

$$F(s) = H(s)^{-1} G(s) R(s) \qquad (39)$$

The form of the restoration filter $R(s)$ depends upon assumptions about the original signal using either stochastic or deterministic models. An example of an approach based on a stochastic model of the signal is the optimal (or Wiener) filtering technique where the product $H(s)^{-1} R(s)$ forms the Wiener filter ([*Andrews and Hunt* (1977)]). The optimal filtering approach seeks to minimize the mean-square error between the restored and true signals. This method requires knowledge of the power spectrum of the signal. Estimates of the original signal spectrum are often made indirectly using the observed spectrum.

Preliminary analysis showed that the final results were rather sensitive to how well the signal spectrum could be estimated from the observed signal. Therefore following an approach similar to that used for LIMS processing ([*Bailey and Gille* (1986)]), the restoration filter $R(s)$ will be a fixed lowpass filter of high order. This approach maintains a consistent frequency response over all profiles. As of the beginning of production (though processing system requirements leave this open to change), the channel-dependent cut-off frequency was chosen to be, for all channels, 0.48 km^{-1}, corresponding to vertical wavelengths of about 2 km. Beyond this cutoff frequency, the observed limb spectrum is dominated by measurement noise. Therefore, it will be possible to distinguish small vertical variations in the limb radiance profiles, and hence in temperature and constituent retrievals, having spatial wavelengths greater than about 2 km. The field-of-view deconvolution process can be efficiently implemented in the Fourier frequency domain by using FFT algorithms. As mentioned in Section 5.3.1, application of the FFT routine will require radiance samples to be expressed on a uniformly spaced grid with spacing consistent with the information content of the limb profile, of which ST 23 will be the most prevalent. The end-points of a profile will be extended and a smooth transition from zero to each end-point added to eliminate end-around leakage in the convolution and the introduction of spurious frequency components generated by an abrupt transition. Finally, computationally efficient FFT routines require the number of data points to be a power of 2, therefore the "conditioned" profile will be extended by zero padding. The restored profile is extracted from the inverse transform of the deconvolved profile and placed onto a uniform grid with a nominal 1 km tangent height spacing.

5.3.3 FOV Response Shift

A shift in angular space is necessary to remove the effect of convolution of the FOV and the filter. Also, the FOV Response functions, an example of which is shown in Figure 31, are not zero-pointed exactly at their respective detector channel's centroid, but slightly up. This FOV Response shift is built into each channel's low pass filter.

5.4 Generating Profiles

The main purpose of the HIRDLS Level 1 Radiance Conditioning processor is to transform the Level 1 time-series data into atmospheric profiles for ingestion into Level 2 processing. This step in the conditioning processor happens after radiance filtering, as the hardware units necessary for radiance filtering are no longer necessary in the remainder of the HIRDLS data processing systems. The remainder of the section details the transform onto a uniform altitude grid, and the alignment method for each channel.

5.4.1 Channel Alignment

The HIRDLS Level 2 processing system expects atmospheric profiles, with extent 0 – 120 kilometers, with a Δ of 1 kilometer, nominally. The extent of the angle space of the atmospheric scans varies, but in almost all cases covers this altitude extent (the exception being ST 30, described in Section 2.7.2.1, with some profiles from the channels on the bottom row of the detector plane having a top altitude closer to 118 km, due to oblateness of the Earth). Each of the 21 channels, in every atmospheric scan in the input file, has altitude geolocation tags for each data point. Those altitude tags are offsets, in meters, from the detector plane boresight altitude. Figure 2, on page 8, details the layout of the detector plane, and included in that layout are nominal offsets of each channel from each other, as would be measured at the Earth's limb, while viewing from HIRDLS. Note that the boresight is at the middle of the plane, on the "left" edge of channel 2, and the nominal distance between channel

centroids, in a given column, is 9 kilometers. Due to the radiance anomaly, detailed in Section 2.6, HIRDLS atmospheric scans are 47° off vertical 0° (the angle used to generate the nominal channel offsets listed in Figure 2), and this rotation necessitated these boresight altitude offset tags for every data point for every channel. As an example, the centroid for channel 2, which would be aligned with the boresight while scanning at azimuth angle 0° (vertical), is in most cases more than 10 meters offset from boresight. These channel-specific altitude offset tags are combined with the detector boresight altitude, for each data point, to align each channel's data points with the other channels. In other words, any atmospheric feature seen by multiple channels was, up to this point, denoted by the different channels at different hardware shaft angles. This step applies the channel-specific altitude offsets to align the channels in altitude space, so that these features are now denoted at the same altitude.

5.4.2 Splining to Uniform Altitude Grid

After channel alignment, each channel's atmospheric profiles are then transformed onto a uniform altitude grid. For HIRDLS, with its high vertical resolution, that grid Δ is nominally 1 kilometer, with an extent of 0 – 120 kilometers distance above the surface of the Earth ellipsoid. The atmospheric data point Δ is roughly 180 meters, and a cubic spline with high tension is used to transform the radiance data from the 180-meter grid to the 1-kilometer grid. After transformation, any data outside the 0 – 120 kilometers range is clipped off, thereby creating the HIRDLS atmospheric profiles that the Level 2 processing system expects. As stated in Section 5.4.1, there will be some cases where the extent of the atmospheric profile does not fully cover the 0 – 120 kilometers range. In those cases, the data points that are not covered are given the "missing data" designator.

5.5 Adjusting Profiles

The Aperture Obscuration Correction, described in Section 4.5, is the only one of the three corrections in the Level 1 Correction processing system that uses HIRDLS pitch-up data exclusively to generate the correction. As such, an effective modification based on normal orientation (nominal, non-pitch-up) data is appropriate and consistent. This modification, known as the Radiance Adjustment step in the Level 1 Radiance Conditioning processing system, is detailed here. This step can be thought of as an empirical correction to the Aperture Obscuration Correction. It is a vertically dependent (in altitude space) fractional correction that is channel dependent and applied once for all profiles in the mission (separately for each channel and for up- and down-scans). The adjustment is also time-dependent, as the Kapton® seemed to drift with time. Due to this drift, there are two different sets of adjustment curves for each directional scan, for each channel. The remainder of this section details the creation and application of this adjustment.

5.5.1 Adjustment Calculation

Three different calculation methods were used to generate the adjustments, and each is detailed in this section. Also, two different sets were generated. The first set, shown in Figure 33, was used for the majority of the HIRDLS mission. The second set, not shown, but similar to the first, was used after the optical chopper started showing effects of contact with the Kapton® contamination.

5.5.1.1 Constant Adjustment

Constant adjustment to the radiances is the most common adjustment, with eight of the channels' radiances adjusted in this fashion. Those channels are the aerosol channels (1, 6, 13, 19), the N_2O_5 channel (14), the $ClONO_2$ channel (16), the CH_4 channel (17), and the NO_2 channel (21). This is also the simplest adjustment, with a constant factor applied to all data points in the atmospheric profiles, and can be thought of as a simple boost or reduction in signal.

5.5.1.2 Correlative Data Ratio Adjustment

Correlative data ratio adjustment is the second most common adjustment, with seven of the channels' radiances adjusted in this fashion. Those channels are the CO_2 (temperature) channels (2, 3, 4, 5) and the O_3 channels (10, 11, 12). This adjustment is determined by computing the 24-hour mean, vertically dependent ratio of each HIRDLS channel radiance (for a fiducial day) to the corresponding radiance that is consistent with correlative data sources, such as the Microwave Limb Sounder (MLS), as calculated by a simulation run of the HIRDLS forward model. Then, either a limited vertical range of this ratio is used as the adjustment profile, or the approximate magnitude is used to select an adjustment factor that is a constant as a function of altitude.

5.5.1.3 Radiance-Species Ratio Adjustment

Radiance-species ratio adjustment is the least common adjustment, with six of the channels' radiances adjusted in this fashion. Those channels are the CFC11 channel (7), the HNO_3 channel (8), the CFC12 channel (9), the N_2O channel (15), and the H_2O channels (18, 20). This adjustment is created for channels whose primary influence on a retrieved species is the radiance of only one or two channels, and is determined using the ratio of retrieved species with the radiance vertical variability, over an arbitrary 24-hour period. This is done by first identifying a common feature in both the radiance-ratio and Level 2 species-ratio (obviously, this ratio cannot be computed without first running the Level 2 processing system on non-adjusted radiances). The radiance adjustment curve becomes the species-ratio profile, which is uniformly scaled so that the magnitude of the feature in the species-ratio profile matches that of the radiance-ratio profile. The radiance adjustment curve done in this way is refined in an iterative process where the iterated adjustment profile, $a_2(z)$, can be described as follows (with z being a given altitude):

$$a_2(z) = a_1(z) + \frac{P_1(z) * (a_1(z) - a_0(z))}{P_0(z) - P_1(z)} \qquad (40)$$

Here, $a_0(z)$ is the first iteration adjustment used to create the first version of the curve, $P_0(z)$ is the daily mean percent difference of the first version of the curve's retrieved species with species reference), $a_1(z)$ is the second iteration adjustment used to create the second version of the curve, and $P_1(z)$ is the daily mean percent difference of the second version of the curve's retrieved species with species reference. Note that for the first iteration, where there is only one previous adjustment, a_0 is a constant adjustment set at unity, and P_0 is the daily mean percent difference of unadjusted retrieved species with species reference. With this method, there will be altitude regions at which this algorithm becomes unstable, resulting in very high values. The adjustment values in these regions are filtered out and replaced very conservatively with interpolated values.

5.5.2 Adjustment Application

The radiance adjustment curve can be thought of as a weighting function, and therefore the values of the curve are simply the weight to apply to a radiance atmospheric profile. These curves, shown in Figure 33, are generated at the same resolution as the HIRDLS radiance data to be stored in the Level 1 Radiance Conditioner output file, or HIRDLS1R. To apply these curves to the unadjusted radiance profiles, the radiances at a given altitude at a given channel are simply multiplied by their respective adjustment weight.

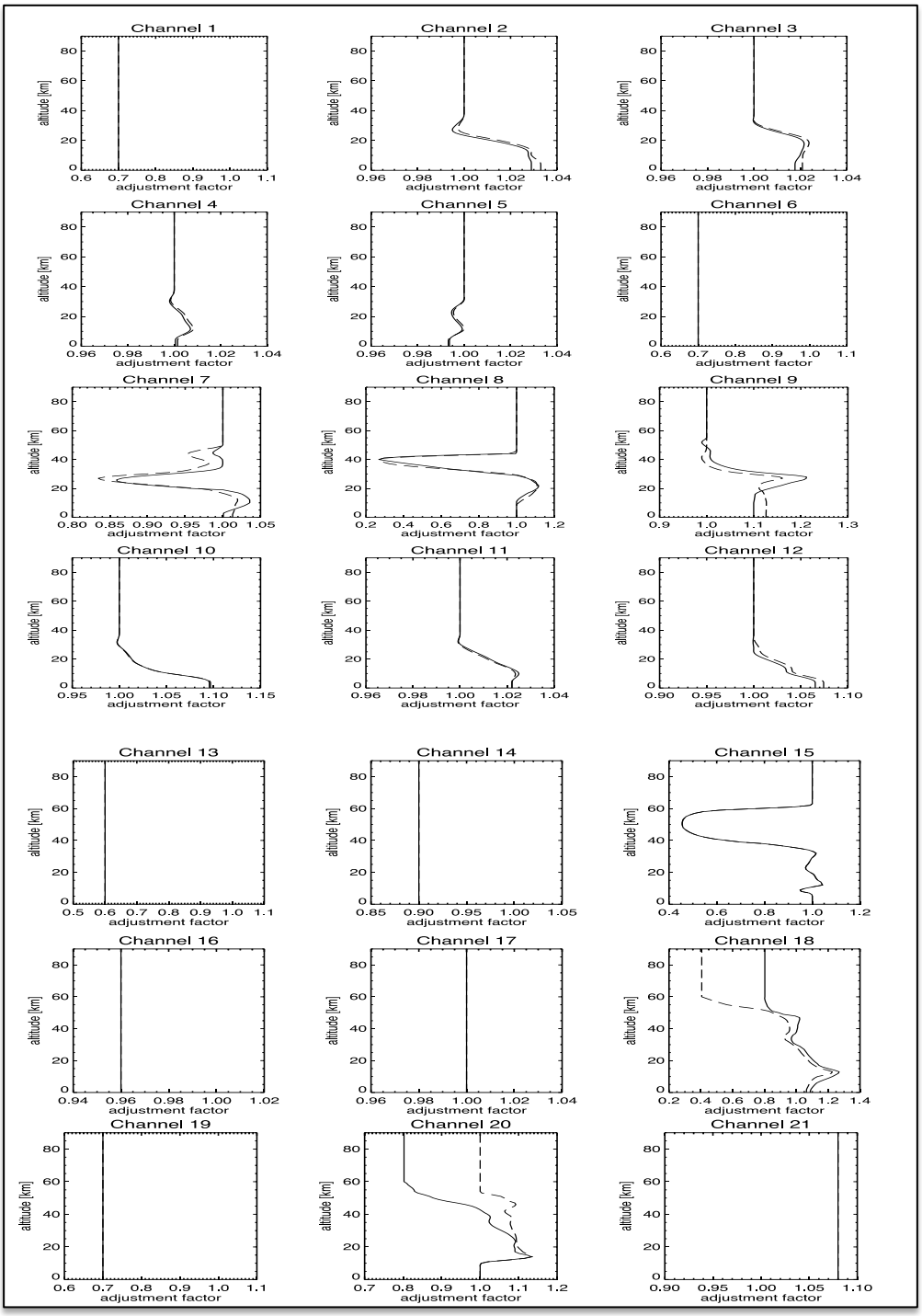

Figure 33. Radiance Adjustment Curves

5.6 Output Level 1 Profile Data

As stated previously in Section 5, the HIRDLS Level 1 Radiance Conditioning processing system is to condition radiance profiles for ingestion into the HIRDLS Level 2 processing system. The format for the output of this step is atmospheric profiles, with extent 0 – 120 kilometers, with nominal spacing of 1-kilometer. However, not all data in the output file is to be put on this grid, as only one reference point is necessary per profile. Examples of these reference points are: time, latitude, longitude, local solar time, and scan direction flag. Please see HIRDLS document SW-HIR-2002, The Requirements of the HIRDLS Level 2 Preprocessor, for an enumeration of all the fields and their respective storage requirements.

Not mentioned at all in this document, due to it being out of scope for HIRDLS Level 1 processing, is a cloud-detection step done before the HIRDLS Level 2 processing system. That step, HIRDLS Level 2 Cloud Detection, ingests this output file, uses the data within, and determines the presence and extent of cloud contamination of HIRDLS radiances. This is mentioned here because the output file described in this section includes placeholders for that cloud data, with field names that all begin with "Cloud". The Requirements of the HIRDLS Level 2 Preprocessor, SW-HIR-2002, includes these cloud fields in the output file description.

5.7 Post-Processing Requirements

There is one conditioning step done in the Level 1 Conditioning processor that is necessary for cloud detection (as introduced in Section 5.6), but is not necessary for HIRDLS Level 2 processing. That conditioning step is the radiance adjustment of aerosol data in channel 6. As shown in Figure 33, the radiance adjustment step adjusts the channel 6 radiances to 70% of the signal. This has shown to be effective in generating robust cloud detection data. However, the Level 2 processing system cannot create convergent profiles of channel 6 aerosol data unless the adjustment is removed and the radiances restored to their pre-adjustment values.

6 Processing Considerations

This section details what the HIRDLS team needs to consider when designing a processing system, including machine capabilities, auxiliary inputs, system outputs, and externally-defined requirements.

6.1 SDP Toolkit

The HIRDLS Level 1 processing system uses the Science Data Processing (SDP) Toolkit, provided by ESDIS, for such functions as Level 0 file ingestion, geo-location, and time stamp conversion. The SDP Toolkit is also used to generate the necessary metadata for each data product. A discussion of that metadata is in Section 6.2. This functionality has an impact on the minimum platform capabilities necessary for processing, and will be further detailed in Section 6.3.

6.2 Metadata

The primary purpose of metadata is to assist with the efficient distribution (e.g. via easy access) and subsequent analysis of data sets. Since data volumes are so large, information about the data (metadata) is used to represent the data to search engines or data base queries, rather than searching the data itself. All components of the HIRDLS science data processing system have followed EOS Data and Information System (EOSDIS) Core Metadata System (ECS) guidelines regarding metadata.

6.3 Diagnostics

Diagnostic data is necessary to perform quality control of all HIRDLS Level 1 data products, and subsequently, the HIRDLS team developed many diagnostic tools to analyze the efficacy of the processing algorithms. An enumeration of these diagnostic tools is out of scope of this document. But it is of note that all three processors detailed in this document produced diagnostic data files as part of their standard output. Those data files, however, were not deliverable files, and therefore not disseminated beyond the HIRDLS team.

6.4 Platform Capabilities

The HIRDLS Level 1 processing system, all three components described in this document, were developed as monolithic, non-graphical, singly-threaded, non-parallelized systems. The throughput of the entire system (all three processing systems) is ingestion of two days of HIRDLS Level 0 data and egestion of one day each of HIRDLS Level 1 data, HIRDLS Level 1 correction data, and HIRDLS Level 1 conditioned data. Therefore, the UNIX platform(s) that hosts these systems must provide at least enough space to simultaneously store the data volume, as described in Table 18. Also, the hosting UNIX platform(s) must allow flexibility in the system's design by not limiting the expected heavy I/O, nor limiting the amount of memory available, within reason. The SDP Toolkit, described in Section 6.1, contains geo-location tools that operate in 64-bit precision. HIRDLS time stamps are also generated and stored using 64-bit precision. Hosting platforms must provide up to 6 Gbytes of memory to be available for each processing throughput thread.

Processor	Input Space	Output Space
Level 1	2 Level 0 Files = 1.5 Gbytes 14 Attitude Files = 6.5 Mbytes 2 Ephemeris Files = 11 Mbytes Total = 1.5 Gbytes	1 HIRDLS1 File = 750 Mbytes
Level 1 Correction	1 HIRDLS1 File = 750 Mbytes 16 EOF Files = 100 Mbytes	1 HIRDLS1C File = 750 Mbytes
Level 1 Conditioning	1 HIRDLS1C File = 750 Mbytes	1 HIRDLS1R File = 270 Mbytes
Total (not including output of previous processor)	Level 1 = 1.5 Gbytes Level 1 Correction = 100 Mbytes Level 1 Conditioning = 0 Mbytes Total = 1.6 Gbytes	Level 1 = 750 Mbytes Level 1 Correction = 750 Mbytes Level 1 Condition = 270 Mbytes Total = 1.77 Gbytes

Table 18. Disc Space Requirements